UNITED STATES AIR FORCE RESEARCH LABORATORY

Economical Occupant/Seat Restraint Model: Integration of ATB and LS-DYNA3D

Robert L. Williams
Bhavin V. Mehta
Shr-Hung Chen

OHIO UNIVERSITY
Russ College of Engineering and Technology
257 Stocker Center
Athens OH 45701-2979

Lee P. Bindeman

LSTC INC.
7374 Las Positas Rd.
Livermore CA 94550

May 2002

Final Report for the Period September 1998 to December 2000

20030805 047

NOTICES

When US Government drawings, specifications, or other data are used for any purpose other than a definitely related Government procurement operation, the Government thereby incurs no responsibility nor any obligation whatsoever, and the fact that the Government may have formulated, furnished, or in any way supplied the said drawings, specifications, or other data, is not to be regarded by implication or otherwise, as in any manner licensing the holder or any other person or corporation, or conveying any rights or permission to manufacture, use, or sell any patented invention that may in any way be related thereto.

DISCLAIMER

This Technical Report is published as received and has not been edited by the Technical Editing Staff of the Air Force Research Laboratory.

TECHNICAL REVIEW AND APPROVAL

AFRL-HE-WP-TR-2003-0017

This report has been reviewed by the Office of Public Affairs (PA) and is releasable to the National Technical Information Service (NTIS). At NTIS, it will be available to the general public, including foreign nations.

This technical report has been reviewed and is approved for publication.

FOR THE DIRECTOR

F. WESLEY BAUMGARDNER, PhD
Chief, Biodynamics and Protection Division
Air Force Research Laboratory

REPORT DOCUMENTATION PAGE

1. REPORT DATE (DD-MM-YYYY) May 2002	2. REPORT TYPE Final	3. DATES COVERED (From - To) September 1998 to December 2000

4. TITLE AND SUBTITLE Economical Occupant/Seat Restraint Model: Integration of ATB and LS-DYNA3D	5a. CONTRACT NUMBER F33615-98-25155
	5b. GRANT NUMBER
	5c. PROGRAM ELEMENT NUMBER 62202F

6. AUTHOR(S) Robert L. Williams, Bhavin V. Mehta, Shr-Hung Chen (Ohio University), and Lee P. Bindeman (LSTC Inc.)	5d. PROJECT NUMBER 7184
	5e. TASK NUMBER 718443
	5f. WORK UNIT NUMBER 71844305

7. PERFORMING ORGANIZATION NAME(S) AND ADDRESS(ES) Ohio University Russ College of Engineering and Technology 257 Stocker Center Athens OH 45701-2979	8. PERFORMING ORGANIZATION REPORT NUMBER

9. SPONSORING/MONITORING AGENCY NAME(S) AND ADDRESS(ES) Air Force Research Laboratory, Human Effectiveness Directorate Biodynamics and Protection Division Biodynamics and Acceleration Branch Air Force Materiel Command Wright-Patterson AFB OH 45433-7947	10. SPONSOR/MONITOR'S ACRONYM(S) AFRL/HEPA
	11. SPONSOR/MONITOR'S REPORT NUMBER(S) AFRL-HE-WP-TR-2003-0017

12. DISTRIBUTION/AVAILABILITY STATEMENT

Approved for public release; distribution is unlimited

13. SUPPLEMENTARY NOTES

14. ABSTRACT
The project objective was to integrate rigid body dynamics software ATB from the Air Force and three-dimensional nonlinear dynamic finite elements software LS-DYNA from LSTC Inc. This combination of existing software allows deformation and stress analysis in addition to rigid body motion within the same system. The purpose was to produce a new tool for integrated modeling and simulation of human body dynamic response in crashes and other hazardous situations. The resulting commercial product, marketed by LSTC Inc., can be used to support design of improved human-safety restraint systems for the aircraft and automobile industries.

15. SUBJECT TERMS
Modeling, Simulation, Finite Elements, Occupant, Crash Safety

16. SECURITY CLASSIFICATION OF:			17. LIMITATION OF ABSTRACT	18. NUMBER OF PAGES	19a. NAME OF RESPONSIBLE PERSON Joseph Pellettiere
a. REPORT	b. ABSTRACT	c. THIS PAGE	UL	106	
UC	UC	UC			19b. TELEPHONE NUMBER (Include area code) (937) 255-1150

THIS PAGE LEFT BLANK INTENTIONALLY

PREFACE

THIS PAGE LEFT BLANK INTENTIONALLY

TABLE OF CONTENTS

LIST OF FIGURES

LIST OF TABLES

THIS PAGE LEFT BLANK INTENTIONALLY

FINAL TECHNICAL REPORT SUMMARY

This is the final report for the project "Economical Occupant/Seat Restraint Model: Integration of ATB and LS-DYNA3D," Agreement No. USAF-F33615-98-25155. The two-year project performance period is 1 September, 1998 through 31 December, 2000. The project was granted a no-cost extension to 31 December 2000, instead of 30 September, 2000 as originally proposed. This final report also serves as the eighth quarterly report and the fourth payable milestone report.

The project objective was to integrate rigid body dynamics software ATB from the Air Force and three-dimensional nonlinear dynamic finite elements software LS-DYNA from LSTC Inc. This combination of existing software allows deformation and stress analysis in addition to rigid body motion, within the same system. The resulting commercial product, marketed by LSTC Inc., can be used to support design of improved human-safety restraint systems for the aircraft and automobile industries.

The specific project goals were to integrate the ATB and LS-DYNA software, deliver a coupled code user manual (included with this final report), verify with known examples during the integration and improvement phase (which lasted nearly the entire project), model restraint systems (seats, seat belts, and airbags) and use the new software to produce models with these elements, and to commercialize project results in the marketplace. All of these goals have been met. The marketing phase is underway and will continue into the future.

The project team was composed of Ohio University, LSTC Inc. and the Biodynamics and Acceleration Branch of the Air Force Research Laboratory. During the first project year KBS2 Inc. was the lead partner in integrating ATB and LS-DYNA for Windows NT. During the second project year LSTC Inc. took over from KBS2 Inc. in charge of the commercializing efforts.

This final report presents an overall summary of the software integration and validation efforts. The final user manual is included. The Business Status report summarizes the fourth payable milestone expenditures and partner matching expenditures; also the Final Business Status report is given. As the eighth quarterly report the final seat, seat belt, and airbag modeling is presented. Full technical details are not given for the entire project: please see the preceding seven quarterly reports for the complete overall technical details.

Payable Milestone 4, 31 December, 2000

"Final software, including pre- and post-processors, completed and ready for commercialization. Software, user manual, and final report delivered."

Teleconferences

Throughout the project teleconferences were held roughly monthly to ensure regular communication of project issues. Teleconference minutes were distributed to all partners by the Air Force after each event.

Conference Papers

Two conference presentations were made based on project results:

S. Patlu, S.-H. Chen, P. Petkar, R.L. Williams II, B.V. Mehta, J.M. Kennedy, L.P. Bindeman, J. Pellettiere, 2000, " Enhanced Modeling Capabilities for ATB by Integration with Finite Element Analysis (LS-DYNA)", 2000 ATB Model User's Group Conference, 28 April, Wichita, Kansas.

S.-H. Chen, S. Patlu, P.N. Petkar, R.L. Williams II, B.V. Mehta, L.P. Bindeman, J.M. Kennedy, and J. Pellettiere, 2000, "Integration of Finite Element Analysis (LS-DYNA) with Rigid Body Dynamics (ATB) for Crash Simulation", 6th International LS-DYNA Users Conference (Simulation 2000), April 9 - 11, Dearborn, Michigan.

Website

LSTC is continuing development of the following website for communicating developments in the coupled ATB/LSDYNA software:

http://www.ATBModel.com/

The site is under further development; all additions and modifications must be approved by the Air Force. This will be the primary vehicle for commercialization efforts following the end of the project. This site is linked to the FEA Information Master Site:

http://feainformation.com/aindex.html/.

Coupled ATB/LS-DYNA User Manual

The final ATB/LS-DYNA user manual is attached to this report. It is available to other parties from the contact author after the end of the project. It can also be made available on the above website.

Technical Status

Ohio University

During the seventh and eighth quarters, Ohio University has completed modeling and verification work in the project. The coupled code has remained stable over this entire period; we were working during this final period with software version 7. Only late in the project (mid-December 2000) we received the final coupled software version, LS960ATB. Our final verification is included with this report, and it appears as if there are some bugs yet to fix and some validation disagreement. In Appendices A,B, and C, we report our work on seat, seat belt, and airbag modeling, respectively, including example cases for each. Appendix D presents the pre-processor developed for the coupled code input. Appendix E presents the final User's Manual for the coupled ATB/LS-DYNA software; this includes a LS-DYNA input deck (*.k file) and an ATB input deck (*.ain file). First we present a project summary of the software integration and verification work on the following page, followed by a two-page report on the verification work for the final coupled code version developed for marketing by LSTC, Inc., LS960ATB.

LSTC

During the eighth quarter, efforts by LSTC include the following:

- Further development and enhancements were made to the ATBModel.com website, which is linked to the FEA Information website.

- Continued LS-DYNA support was provided to Ohio University.

3

FINAL INTEGRATION/VERIFICATION SUMMARY

Throughout the project KBS2, Inc., and then LSTC, Inc. was responsible for providing the coupled ATB/LS-DYNA code; Ohio University was responsible for verifying the coupled code and all changes to ensure that correct functionality was maintained throughout as improvements were made.

For verification, five separate cases were modeled and analyzed to compare the results and verify the integration of the two software. The verification cases are given in Table 1 below.

Table 1. Verification Cases

Verification Case
ATB sphere, plane and motion
ATB manikin, seat and motion with no seat belt
ATB manikin, seat and motion with LS-DYNA seat belt
ATB manikin, seat and motion with LS-DYNA airbag
ATB manikin, seat and motion with LS-DYNA seat belt and airbag

Table 2 summarizes the Version history throughout the project for the coupled ATB/LS-DYNA software.

Table 2 Bug or Upgrade and Version Number Summary

Description	Version	Date
Windows NT Beta version	1	4/1999
View missing ellipsoid of ATB manikin leg	2	7/1999
Visualize ATB seat and floor planes	3	7/1999
Visualize ATB seat belts	4	8/1999
Fix acceleration bugs (X,Y zero, Z constant)	5	10/1999
ATB Fortran 90 upgrade	6	12/1999
Eliminate seat belt slack in the first step	7	2/2000
Seat accelerations are zero	LS960ATB	12/2000

The following two pages present our final verification results, comparing LS960ATB with the previous version 7, as it had been compared with the previous version 6 and so on. This final report then concludes with the last payable milestone and final business status reports, plus the appendices.
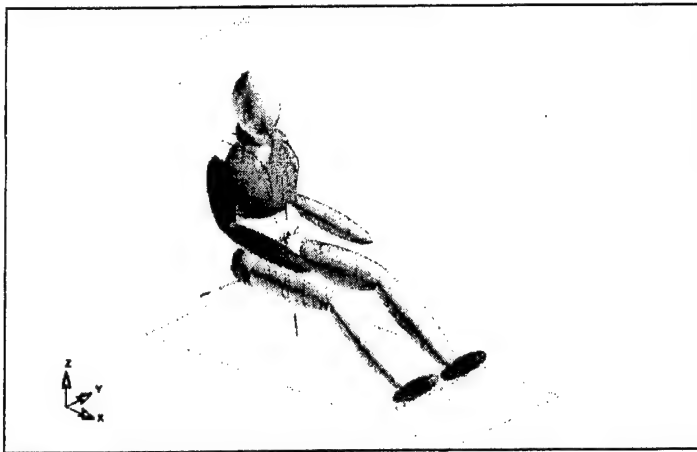
LS-DYNA Version 7 Result – Frame 1
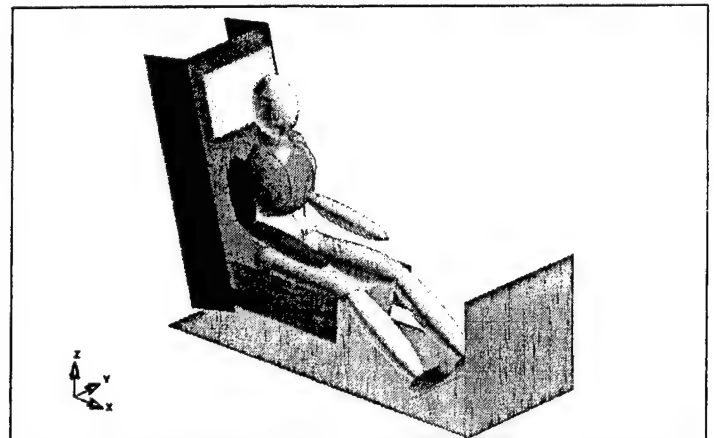
Ls960ATB Result – Frame1
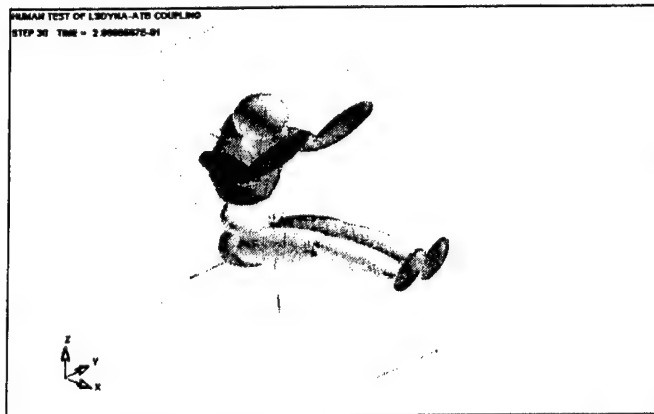
LS-DYNA Version 7 Result – frame 30
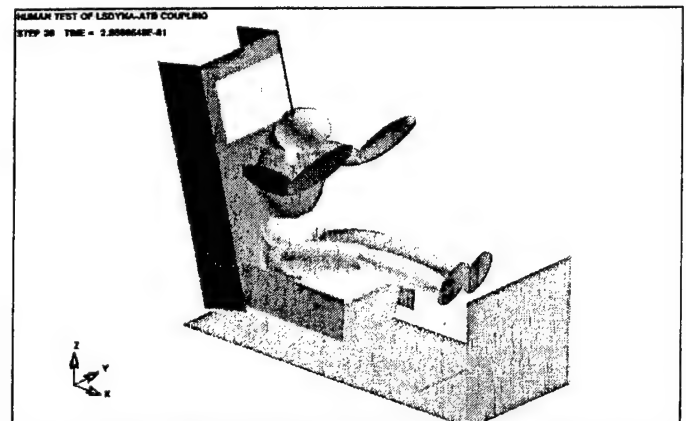
Ls960ATB Result – Frame30

Figure 1 The Comparison of result between LS-DYNA version 7 and ATB

The ls960ATB could show all the planes that were setup in the ATB file, but the lsdyna7 (LS-DYNA version7) only showed the plane that were in contact.

The figures below show a comparison of ATB manikin, seat and motion with LS-DYNA seat belt and airbag between lsdyna7 and ls960ATB versions. The results are almost identical, which was expected since LSTC did not modify anything in the code other than display of the planes.
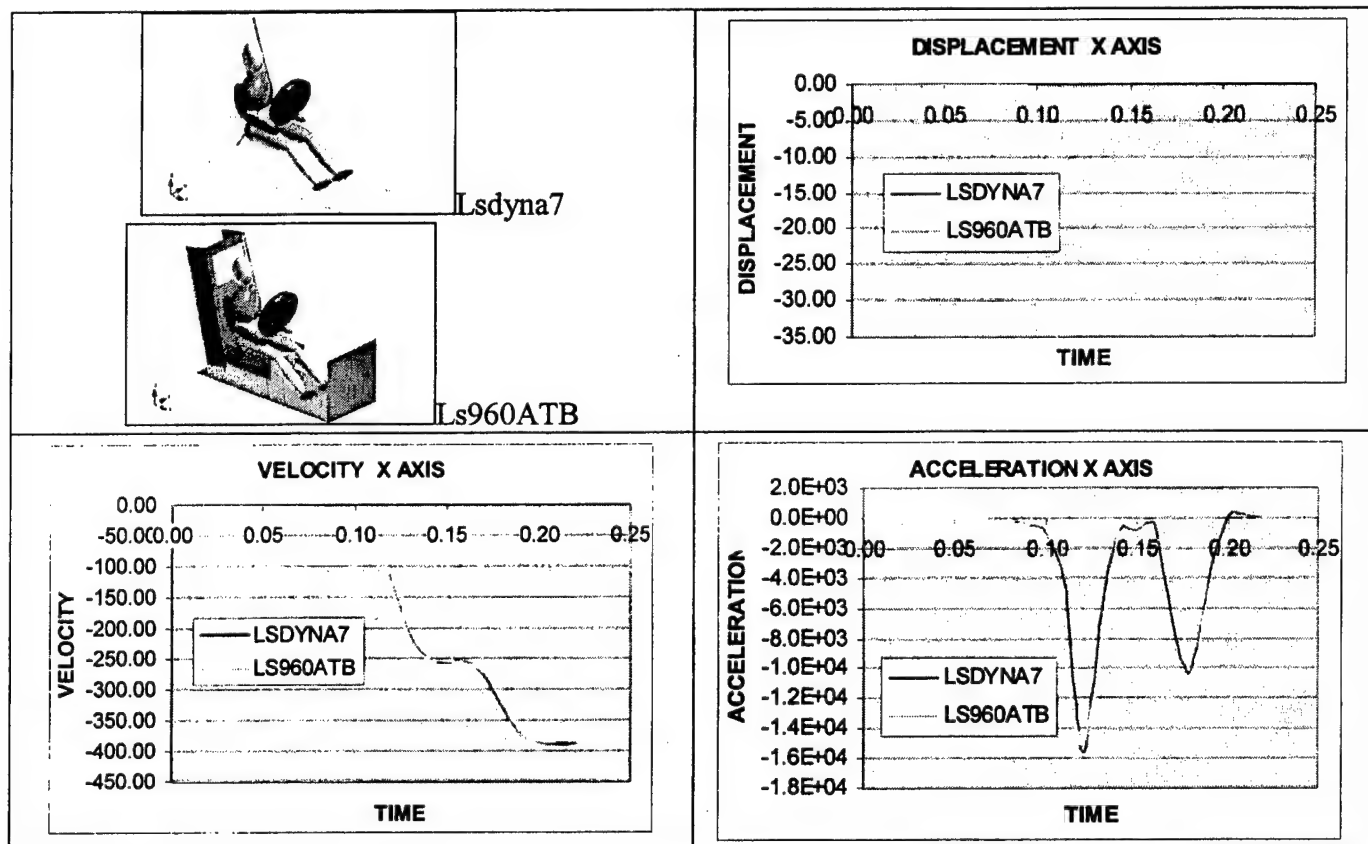
Figure 2 The Comparison be between lsdyna7 and ls960atb

APPENDIX A. MODELING OF SEAT STRUCTURES

Overview

Modeling of seat structures (often with foam cushions) is one of the challenges for current car crash and occupant safety analysis and modeling. The following input is needed for the simulation of gross body dynamics of occupant in vehicle crash.

1. Geometric and mechanical properties of the occupant
2. Geometry of the interior parts of the vehicle, which interact with occupant model during the crash

Occupant Model

The occupant model is provided by rigid body dynamics program ATB Model. The dummy model used for the research was Hybrid III (Fiftieth percentile adult human male).

Geometry of Vehicle Interior

A vehicle interior from the crash analysis research point of view consists of the seat, floorboard, the toe board and initial seating positions. For sled tests, dashboard and the steering wheel are not included.

Solid modeling of seat parts

3-Dimensional solid model of the seat was created using software package Solid Edge-version 7 by Unigraphics solutions. Each part was modeled separately in Solid Edge Part. All the parts were then assembled in Solid Edge Assembly for relative positioning to make complete 3-D model of the seat. Figure A.1 shows the exploded view of the seat assembly.
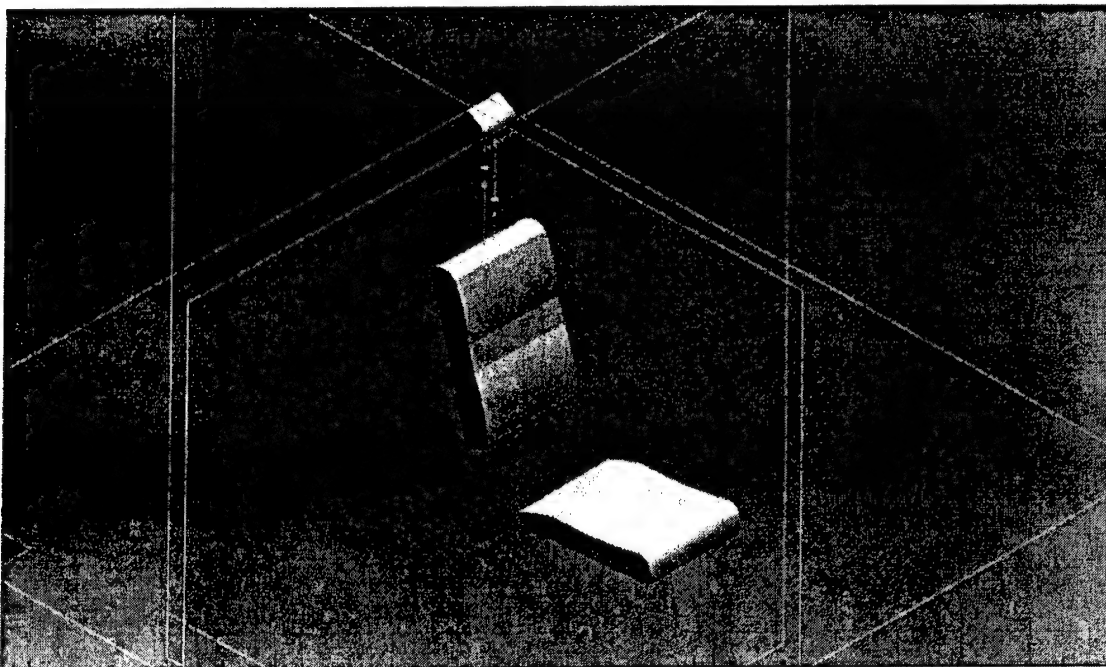
Figure A.1 Exploded view of the seat assembly in Solid Edge

The above seat assembly consists of 5 parts modeled in Solid Edge Part

1. Seat Cushion – It forms base of the seat
2. Seat Back – It is the back rest of the seat
3. Left Pin – It supports the head rest on the top of the seat back
4. Right Pin – Second support pin for the head rest
5. Head Restraint – It forms the support for the head of the occupant in rear impact crash situations.

Export of Solid Model to HyperMesh

The seat model created has to be exported to the pre-processor HyperMesh for creating solid mesh. This is done by exporting each part separately and creating a solid mesh on each part. As HyperMesh does not recognize the .par file format of the solid geometry created in Solid Edge, the parts were saved in IGES format.

Maintaining the relative position of the parts with respect to each other in the seat assembly was important while exporting them. For this reason, after all the parts were assembled in their respective position, all of them except one were deleted. Now
the remaining part was saved in IGES format. This procedure was repeated for each part. Figure A.2 shows one of the parts left in the Solid Edge assembly after all other had been deleted. The last part retains its position in the assembly even if all other parts are deleted.
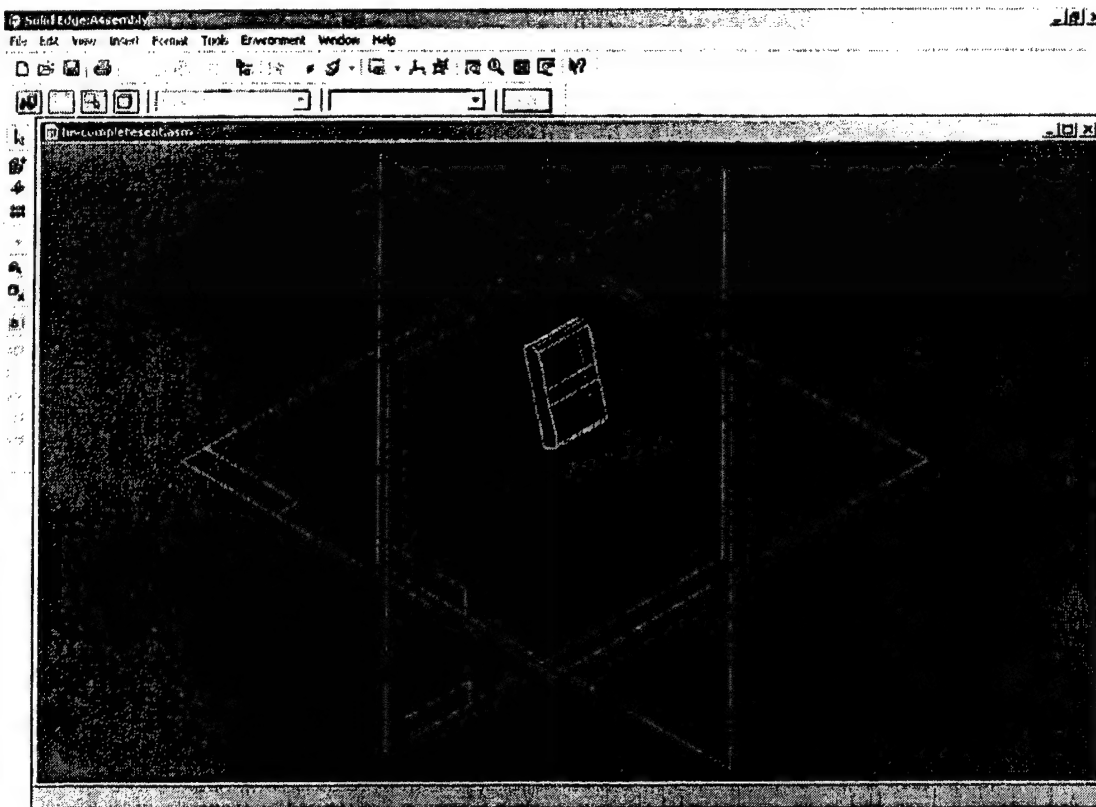
Figure A.2 View of the seat back after deleting all other parts of the seat assembly

9

This procedure was implemented to avoid the misalignment of the parts at the final stage before analysis in LS-DYNA pre-processor. It would have been much more difficult to reposition them correctly at that stage.

Discretization of the parts

Altair® HyperMesh® is a high performance finite element pre- and post-processor that enables engineers to quickly and efficiently create finite element and models for engineering simulation and analysis. It is used to discretize 3-Dimensional parts of the seat.

The parts saved in the IGES file format are imported in HyperMesh using an IGES translator. In this file format, the solid is saved in the form of surfaces. For creating a solid mesh for the part, first a suitable surface, which retains its cross sectional area throughout the length of the model, is chosen. Using 2-Dimensional auto-meshing algorithm, a surface mesh is created on that surface. Four nodded quadrilateral elements are used for the mesh. The mesh density is manually adjusted to avoid mesh distortion and obtain smooth mesh. Figure A.3 shows meshed side surface of the seat back.
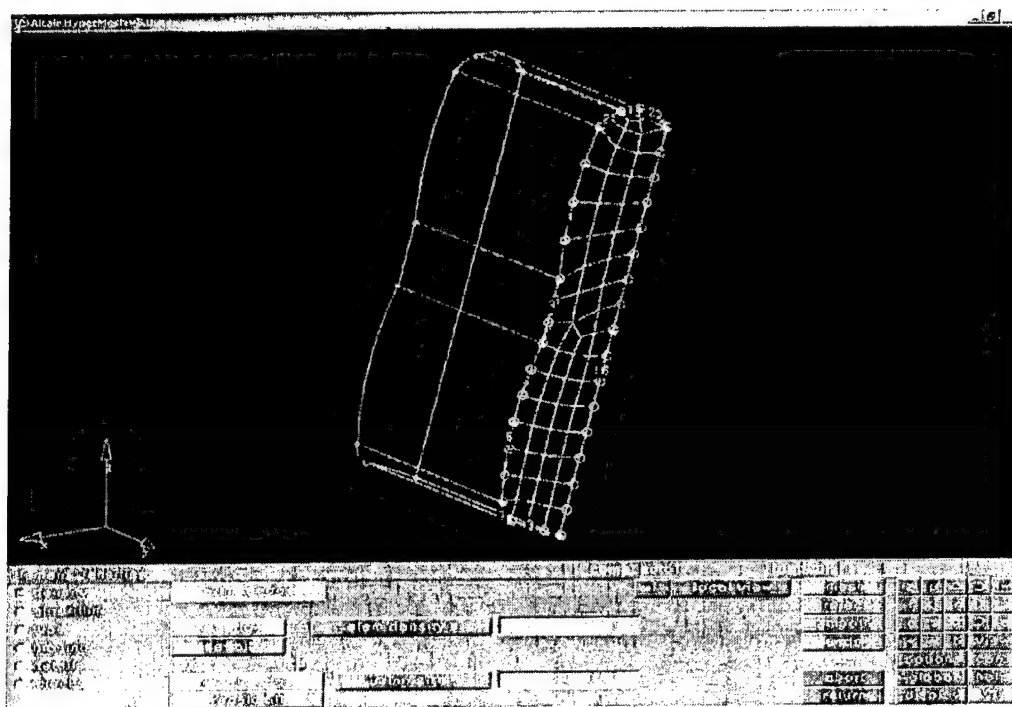
Figure A. 3 Surface mesh generation on the seat back surface using HyperMesh

After the surface mesh is completed, all the shell elements on the surface are   dragged along the continuous path throughout the width of the model to create eight-node brick elements. The element density can be controlled by specifying the number of elements along the drag. Figure A.4 shows the seat back model with solid elements generated by dragging the shell elements. Figure A.5 shows discretized solid model of the seat cushion. Similarly, FigureS A.6 and A.7 shows models of support pin and head restraint with eight-node brick elements.

After creating the solid mesh, previously created surface mesh has to be deleted. Otherwise, the shell elements are passed along with the solid elements when the geometry is exported to LS-DYNA pre-processor. As these shell elements are redundant to the analysis, it might cause confusion at a later stage.
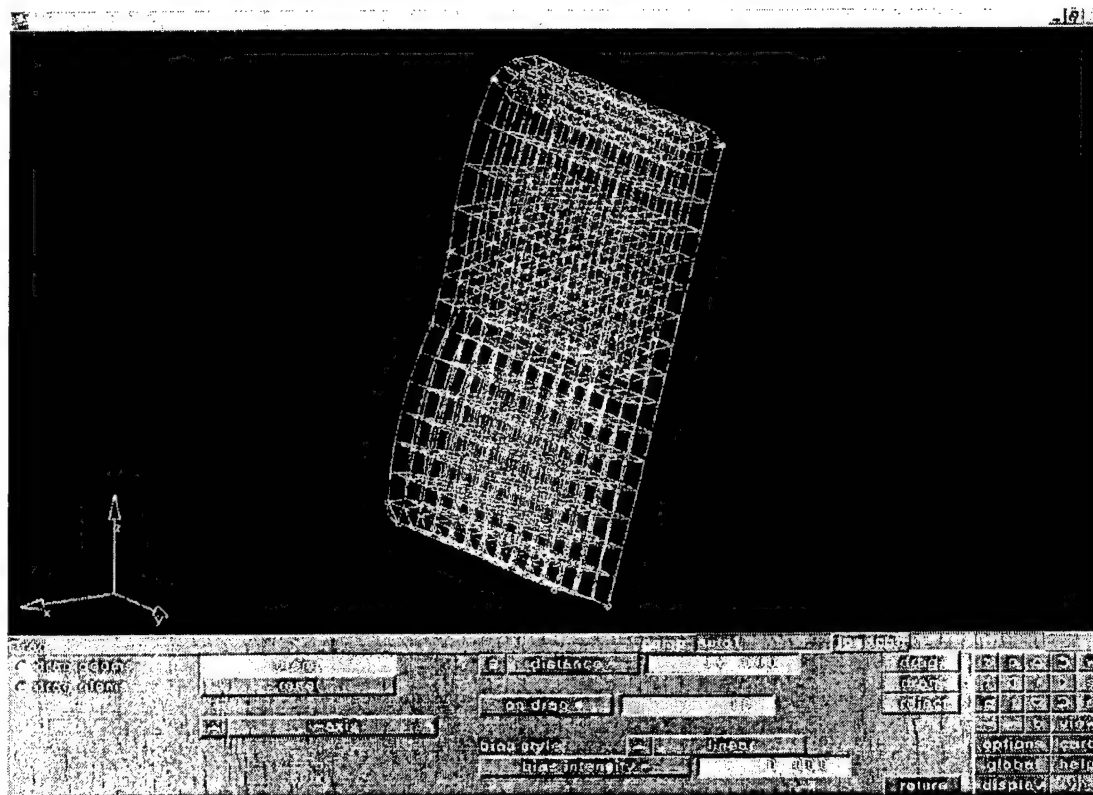
FIGURE A. 4 DISCRETIZED SOLID MODEL OF SEAT BACK
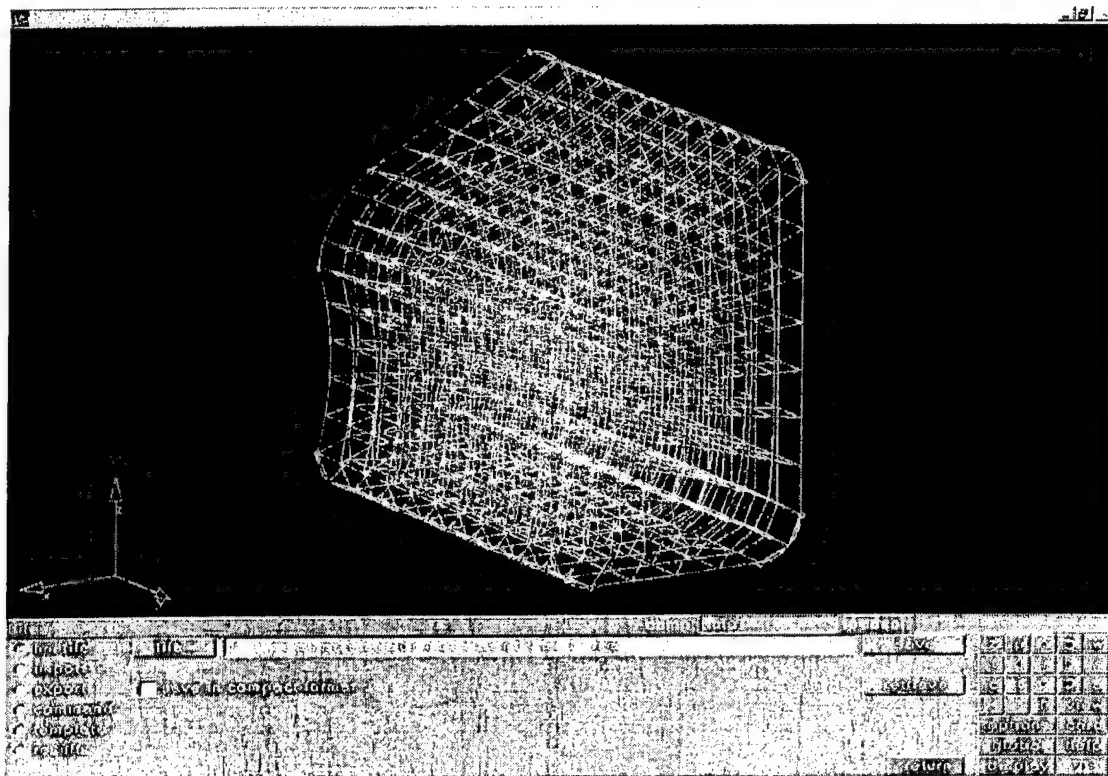
Figure A. 5 Discretized solid model of head restraint
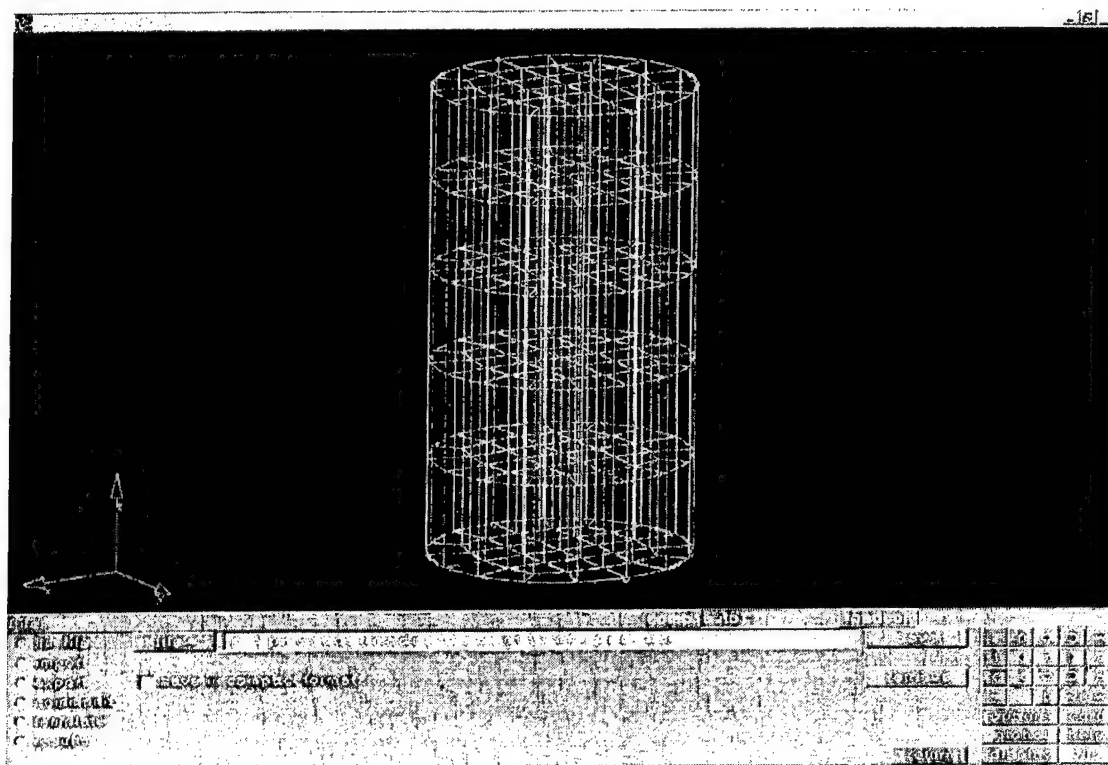
Figure A. 6 Discretized solid model of head restraint support pin

Pre-processing of the seat model

After the model has been discretized, the next step is to define boundary conditions, constraints and contacts. This part of the pre-processing is handled by specialized LS-DYNA pre-processor Finite Element Model Builder (FEMB). HyperMesh exports a LS-DYNA file as an output. It is in the form of nodal and connectivity data which can be read by FEMB after saving in LS-DYNA3D (.dyn) format.

Single part seat model

Before designing the 5-part seat model, to validate the accuracy of above procedure, a single part seat model was developed.
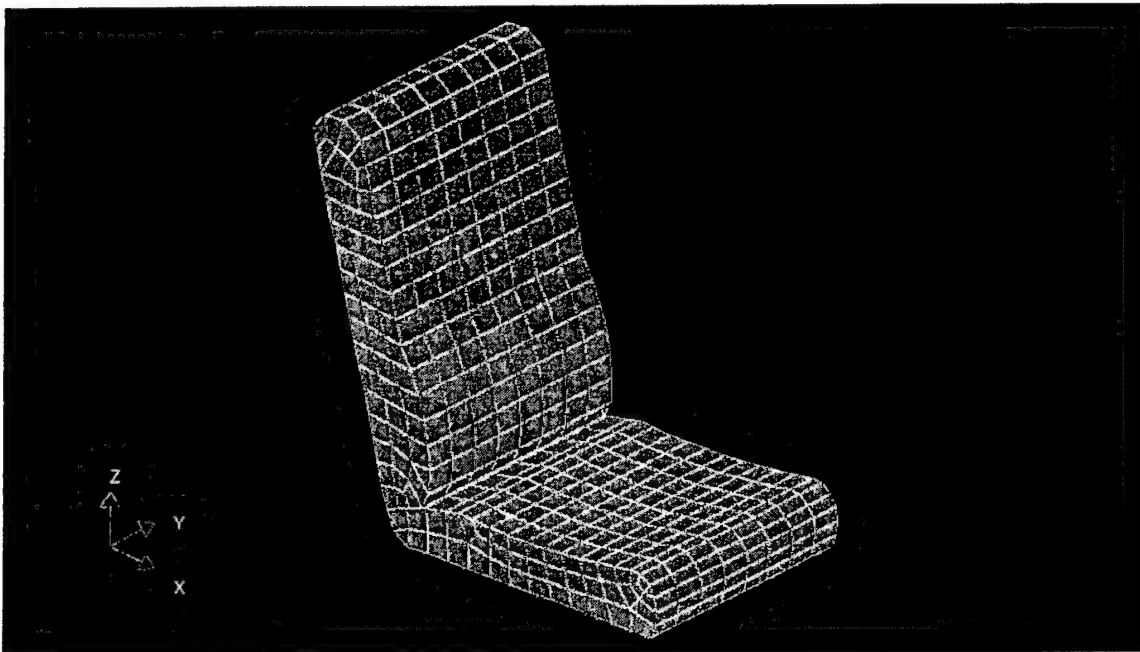
Figure A. 7 Discretized single part seat model

Modeling of the rigid planes

Two more parts were added to the seat structure in FEMB as two planes. These two planes were modeled at the base of seat cushion and at the back of the seat back respectively. These planes are needed to form a rigid support for seat cushion and seat back made up of foam material. In addition, the motion of the vehicle floor, specified in ATB input deck, is transferred to seat via these rigid planes. The rigid planes, as separate but adjoining parts are needed to model the joint between seat cushion and seat back.

Figure A.8 shows an exploded view of the rigid seat planes in FEMB. This view is created by copying and moving the planes parallel to the axes and modeling them as separate parts, as there is no facility to move parts in FEMB. This was done to clarify the position of the planes. The two planes were aligned perfectly to the seat cushion and back.
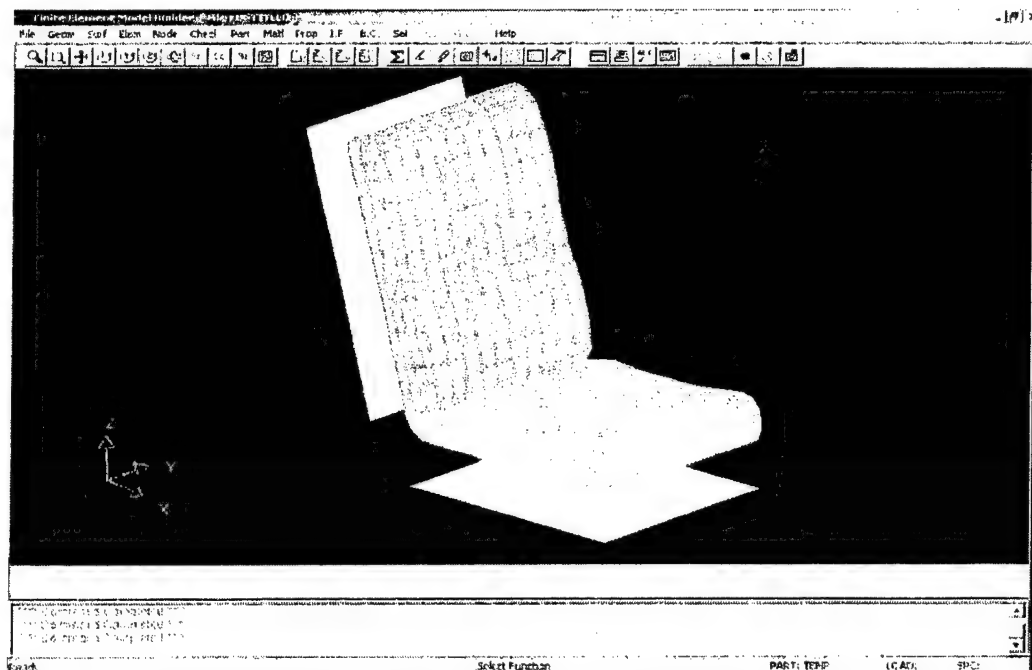
Figure A. 8 Exploded view of the rigid planes in FEMB

Seat Positioning

In order to position the seat correctly with respect to the ATB dummy, various trial and error steps were taken. Firstly, a simple seat model consisting of 2 rectangular blocks, one for seat cushion and one for the back rest, was modeled and meshed using the technique stated above. Both the blocks were modeled as single part to simplify the analysis. The dimensions of the block were approximately determined from the Hybrid III dummy segment geometry information from ATB. This was done to model the seat proportional to the dummy.

After the initial seat model was completed, both LS-DYNA seat file (.k format) and ATB Hybrid III dummy file (.ain) were run together using coupled code for one time step. During this time step, both LS-DYNA seat and ATB Dummy were coupled and visualized in the post-processor.

Figure A.9 shows one of the trial and error attempts to position the seat with respect to dummy. In this case, the seat is misaligned in Y-axis and the seat cushion block is penetrating in the Lower Leg segment of the dummy. In the next step, shown in Figure A.10, both these problems were corrected. In this case, seat cushion block is penetrating in the Upper Leg segments of the dummy. To avoid this, the Z-axis positioning of the seat was adjusted.

The correct position of the seat was thus achieved by trial and error, adjusting the seat position and running the coupled code each time to check the accuracy. Figure A.11 shows the final adjusted seat position. This position is taken as reference for developing more accurate seat model described in the first section of the chapter.

14
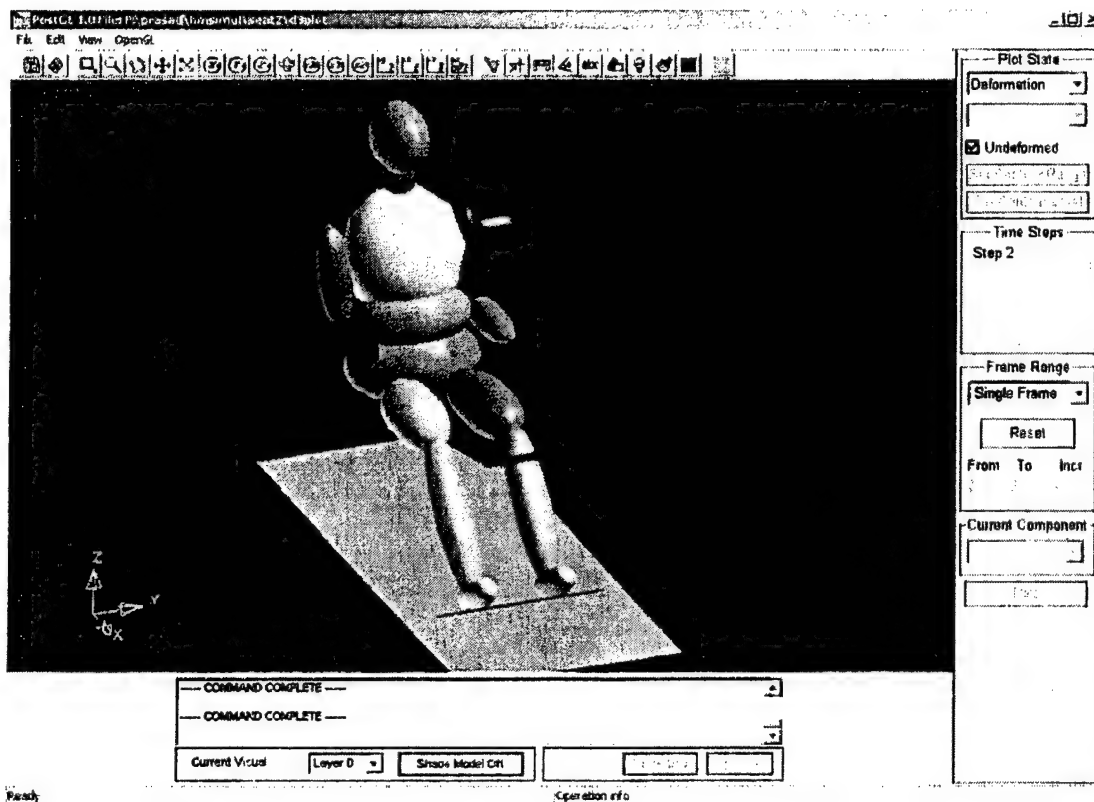
Figure A. 9 Positioning of the seat with respect to dummy – Step 1
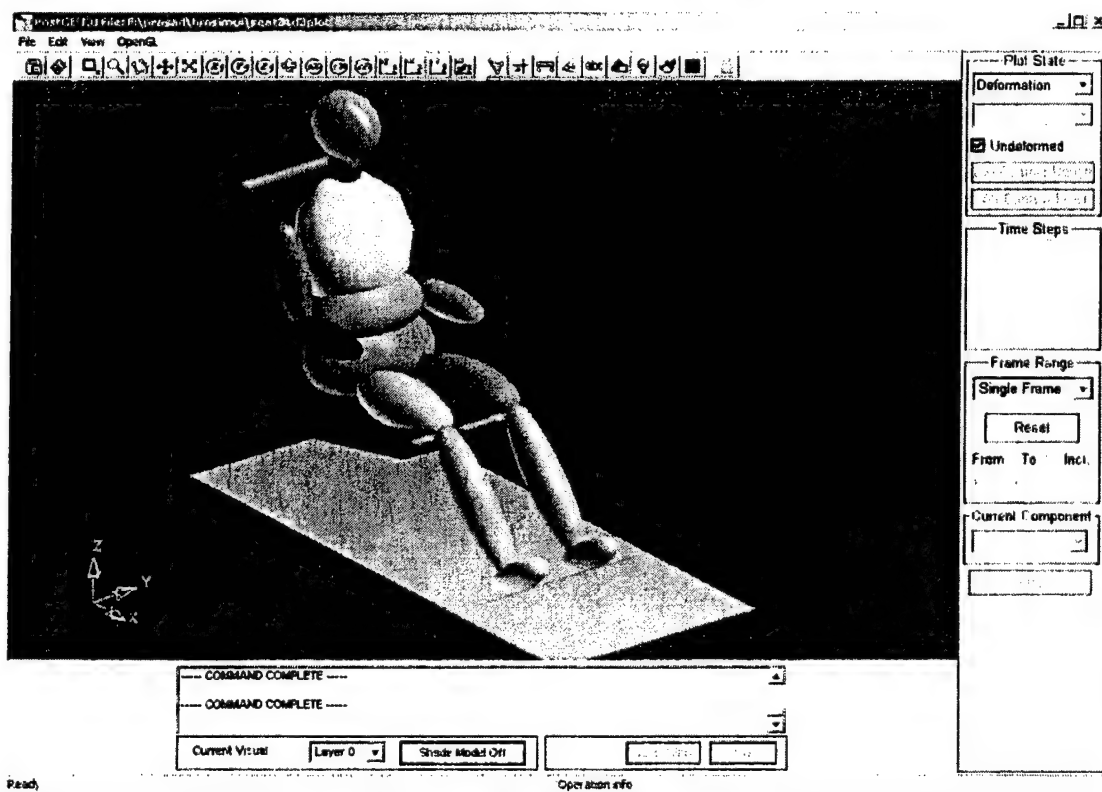
Figure A. 10 Positioning of the seat with respect to dummy – Step 2
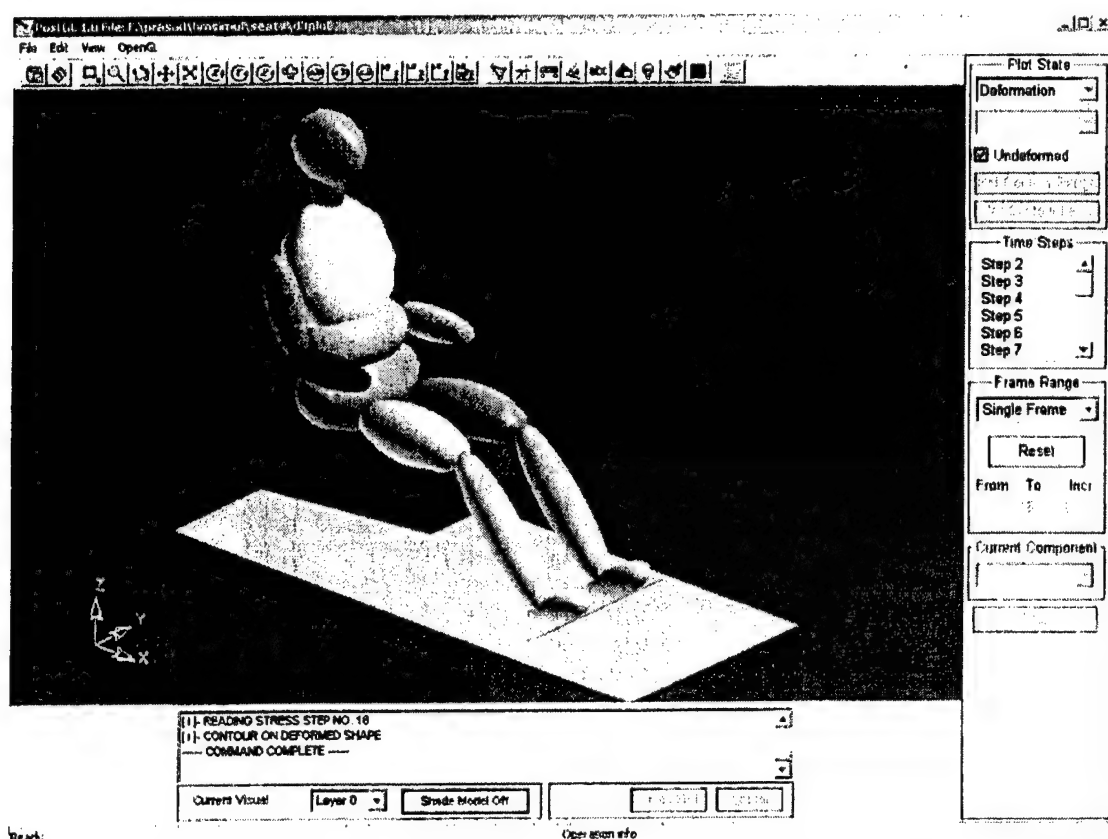
Figure A. 11 Positioning of the seat with respect to dummy – Correct Position

Node and element numbering scheme

To create various models of the seat, it is necessary to change the positions or orientations of different parts individually without changing orientation of other parts of the seat. Hence, it is very convenient if node and element numbers of all parts are separated in order to facilitate the change. Table A.1 shows the numbering scheme for nodes and elements for all seat parts. In order to replace any part, new part is modeled and saved separately with appropriate node and element numbers. Element and node renumber function in FEMB is used for this purpose. Later, the nodal and connectivity data is inserted in original LS-DYNA data deck replacing previous nodal and connectivity information of that part. This technique avoids building of LS-DYNA data deck from scratch every time the change is to be done in the model.

Table A. 1   Node and Element Numbering scheme for each part

Sr. No.	Part Name	Part Number	Start Node Number	Start Element Number
1	Seat back Plane	31	100	100
2	Seat Back	32	1000	1000
3	Left Pin	33	5000	5000
4	Right Pin	34	6000	6000
5	Head Restraint	35	7000	7000
6	Seat Cushion Plane	36	10000	10000
7	Seat Cushion	37	11000	11000
8	HR Support - Bottom	38	15000	15000
9	HR Support - Top	39	16000	16000
10	Seat belt	21	21000	21000

Head Restraint Modeling

Two important considerations for head restraint modeling were the support and position of head restraint. Figure A.12 shows exploded view of meshed head restraint model. It can be seen that it consists of 5 parts. Description of each part is given below.

Head restraint foam

The most important part of the head restraint is energy absorbing foam part (part # 35). It is the part which absorbs the impact of head during rear-end impact. It was modeled while keeping its shape proportional to the head and seat dimensions. It is discretized using hexahedral solid elements made up of low-density foam material   (LS-DYNA material model # 57) due to its high energy absorption efficiency, light weight and moldability. It is the same material used for seat back foam.

Head restraint support pins

Left and right support pins were modeled to join the head restraint to seat back and to give it vertical position adjustment flexibility. Height of both the pins can be varied to get the desired head restraint position relative to the dummy head segment. The support pins were modeled as two solid cylinders with elastic material with properties of a metal. They connect top and bottom head restraint support rigid planes.

Head restraint support planes

In order to rigidly connect head restraint foam part to seat back, two rigid support planes were modeled. The top support plane connects the top of support pins with head restraint bottom nodes. It also extends and supports back of head restraint to avoid head restraint solid foam element deformation due to high velocity of impact and head impact and keep them in shape. The bottom support plane rigidly connects seat back with nodes of support pin bottom surface. Thus the support planes act as a rigid structural support to the head restraint.
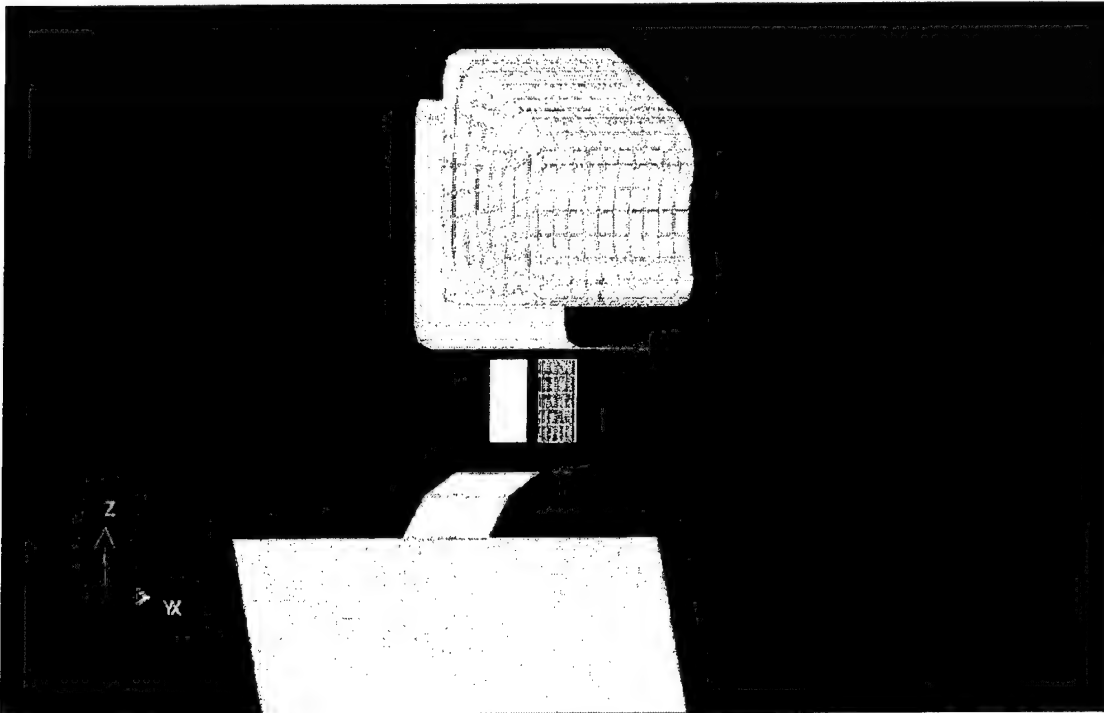
Figure A. 12 Exploded view of head restraint assembly

Seat Joints and Constraints

The parts in the seat model were connected using three types of joints: Revolute hinge joint, Nodal rigid body constraint and deformable to rigid body constraint. The description of each of the joint is given below

Revolute Joint

The connection between the seat back and seat cushion is not a rigid one. To simulate the real life crash situation, a hinge joint needs to be defined for the seat back. The joint is needed to deflect the seat back in the direction of body motion in the event of the crash. This additional cushioning effect is needed to avoid large forces on the thorax of the occupant due to the impact against a rigid seat back. For the seat model, first a joint is defined and then stiffness is imparted to the joint to avoid additional rotation of the seat back.

Joint Definition

The seat joint is defined between the seat cushion and seat back planes. The *CONSTRAINED_JOINT_REVOLUTE card was used for the joint definition. Using this card a revolute joint can be defined between two rigid bodies sharing a common edge along which the joint can be defined. The common edge for seat planes is the line of contact between them. Even though the planes share a common edge, the coincident nodes along this common edge must not have been merged in order for this joint definition to work. Otherwise, the joint cannot be defined, as both the planes will be constrained rigidly to each other. The two rigid bodies, which form the contact plane, will rotate relative to each other along the axis defined by the common edge. Figure A.13 shows the position of the joint with the corresponding planes.
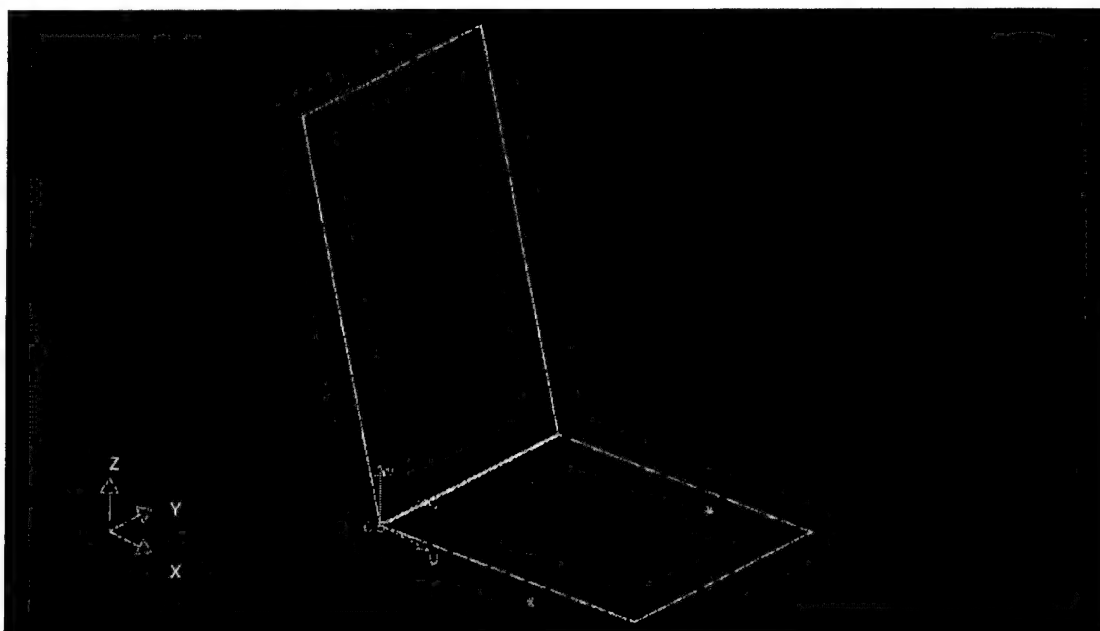
Figure A. 13 Revolute joint between seat back and seat cushion planes.

Joint Stiffness Definition

Defining a revolute joint between the two seat planes allows the free rotation of the planes. However, to avoid unrestricted rotation of seat back, rotational joint stiffness needs to be defined for the joint. Joint stiffness is defined by the card *CONSTRAINED_JOINT_STIFFNESS_GENERALIZED. In this card, a stop angle in the direction of the rotation is specified for the seat back rotation. The joint allows the rotation until the stop angle and then imparts an elastic stiffness to prevent further rotation. The elastic stiffness per unit radian for the stop angles is also specified in the card. To define the revolute angles, a local coordinate system along the revolute axis has to be defined.

Deformable to Rigid Body Constraint

The seat model consists of four rigid and five deformable parts. It is necessary to constrain the degrees of freedom of these parts to move them together to integrate the seat model. This constraint between deformable and rigid bodies is achieved by LS-DYNA keyword *CONSTRAINED_EXTRA_NODES_SET. Using this option, the nodes of the deformable body are defined as extra nodes of the rigid body to which they are to be joined thus providing the rigid link between the two parts. This constraint is used to join the following parts:
1. Seat Back Foam (part # 32) to Seat Back Plane (part # 31)
2. Seat Cushion Foam (part # 36 to Seat Back Plane (part # 37)
3. Head Restraint Support Pins bottom nodes (Part # 34 and 35) to Head Restraint Support-Bottom plane (Part # 38)
4. Head Restraint Support Pins top nodes (Part # 34 and 35) and Head restraint surface nodes to Head Restraint Support-Top plane (Part # 39)

This constraint was used most frequently to build the seat model. The inputs needed for this constraint cards are the part number of the rigid body to which the deformable nodes are to be attached and node set ID of attached nodes.

Nodal Rigid Body Constraint

This constraint is used to join the head restraint- bottom support with the seat back plane. The LS-DYNA keyword *CONSTRAINED_RIGID_BODIES was used for this definition. Using this keyword one rigid body, master rigid body, is merged into second rigid body, called as slave. In the seat model, seat back rigid plane is master body whereas the bottom support is slave body. When two bodies are thus constrained, all constraints, motion definition, displacements valid for master body are applicable to the merged body as well. Thus head restraint also gets displaced with seat back deformation after the impact.

Seat Material

Material for an automobile seat plays an important part in the occupant protection in the situation of a rear impact. One of the main requirements of the seat material is the energy absorption capacity. The material used in the study for modeling the seat cushion is low-density foam (LS-DYNA foam material model number 57). The advantages of using this material are its high-energy absorption efficiency, light weight and moldability. The light weight and moldability properties are important from vehicle design and manufacturing aspect. A input data of nominal stress-strain curve. Figure A.14 shows the stress-strain curve obtained by conducting a test on polypropylene foam specimen during a study.

mat57-Stress/Strain curve
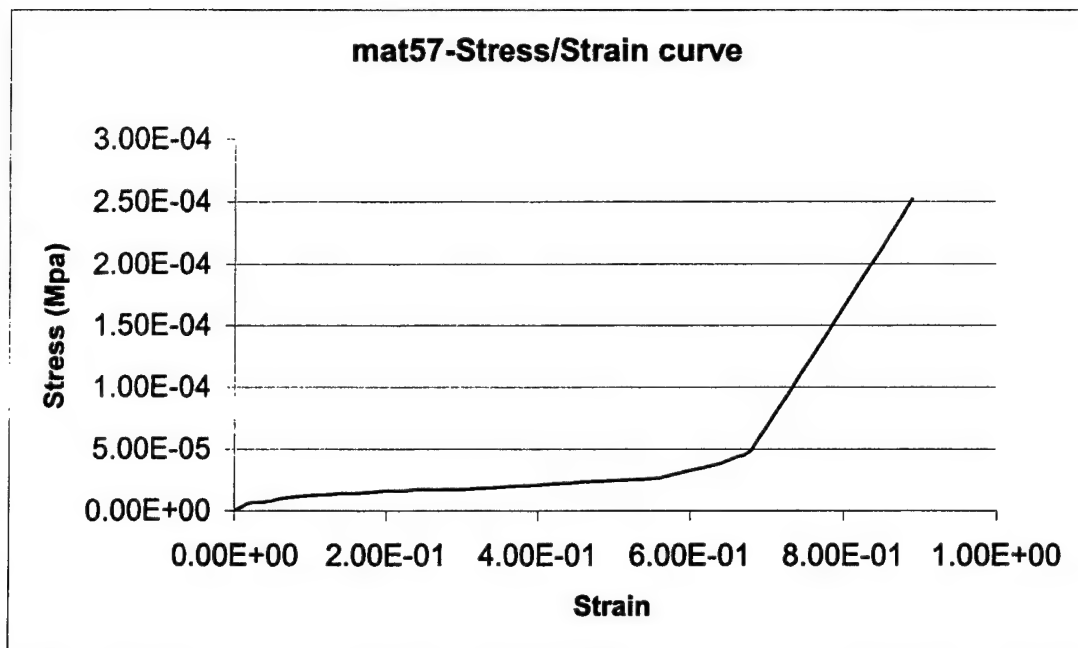
Figure A. 14 Stress-strain curve for low density foam (material model #57)

The complete seat model

The final seat model consists of 10 parts including joint between seat cushion and seat back plane. Following tables give statistics of the number of nodes, elements, types of elements etc.

Summary of the parts and modeling technique

 The final seat model consists of ten parts. Table A.2 shows the summary of all the parts with their modeling technique. Figure A.15 shows the complete seat model made up of all ten parts.

Table A. 2 Summary of the seat model parts

Sr. No.	Part Name	Part Number	Modeled In	Meshed In
1	1.7.1 Seat back Plane	31	FEMB	FEMB
2	Seat Back	32	Solid Edge	HyperMesh
3	Left Pin	33	Solid Edge	HyperMesh
4	Right Pin	34	Solid Edge	HyperMesh
5	Head Restraint	35	Solid Edge	HyperMesh
6	Seat Cushion Plane	36	FEMB	FEMB
7	Seat Cushion	37	Solid Edge	HyperMesh
8	HR Support - Bottom	38	FEMB	FEMB
9	HR Support - Top	39	FEMB	FEMB
10	Seat belt	21	FEMB	FEMB
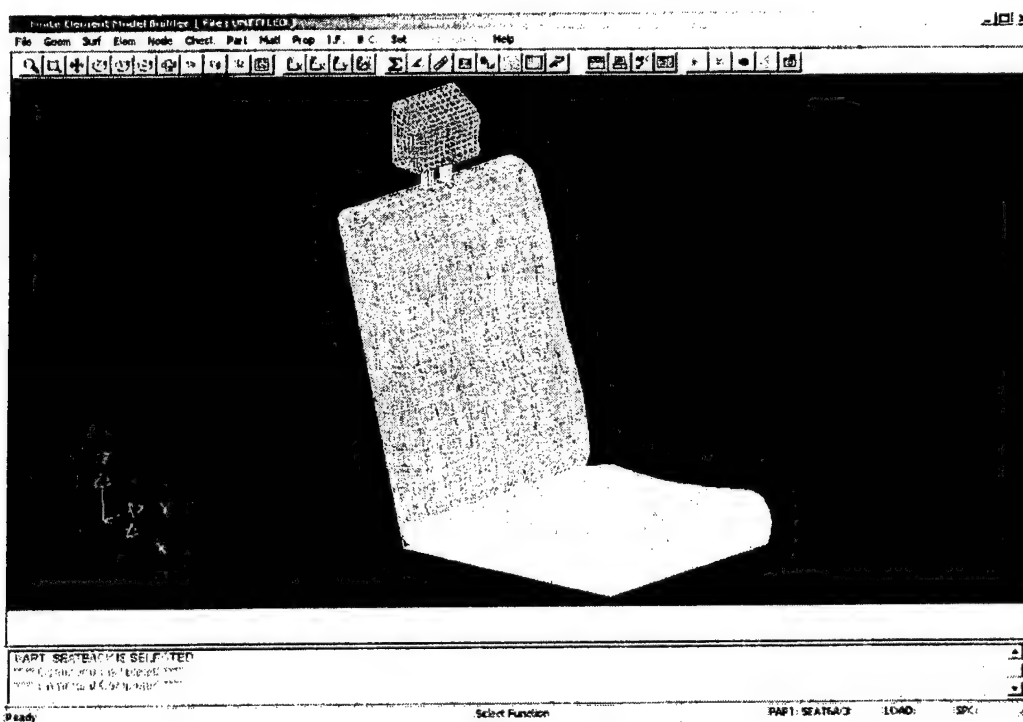
Figure A. 15 The complete seat model in FEMB

Summary of the Nodes and Elements

Table A.3 shown below gives total summary of the seat geometry and meshed parts.

Table A. 3 Summary of complete seat model

Sr. No.	Model Attribute	Value
1	Number of Parts	10
2	Number of Nodal Points	2942
3	Number of Beam Elements	1
4	Number of Shell Elements	10
5	Number of Solid Elements (Hexahedral)	1970
6	Number of Solid Elements (Wedge)	58
7	Number of Joints	1

Main factors considered in the seat model design

Various seat models were built to analyze the effectiveness of the seat and seat belt restraint system for occupant protection in rear impact situation. Table A.4 shows the factors, which were considered from design and analysis point of view to carry out the crash simulation.

Table A. 4 Main factors considered for seat model design in the study

Sr. No.	Factors	Levels		
		1	2	3
1	Head Restraint	Present	Absent	
2	Seat Belt	Present	Absent	
3	Seat Back Angle (^{o} from vertical)	10	15	
4	HR- horizontal distance (in.)	0	1.65	2.9
5	HR- vertical Distance (in.)	1	2	
6	Joint Stiffness	Low	Medium	High

Seat back angle

This is the angle between the seatback and vertical plane. Typically, it is reclined 15-25 degrees from vertical thus giving 10 degrees as range of adjustment. Recommendations for optimal seat back angle range from 15 to 30 degrees. Increasing seat back angle decreases pressure on the disc. In the study, two seat models were built with angle 10^0 and 15^0 to analyze the effect of seat back adjustment on the result. As seat back angle changes, distance of head restraint from head as well contact of seat back with upper and middle torso changes. Figure A.16 shows the seat back angle for one of the models measured from the horizontal planes.
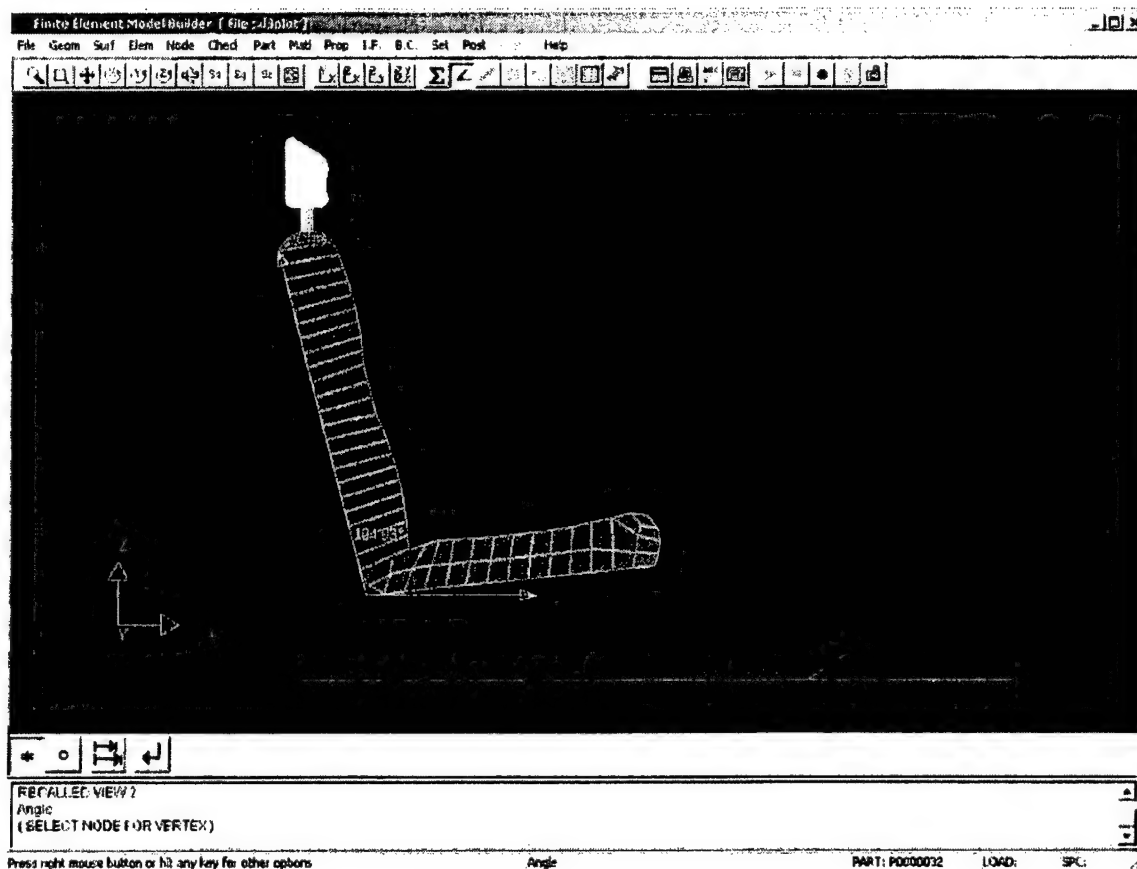
Figure A. 16 Seat back angle measurements

Gap –Horizontal Distance between head restraint and back of the head

To study the effect of adjustable head restraint on the result, the distance between the back of dummy head and head restraint was varied. This gap affects the time duration between the crash and contact of head with head restraint. As the gap increases, rearward rotation of the head increases delaying the contact between head and the headrest. Figure A.17 shows the distance measured between dummy head and headrest model in shown in FEMB pre-processor. The distances used in the study were 2.90 and 1.65 in. This was achieved by changing the position of the dummy by rotating the upright body relative to horizontal upper leg segments and moving it closer or away from the head restraint.
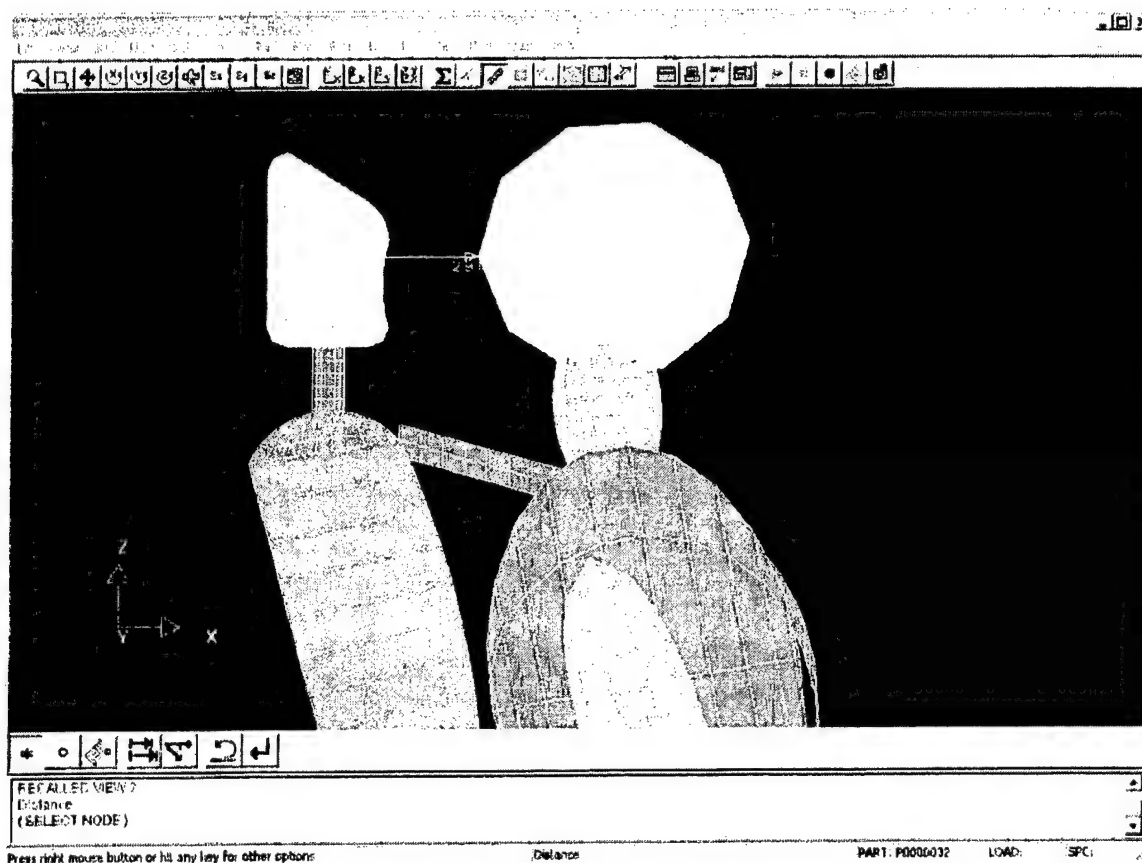
Figure A. 17 Side view of the seated dummy with respect to head restraint

Offset - Vertical Distance between head and top of the restraint

In order to simulate the conditions observed while actual driving, an adjustable head restraint is considered in the study. The seat geometry was modified to provide two different heights of the head restraint from top of the seat back. This was achieved by varying the height of head restraint support pins. The support pin height was varied from 1 in to 0.5 in. to achieve the vertical offset between head and head restraint.

Joint Stiffness

The analysis was carried out using two different values of joint stiffness defined between the seat cushion and seat back plane. The varied stiffness was taken into account to consider elastic seat-back rebound while analyzing the result. As the joint is taken into consideration, it can be assumed that analysis is carried out particularly for front seats for an automobile. The back seats of an automobile are rigidly fixed to the vehicle body. The joint stiffness is defined in such a way to avoid excessive bending of seatback, thus resulting in large rebound due to high elastic energy stored in the seatback joint. If large seat-back rebound occurs due to high elastic energy stored init, torso is pushed forward before head begins rotating backward and thus delaying contact between head and head restraint. This increases relative linear and angular velocity of head with respect to torso. The joint is defined at the seat pivot to simulate the real seat back, which would deform backwards under the impact of the body torso. Due to

26

this deformation, the distance between the head and head restraint increases thus delaying the head response.

Motion Definition

Rear-end impacts can be classified into two major categories, Lead Vehicle Moving (LVM) and Lead Vehicle Stationery (LVS). LVS accounts for approximately seventy percent of the rear-end collisions where as LVS is accountable for remaining thirty percent. Thus study of LVS crashes is more important for occupant protection. To simulate the LVS rear-end collision, the seat cushion plane (rigid) was given initial velocity in forward direction. The situation can be compared to the stationary car hit by other vehicle from behind. This initial velocity is imparted using LS-DYNA card *BOUNDARY_PRESCRIBED_MOTION_RIGID. This card is used to define an imposed motion (velocity or displacement) on rigid bodies.

Inputs to the motion card

1. Rigid body part ID – Part ID of rigid seat cushion plane
2. Applicable Degrees-of-freedom – Only X translational degree-of-freedom is specified as seat, being rigidly fixed to vehicle floor, translates only is x direction.
3. Velocity/Acceleration/Displacement Flag – Velocity flag as initial velocity is specified in rear impact crash situation.
4. Load curve ID to describe Motion value versus Time – The velocity, to be imparted to the seat, is not specified from the start of the simulation. A time gap is given between start of the simulation and start of the motion to allow the dummy to settle in the seat.

Velocity at the crash

In the study, a rear end crash was simulated using pre-impact velocities of 10.0 km/h (approximately 100 in/sec) were used. The value of the velocity was within the range used during an actual physical study in Department of Injury Prevention, Chalmers University of Technology in Sweden.

Secondary factors in the seat model design

Along with the gender difference, which were varied to analyze the seat models, some other factors were also taken into account during the seat design. Those factors either were kept constant or were proved insignificant to achieve consistent results by varying main factors. These factors are listed below.

Seat back mesh density

During the simulation, it was found that due to the numerical problems (negative volume), the analysis was abnormally terminated. This was due to the significant mismatch between the stiffness of the seat foam material and rigid dummy material and large forces exerted on the foam by the dummy segments at the time of the crash. This results in foam element becoming extremely compressed and inversion of the elements (negative volume). To avoid this *CONTACT_INTERIOR option was used that is designed to artificially keep solid elements from inverting. Also the longer elements were used with more length in the direction of impact. In order to assure that changing the element density does not affect the analysis,

the seat back density was varied and it's effect was analyzed. It was found that the variation in the seat-back density did not produce significant variation in the result. Figure A.18 shows the graph of dummy's Head segment acceleration comparison in case of low and high seatback element density. It can be concluded that there is insignificant difference in the plots in both the cases. Similar verifications were carried out with other dummy segments that verify the result.

Head - X Acceleration
High Mesh Dnesity (7000 - 8000 elements)
Low Mesh Density (2000 - 3000 elements)
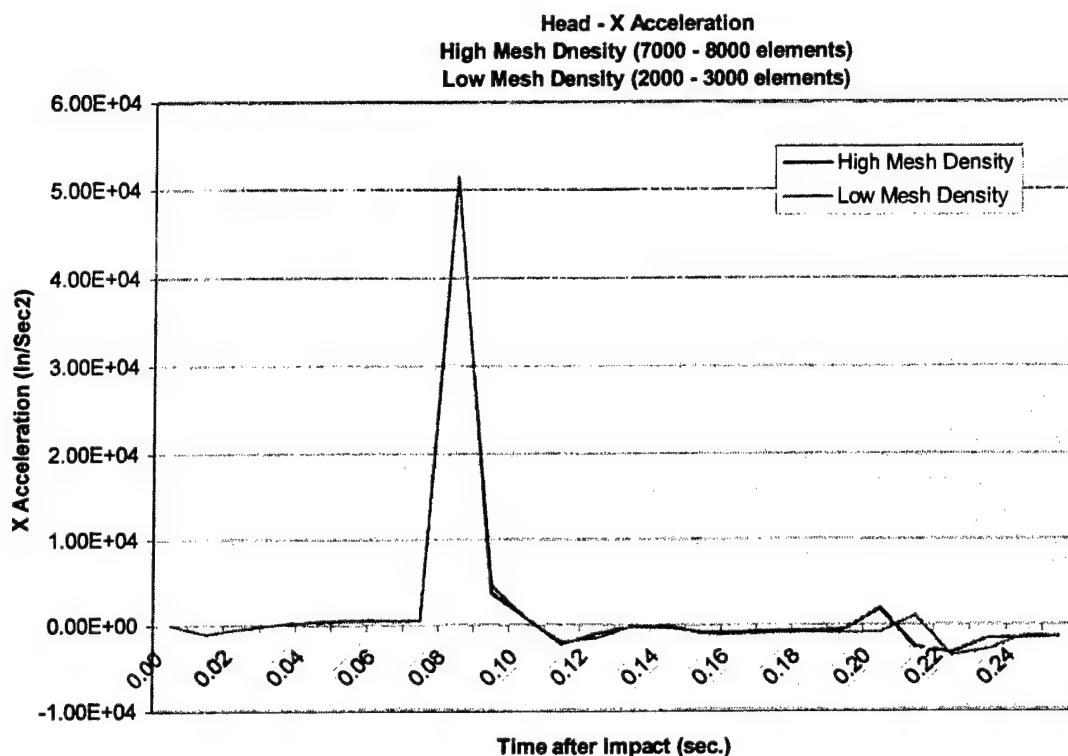
Figure A. 18 Plot of Head X Acceleration with low and high seat back mesh density

Seat Belt

As the analysis of the seat models is for front seats, a three-point belt restraint system was provided for the dummy. It consists of a shoulder belt running across the upper and middle torso dummy segments and a lap belt running across the lower torso. One end of shoulder and lap belt are connected to the seat at a single point on the seat cushion plane; thus, the belt system is anchored at three points. The two ends of shoulder belts are rigidly connected to the seat cushion and seat back plane respectively whereas two ends of lap belt are rigidly connected to the seat cushion plane. Figure A.19 shows the three-point belt restraint system anchored at three points on the seat.

28
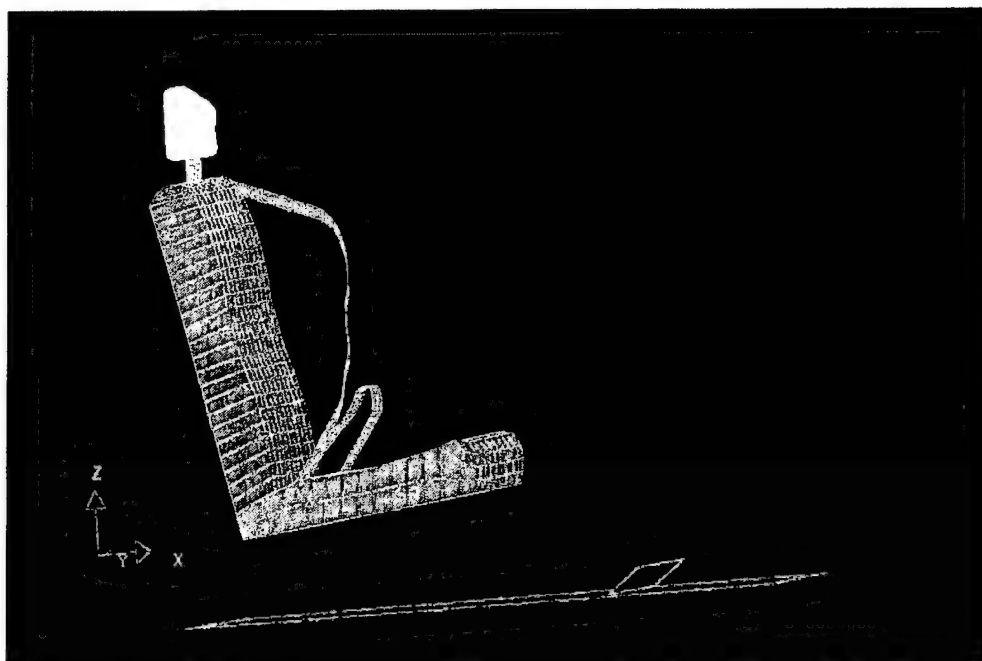
Figure A. 19 Three-point belt restraint system

Modeling of Seat Belt

To get the co-ordinates of the points for modeling the belt, the analysis is run with LS-DYNA seat model and ATB Hybrid III dummy model for 0.01 seconds. After this run, when the output is viewed in LS-DYNA pre-processor Finite Element Model Builder (FEMB). This output contains both seat and dummy model placed relative to the seat in the initial condition. The seat model is built by following the contour of the torso segments while the dummy model is in position. The seat belt modeled for the study is 2-dimensional and is made up of rectangular shell elements. After the model is drawn and meshed, all other parts except the seat belt are deleted and the seat belt model is saved in a separate LS-DYNA data deck. Later the node coordinates of the seat belt and the connectivity table from that data deck are inserted in the original seat data deck to build the final DYNA data deck with both seat and seat belt in place. This complete data deck was used for the further simulations.

Effectiveness of seat belt in rear-end impacts

In the rear impact crash simulation, the dummy is first thrown backwards. It hits the seat back and head restraint and rebound in the forward direction. The seat belt does not play any effective role during rearward movement of the dummy, but it does play an important role during the forward dummy movement as it arrests the motion beyond a point to avoid the impact of the head or chest on the cars interior parts, such as the steering wheel or front panel. Hence, it is important to fasten the seat belt at all times during driving. Figure A.20 shows the dummy position after rebound from the seat during a rear impact. It can be seen that the excessive forward movement of the upper torso and, in turn, head is arrested by the shoulder belt.
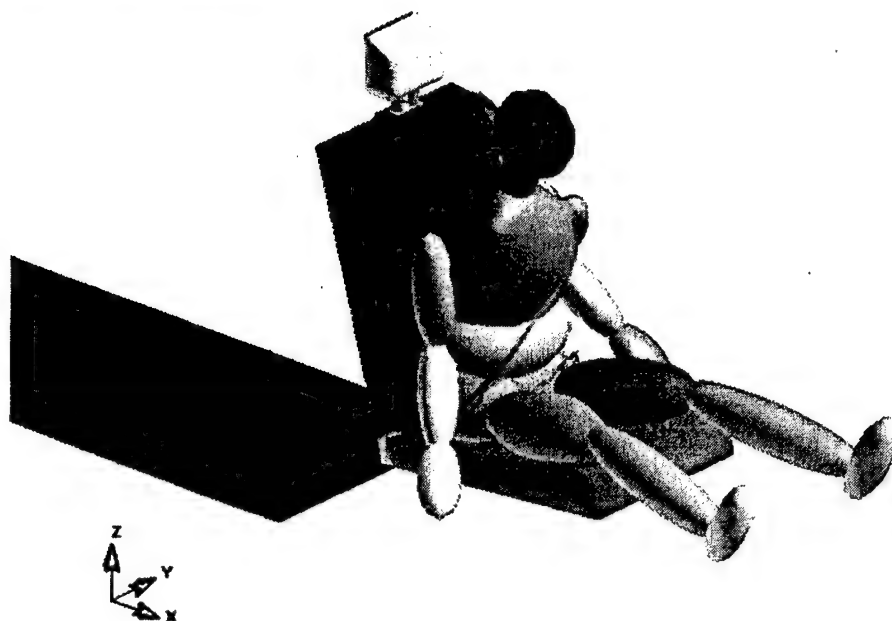
Figure A. 20 Effectiveness of the seat belt during rear-end impacts

Figure A.21 shows the displacement of dummy upper torso segment with and without seat belt. The upper torso displacement is more without seat belt.
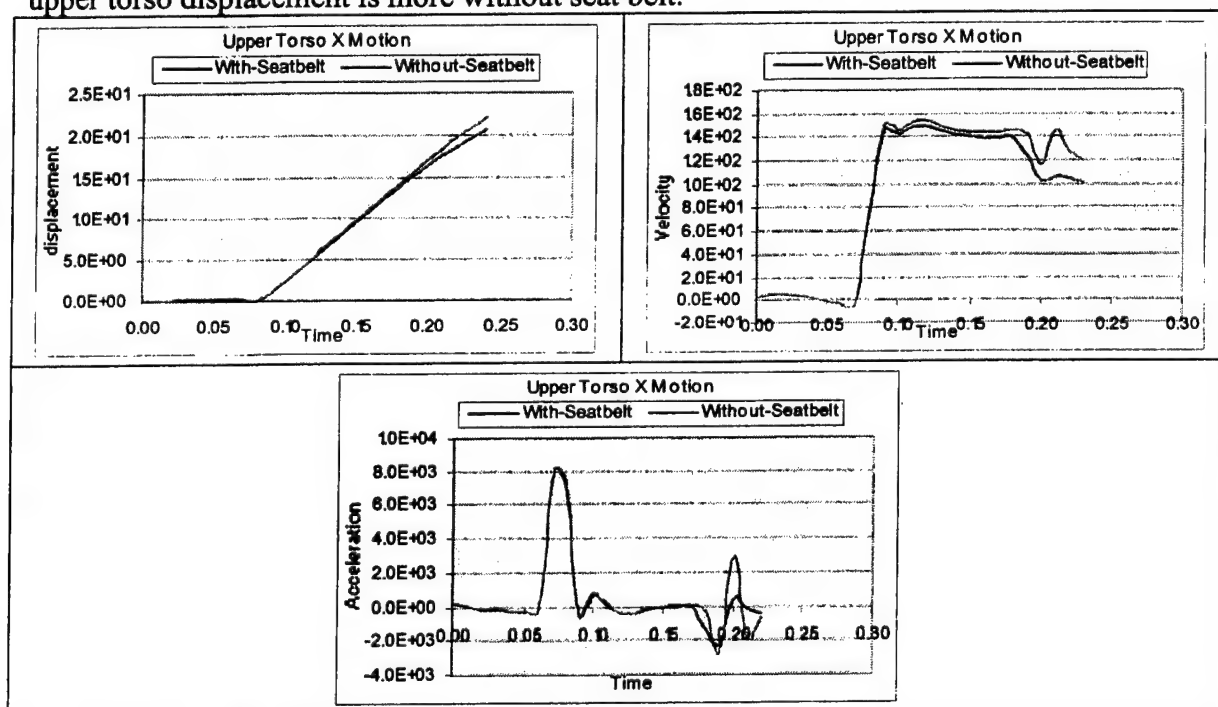
Figure A. 21 Plot of X Motion of Upper Torso with and without Seat belt

Simulation Runs and Analysis

The simulations were performed on a Windows 2000, Pentium III, 800Mhz machines. The cases involving the dummy models were run for 250 milliseconds of simulation time. The time step was set at 0.13 secs. Average CPU times for the simulations were around 4 to 5 hours.

In order to analyze the effect of various seat design factors on whiplash and head injury, rearward horizontal translation and angular displacements between head and upper torso were plotted in each case. This relative angular displacement is a measure of the neck extension, which is closely related to whiplash injury mechanism. From the plots, the significant factors in the seat design were discussed.

Effectiveness of head restraint

Figure A.22 shows the dummy behavior without a head restraint. It can be seen that the head goes under excessive rearward angular displacement in this case. This may lead to neck injury due to neck extension. Figures A.23 and A.24 show comparative plots of rearward head displacement and relative angular displacement of the head with respect to upper torso, both with and without a head restraint. It can be seen that there is considerably more rearward head displacement and relative angular displacement if the head restraint is not provided to resist this motion.
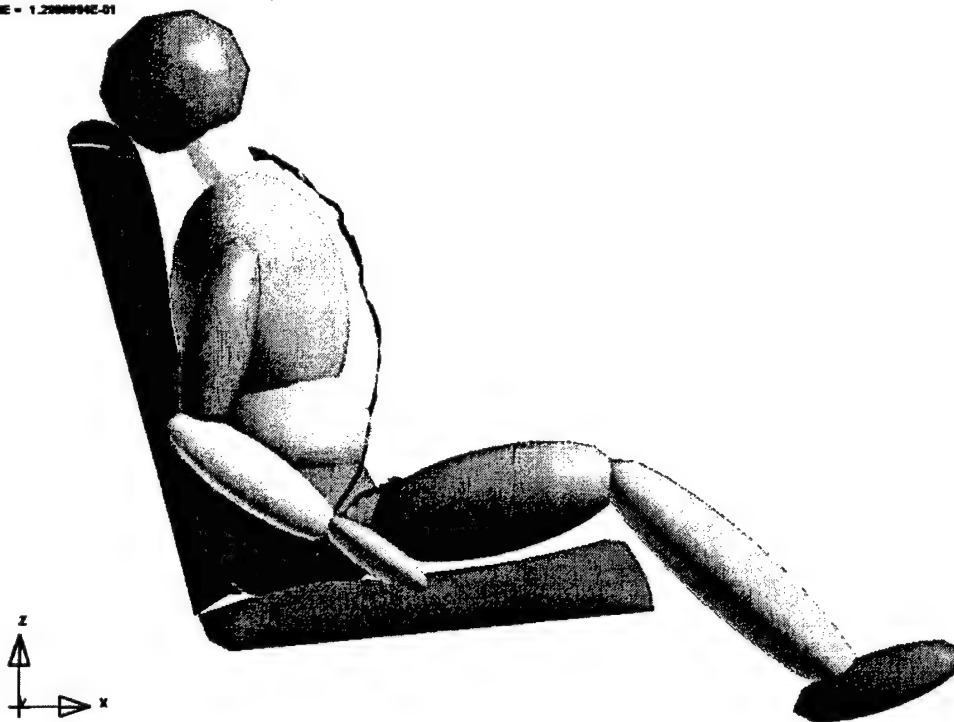
Figure A. 22 Head rotations in seat without head restraint
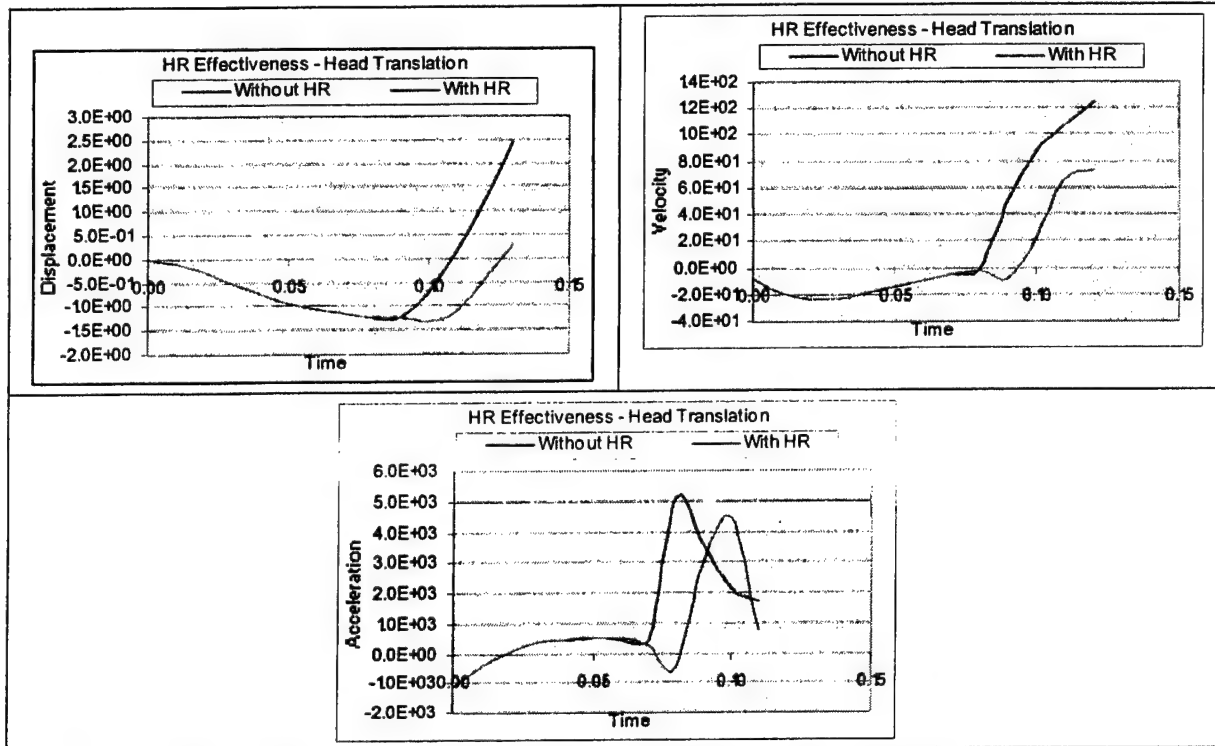
Figure A. 23 Plot of Head translation with and without Head Restraint
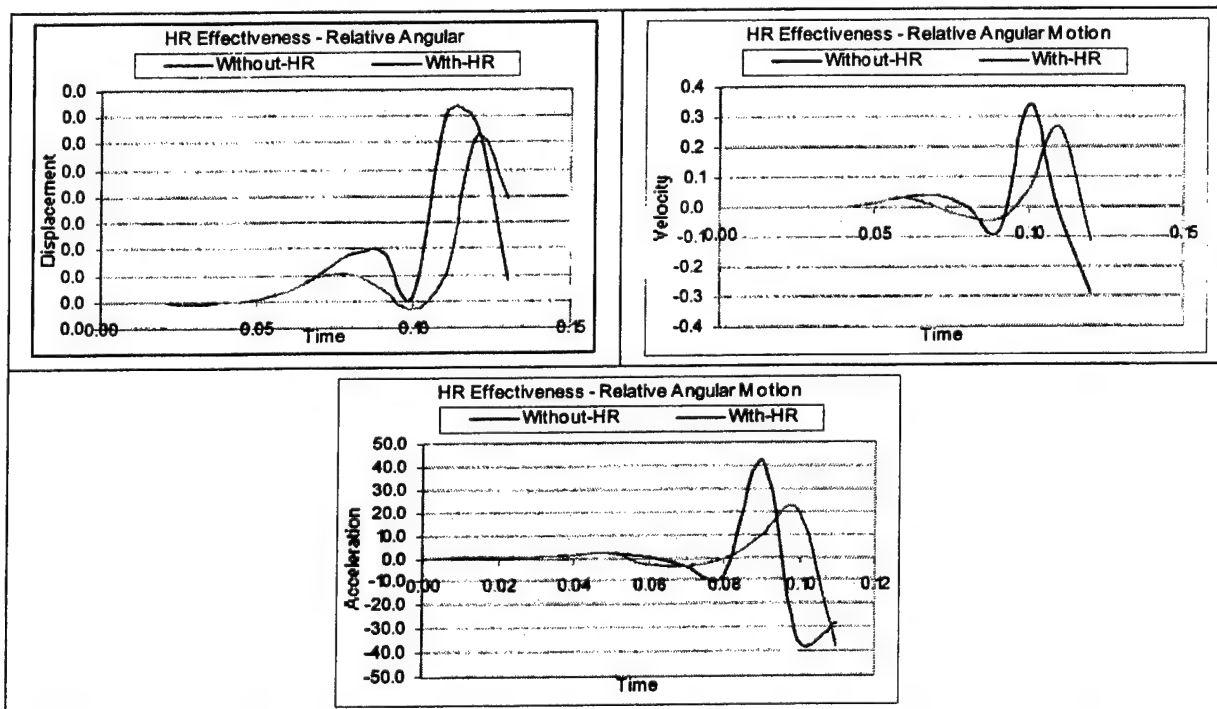
Figure A. 24 Plot of Head Relative angular Motion with and without Head Restraint

Head and head restraint gap

Two seat models were developed with the gap between head and head restraint maintained at 0.0, 1.6 and 2.9 inches. The simulation is carried out keeping all other factors held constant. Figure A.25 shows the dummy position with large gap (2.9 in.) between dummy head and head restraint. Figure A.26 shows the dummy position with no gap between dummy head and head restraint. This was achieved by changing the dummy position by rotating the lower torso thus bringing the head closer to the head restraint. Figures A.27 and A.28 show comparative plots of rearward head displacement and relative angular displacement of the head with respect to upper torso in three gap positions. It can be seen that rearward displacement is least for the no gap position whereas the relative angular displacement is midway between the large and small gap positions.
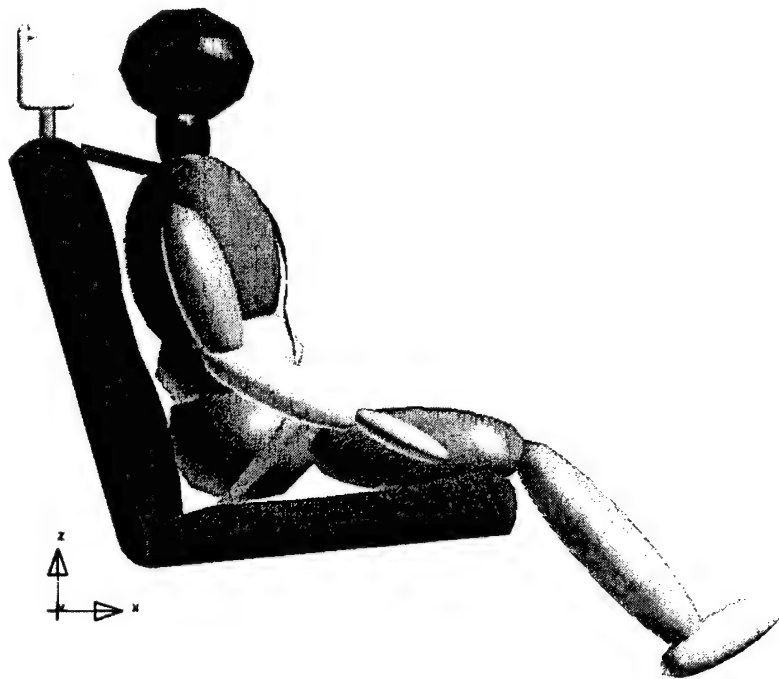
Figure A. 25 Dummy with large Head/ head restraint gap
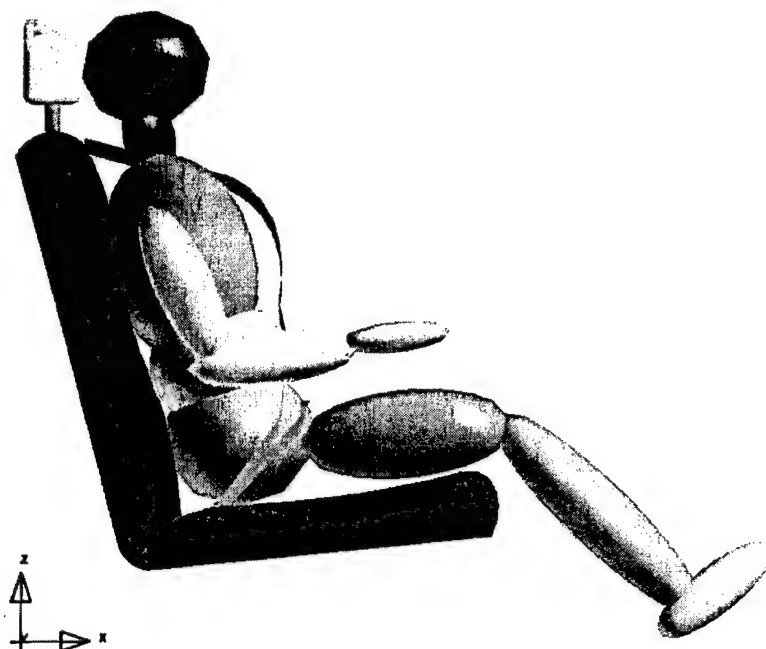
Figure A. 26 Dummy without Head/Head Restraint Gap
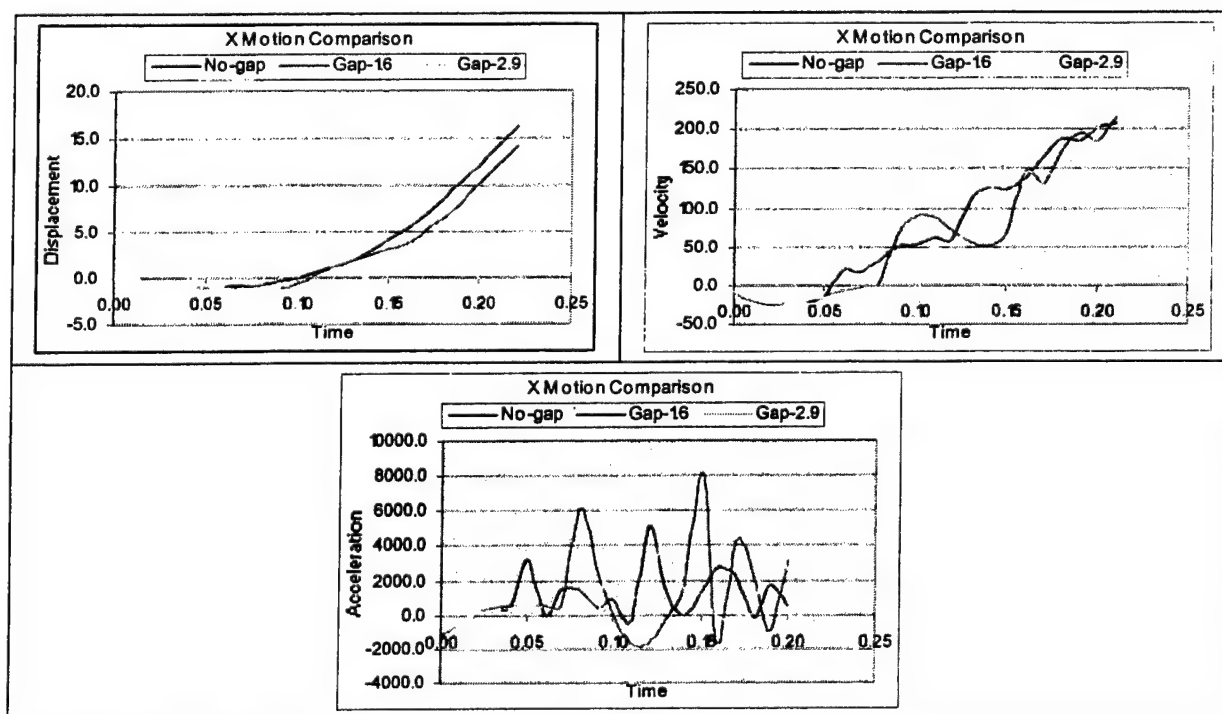
Figure A. 27 Plot of Head X displacement for three gap conditions
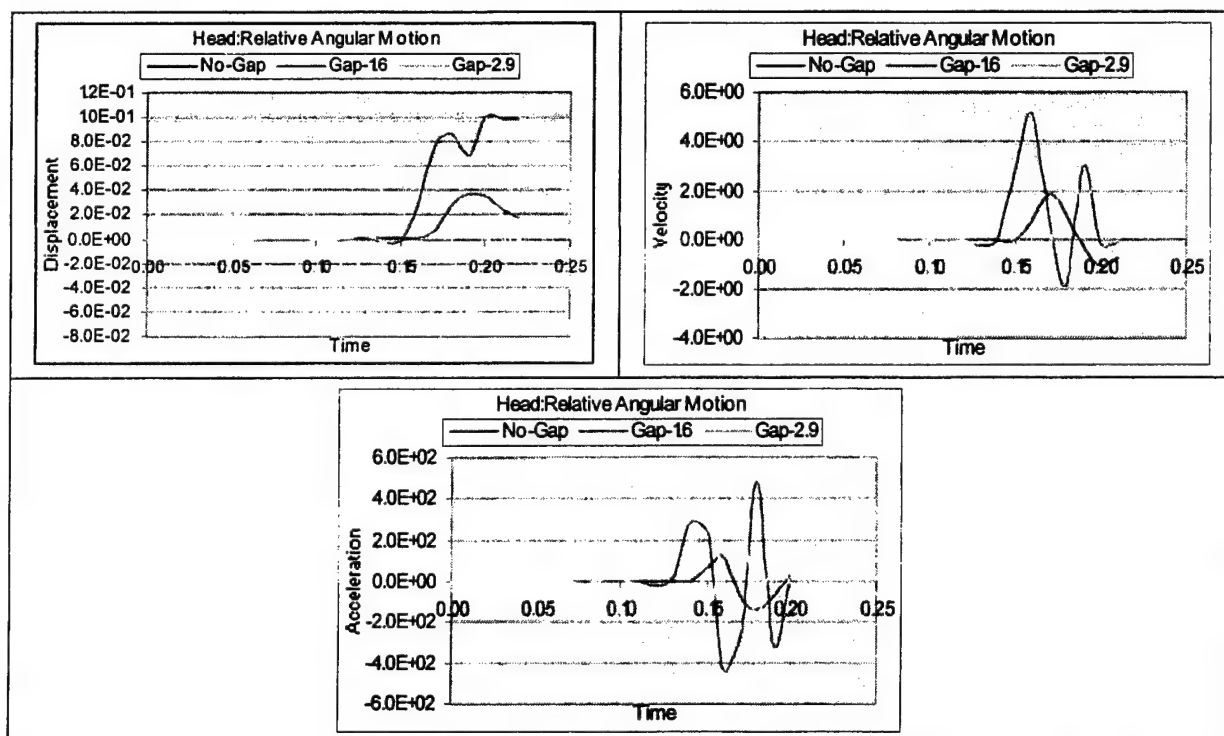
Figure A. 28 Plot of Head Angular displacement for three gap conditions

Vertical positioning of the head restraint

Figure A.29 shows the lower position of the head restraint. The head restraint is lowered by reducing the height of the support pins as shown. In the case studied, the height of support pins was lowered from 2 inches to 1 inch. Figures A.30 and A.31 show comparative plots of rearward head displacement and relative angular displacement of the head with respect to upper torso in low and high head restraint offset positions. The displacement plot shows less rearward displacement for low offset position as well as less angular displacement for the same position.
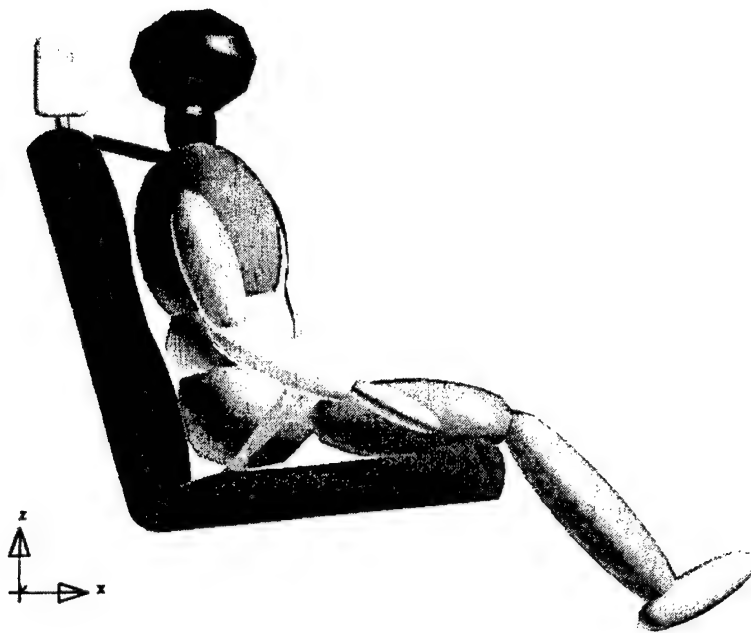
Figure A. 29 Seat model with lower height Head Restraint
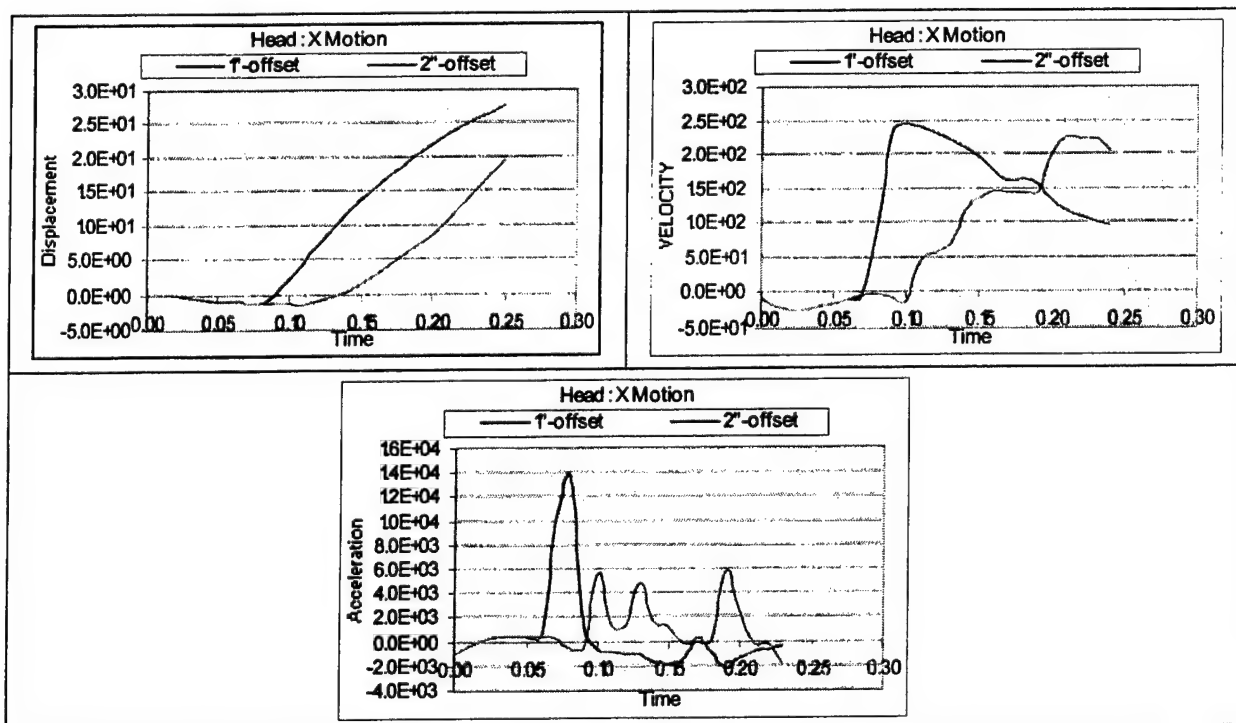
Figure A. 30 Plot of Head X Motion for two offset conditions
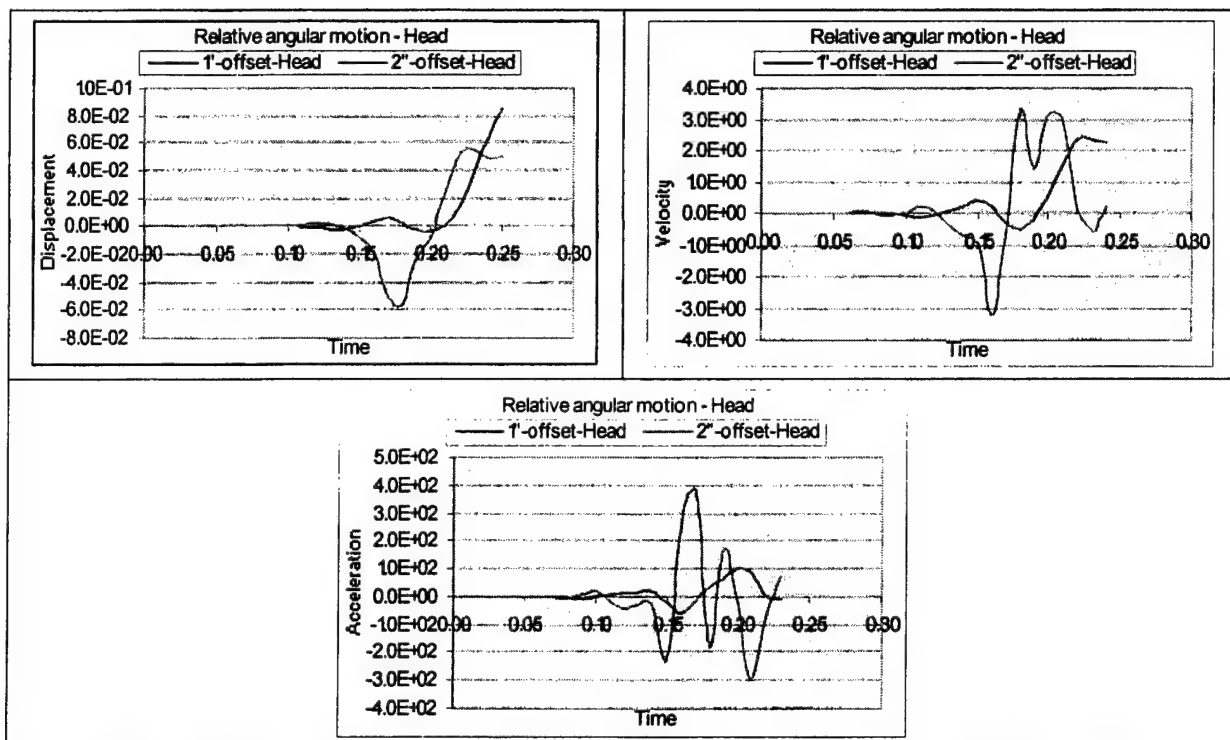
Figure A. 31 Plot of Head X relative angular Motion for two offset conditions

Effect of Seat back angle

In order to study the effect of the increased initial seat back angle, the seat back and head restraint assembly attached to it was tilted backward by 5 degrees. Figure A.32 shows the seat geometry with the increased seat back angle. It can be seen that the gap between head and head restraint as well as that between dummy upper and middle torso and seat back also increases. Figures A.33 and A.34 show comparative plots of rearward head displacement and relative angular displacement of the head with respect to upper torso in small and large seat back angles. The displacement plot shows less rearward displacement for small seatback angle as well as less angular displacement for the same angular position.
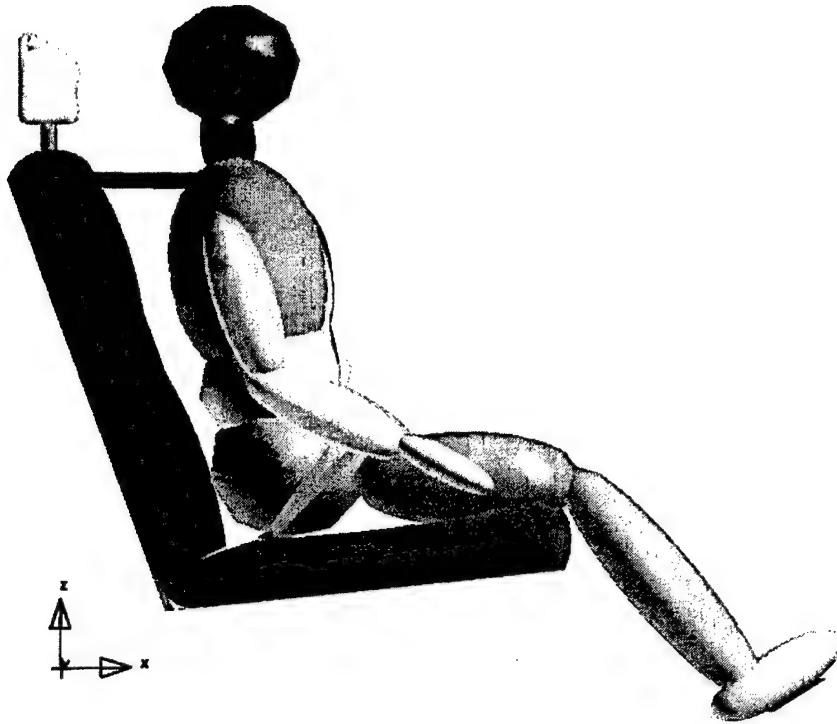
Figure A. 32 Seat Model with Large Seat Back Angle
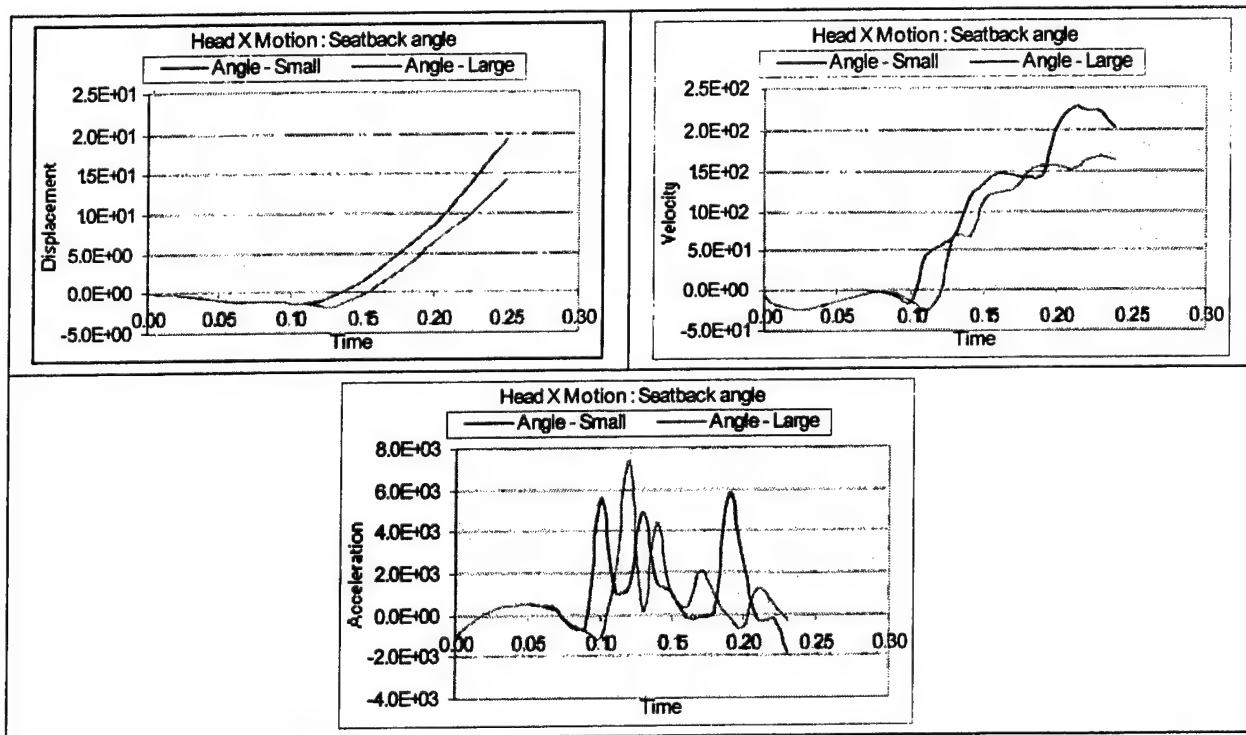
Figure A. 33 Plot of Head X Motion for two seatback angles
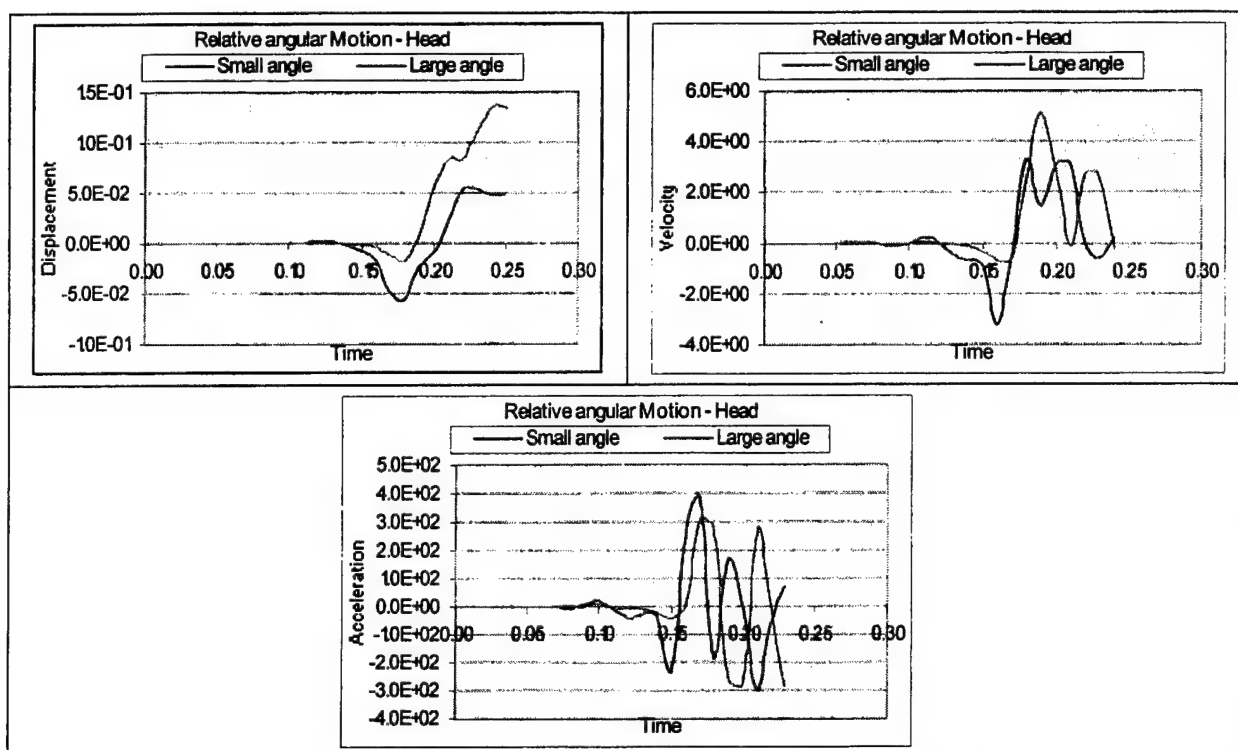
Figure A. 34 Plot of Head X relative angular Motion for two seatback angles

Effectiveness of joint stiffness

Joint stiffness between the seat cushion plane and the seat back plays an important part in rear-end impacts as it partially absorbs the shock of the impact and avoids the damage to body segments by excessive acceleration. Figures A.35 and A.36 show comparative plots of rearward head displacement and relative angular displacement of the head with respect to upper torso in three joint stiffness specifications. It can be seen that the rearward head displacement is slightly less for a stiffer joint, but the relative angular displacement is very high. For middle value of joint stiffness, both rearward head displacement as well as relative angular displacement is decreased.
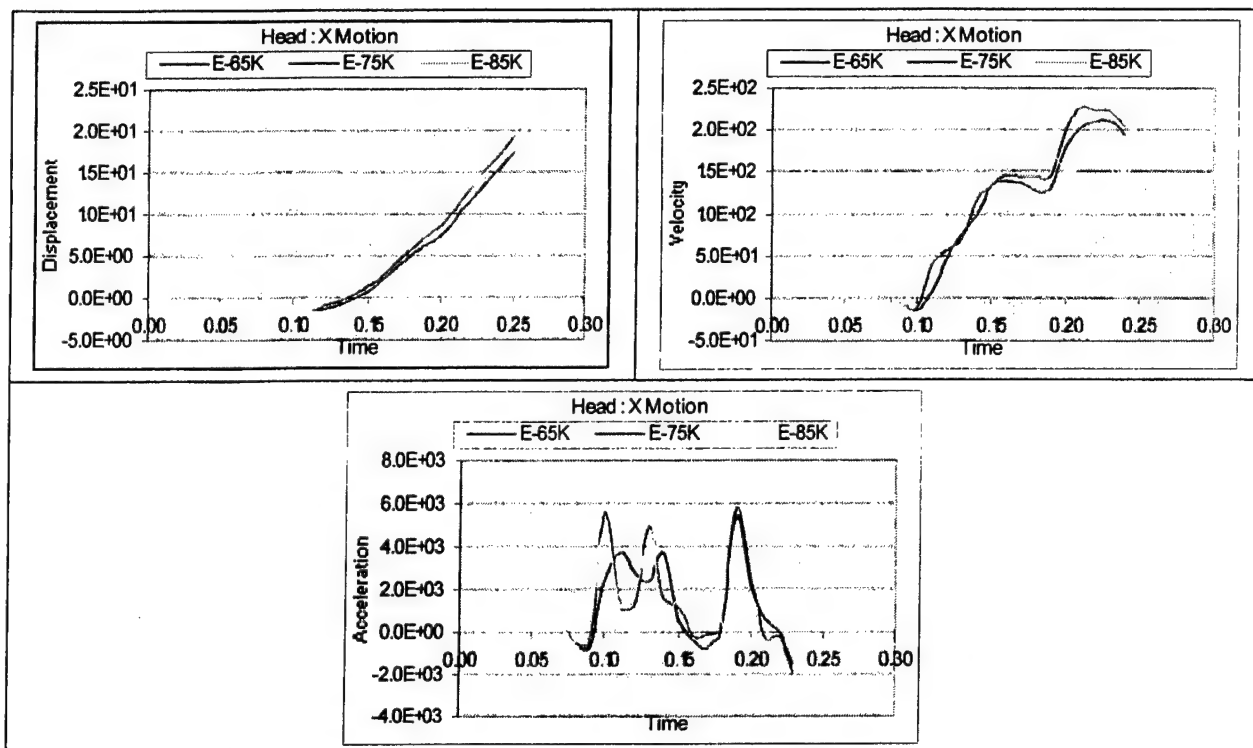
Figure A. 35 Plot of X Motion of Head for 3 seatback stiffness conditions
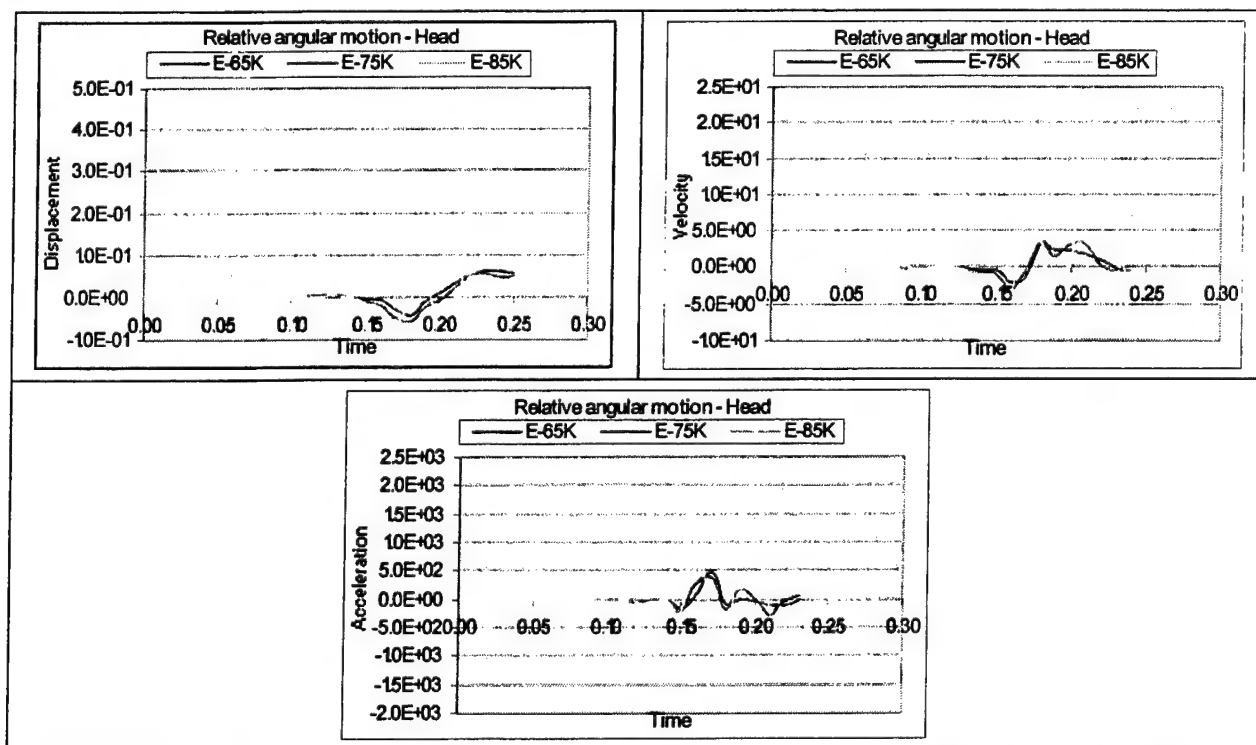
Figure A. 36 Plot of Relative Head angular Motion for 3 seatback stiffness values Software

40

This research has been successful in creating a complete crash environment for crash simulation and occupant protection. The software packages ATB (Articulated Total Body) and LS-DYNA were coupled and integrated to provide researchers the capabilities of performing advance crash simulations in which one can include the dummy model from ATB and the seat belt, airbag, seat and other restraint system models from LS-DYNA. Five test cases were developed during the research to verify the coupled code. The test cases consisted of various combinations of dummy and restraint systems. The output in terms of displacement, velocity and acceleration of the critical dummy segments was compared with the already verified ATB program results. The results compared within acceptable limits. Thus the coupled code was verified.

The objective of the research was to analyze the effect of these parameters on linear and angular rearward motion of the head relative to the torso. This motion is responsible for the risk of the neck injury during a rear-end impact situation. Various seat models were developed in the LS-DYNA with the help of Solid Modeler "SolidEdge" and high performance finite element pre-processor, "HyperMesh". Various parameters considered during the modeling were

1. Seat back angle
2. Vertical position of head restraint with respect to the occupant's head
3. Horizontal gap between back of occupant's head and head restraint
4. Seat back joint stiffness
5. Presence and absence of head restraint
6. Presence and absence of seat belt

By varying the above factors, the seat models were developed. Numerous rear-end impact simulations were carried out with the seat models to analyze the effect on the dummy models. Table A.5 shows the maximum rearward displacement values for all seat models. The result of the simulations is summarized below.

Table A. 5 Maximum rearward displacement results for seat models

Sr. No.	Factors	Levels	Maximum Rearward Displacement
1	Seat Back Angle (° from vertical)	10	-1.46
		15	-1.76
2	HR- Horizontal Distance (in.)	0	-1.09
		1.65	-1.22
		2.9	-1.46
3	HR- vertical Distance (in.)	1	-1.23
		2	-1.46
4	Joint Stiffness	Low	-1.47
		Medium	-1.46
		High	-1.33

Table A.6 shows the rearward angular displacement of head segment with respect to upper torso for different seat configurations.

Table A. 6 Maximum relative rearward angular displacement of head for seat models

Sr. No.	Factors	Levels	Maximum Rearward Angular Displacement (Rad.)
1	Seat Back Angle (° from vertical)	10	-0.061118
		15	-0.02911
2	HR- Horizontal Distance (in.)	0	-0.00036498
		1.65	-0.0025598
		2.9	-0.061118
3	HR- vertical Distance (in.)	1	-0.0133384
		2	-0.061118
4	Joint Stiffness	Low	-0.056958
		Medium	-0.061118
		High	-0.052313

The results from the plots as well as the two tables above can be summarized as follows.

1. The research shows that there is considerable rearward translation and rotation of the head segment of the dummy without seat belt. Hence it can be concluded that the head restraint is a very critical occupant protection device. Absence of head restraint will lead to severe neck injury due to neck extension.
2. It was found that the gap between the occupant head and head restraint is also a significant factor during the research. Least head rotation and translation was found for the dummy position where there is almost no gap between the head and head restraint. Thus it can be concluded that lesser the gap, more effective is the head restraint. So it is advisable to adjust the head restraint to the position as close to the head as possible.
3. In the research, two vertical offset positions of the head restraints were modeled. This was studied to analyze the effect of vertical adjustment of the head restraint in the automobile. It was found that the lower position of the two was more effective in avoiding excessive rearward displacement of the dummy head.
4. In order to study the effect of seat back angle on the dummy, two seat models with large and small seat back angle were developed. Results showed that the rearward displacement of the head is less for small seatback angle. It is consistent with the previous result of the gap factor, as higher seat back angle increases the gap thus leading to larger head angular and horizontal displacement.

5. Effect of the stiffness of the joint between seat cushion and seat back was also studied during the research. The analysis showed that though rearward displacement is less for the stiffer joint, but it can be attributed to the fact that rearward movement of the seatback itself is less for the stiffer joint. Large forward angular movement was found for the stiffer joint as less energy is absorbed during the impact in the seatback, which results in forward bouncing of the dummy.

Thus the research proved successful in identifying the significant factors in seat design for occupant protection during the rear-end impact. The results were consistent with the studies done so far with physical dummy model. The coupled code provided a very powerful simulation tool for crash and safety analysis leading to reduced test costs and time delays due to physical testing by fast and accurate analysis.

APPENDIX B. SEAT BELT MODELING, ANALYSIS, AND RESULTS

Need for seat belt modeling

The most widely used seat belt type is the three-point seat belt or more commonly known as the lap/shoulder belts. In this research work, the database of seat belts was developed in order to determine the most effective belt model for frontal crashes. The parameters that were considered for modeling the belts were, shape of the seat belt and the width of the belt strap. In all, four different shapes of seat belts were developed. Also, various versions of each of the same belt were developed by varying the width of the seat belt strap.

Different models of seat belts and modeling approach

The different seat belts models are three-point belt, lap/shoulder belt, H belt, V belt and X belt. The lap/shoulder belt is similar to the three-point belt except for the fact that in the case of three-point belt, the lap and shoulder portion share a common point. As shown in Table B.1, the lap/shoulder belt, H belt and X belt were modeled with width of 0.8in, 1in and 1.5in. The V belt was modeled for width of 0.2in and 0.4in and the three-point belt was modeled for width of 1in.

Table B. 1: Seat belts used for simulation

	Lap/Shoulder belt	Three-Point belt	H belt	X belt	V belt
Thickness	0.8	-	0.8	0.8	0.2
	1	1	1	1	0.4
	1.5	-	1.5	1.5	-

- **Lap/shoulder belt**
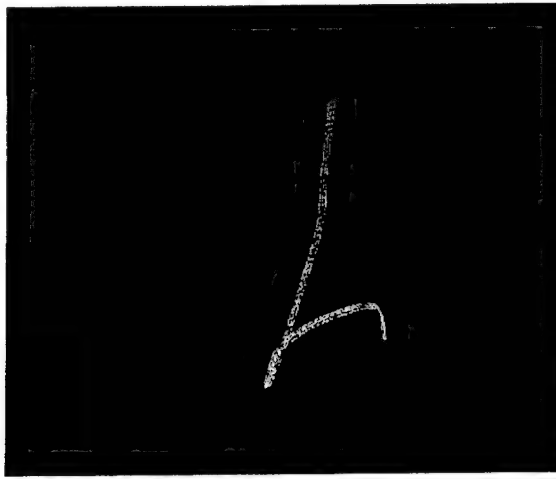
Figure B. 1 LAP/Shoulder Belt
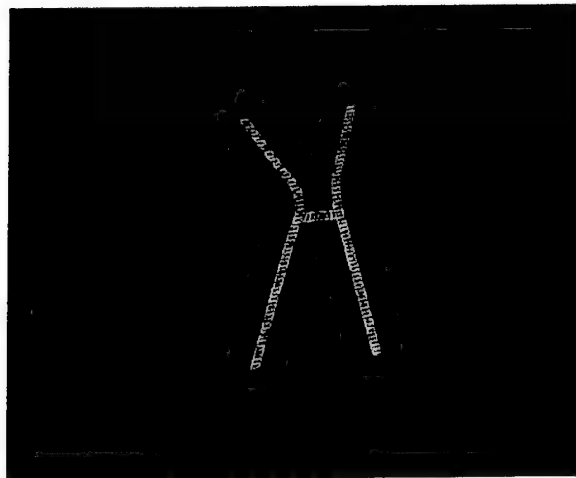
- **H belt**

Figure B. 2 H belt

- **V belt**

Figure B. 3 V belt

- **X belt**
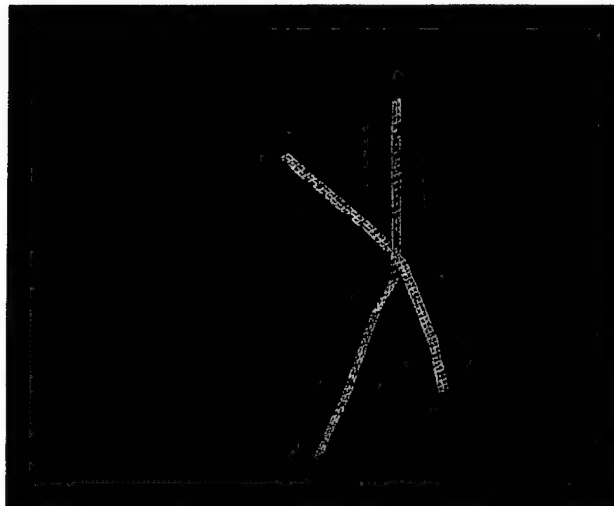
Figure B. 4 X belt

Modeling technique

The factors that determined the choice of the shape of the seat belt include, effectiveness in reducing the excursion of head, upper torso and lower torso towards the steering wheel and dashboard, effectiveness in minimizing the acceleration of these body segments, comfort in wearing the seat belt, ease in wearing the seat belt and manufacturing related issues.

The seat belts were modeled using the LS-DYNA pre-processor, FEMB. The approximate shape of the seat belt was first drawn using the line/arc drawing features of FEMB, with the dummy segment nodes as the reference points. The COPY/MOVE features of the FEMB were used to develop a 2D model of the belts.

The belts were meshed using the quadrilateral shell elements of thickness 0.08in. The *CONSTRAINED_EXTRA_NODES_SET cards were used to attach the belts to the seat. The material of the seat belt was defined using the *MATERIAL_FABRIC (The LS-DYNA Example: airbag_deploy.k) cards. The contact between the dummy segments and the seat belts was defined using the *CONTACT_SINGLE_SURFACE_TITLE cards.

```
*MAT_FABRIC
$    mid       ro      ea      eb      ec     prba    prca    prcb
      3 1.00e-4 2.00e+6 2.00e+6 2.00e+6   0.35    0.35    0.35
$    gab      gbc     gca     gse     el     prl   lratio    damp
 1.53e+6  1.53e+6  1.53e+6
$
```

Also, in this research work, seat belt systems were developed with retractor and pretensioner elements. But, in this case the seat belt was modeled as 1D belt using the *ELEMENT_SEATBELT option of LS-DYNA. This is due to the limitation posed by LS-DYNA in modeling seat belts in 2D, with retractor and pretensioner elements. The effectiveness of the 1D lap/shoulder belt with retractors and pretensioners and, 2D lap/shoulder belt has been shown in Figures B.1.

Simulations employed

In order to evaluate the effectiveness of the seat belts, two types of simulations were employed, namely sled deceleration simulation and 30 mph frontal crash simulation. For all the simulations, the simulation time was set to 0.2 sec. The acceleration pulse curve used for the above two simulations are shown in Figure B.2a. A comparison of the motion of the vehicle for these two simulations is shown in Figure B.2b.

Figure B. 5 Sled and Frontal simulation pulse curves
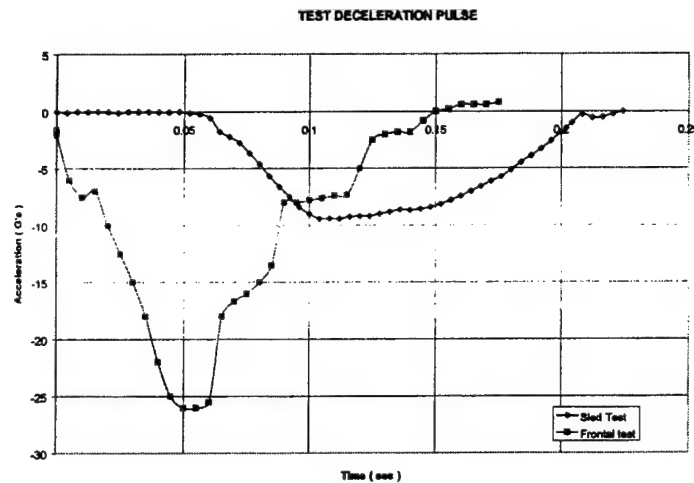

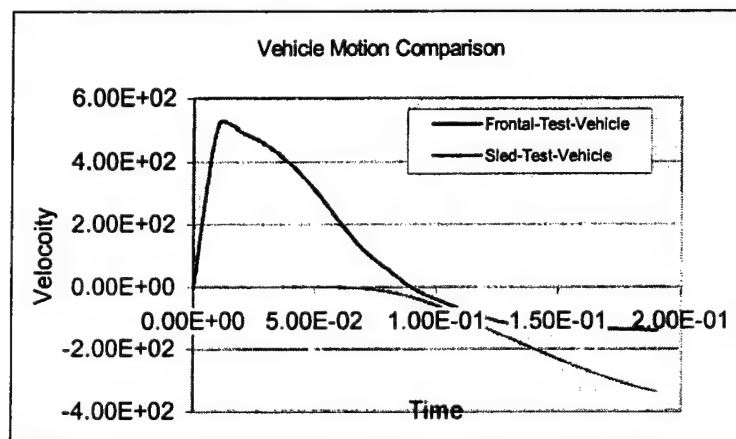**Figure B. 6 Sled and Frontal simulation motion comparison plot**

49

Effectiveness of belt use

- ### Sled Simulation
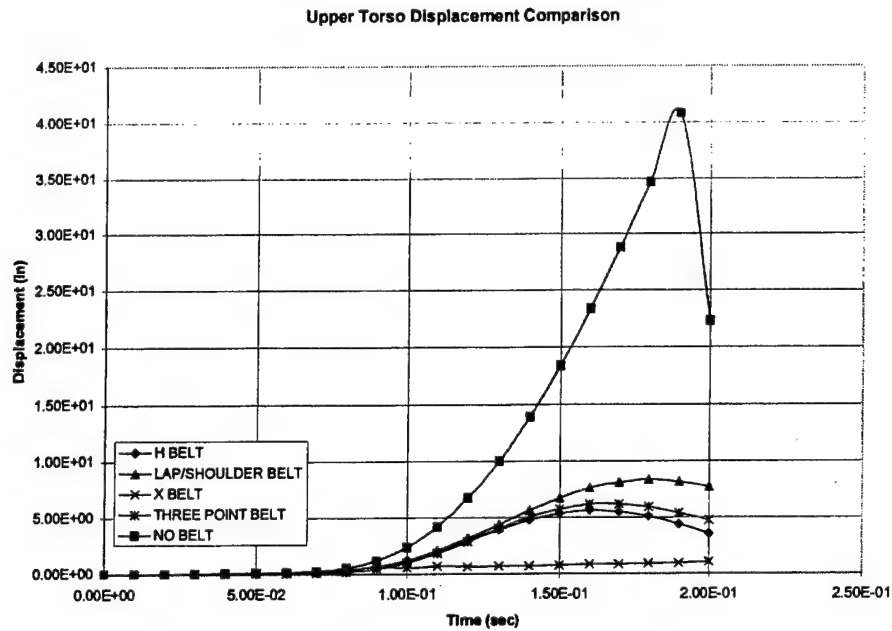
Upper Torso Displacement Comparison

Figure B. 7 Sled simulation displacement comparison plots

- ### Frontal simulation

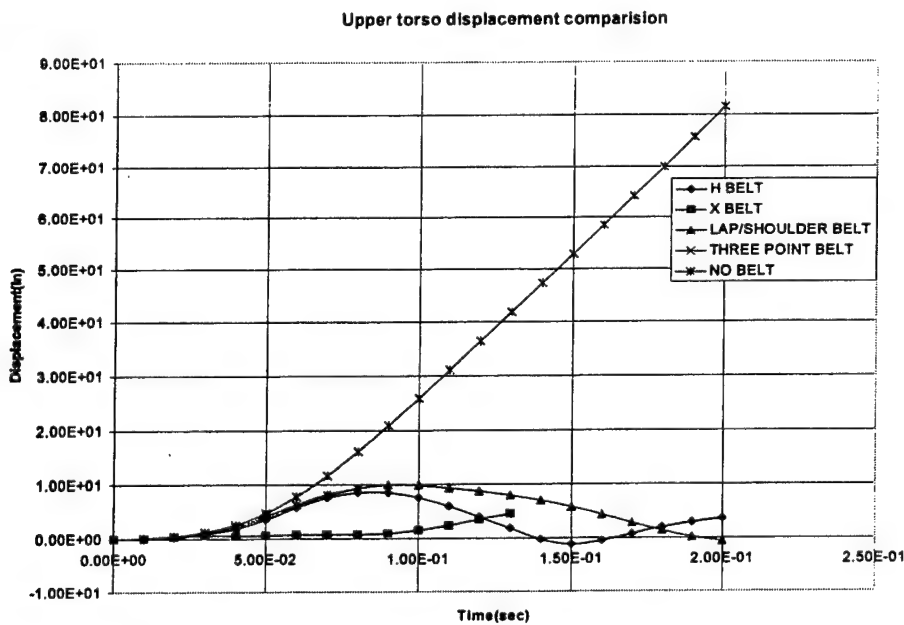**Upper torso displacement comparision**

Figure B. 8 Frontal simulation displacement comparison plots

From the sled simulation displacement plots (Figure B.3a) for upper torso, we see that the maximum displacement of the upper torso is 40.84 in when no belt is used and is 6.2 in when three-point belt is used. The values for lap/shoulder belt, h belt, v belt and x belt are 6.02, 5.6 4in, 2.90 in and 1.0 6in respectively.

Similarly, from the frontal simulation displacement plots (Figure B.3b) for upper torso, we see that the maximum displacement of the upper torso is 81.5 in when no belt is used and is 10 in when lap/shoulder belt is used. The value for h belt is 8.65 in. In this case, the simulation fails with the use of the three-point belt, V belt and X belt.

The above numbers reiterate the fact that seat belts are highly effective in preventing the contact of critical body parts with the vehicle interiors, thus minimizing the risk of fatality or injury. Table B.2 lists the maximum displacement of the upper torso for the sled and frontal simulations, for 1in lap/shoulder belt, three point belt, H belt, X Belt and 0.2 in V belt.

Table B. 2 Upper Torso maximum displacement

Belt	Sled Simulation Max Displacement (in)	Frontal simulation Max Dislacement (in)
No belt	40.84	81.5
H belt	5.64	8.65
X belt	1.06*	4.63*
V belt	2.9*	12.8*
Three Point belt	6.2	9.36*
Lap/Shoulder belt	6.02	10

Comparison of effectiveness based on shape of the belt

In order to determine the shape of the seat belt, that would be most effective for the majority of accident situations, sled and frontal simulations were performed using each of these belts. The dummy used was the 50th percentile male.

Figure B.4a to B.4m show the plots of the displacement and acceleration of the lower torso, upper torso and head, for the sled and frontal simulations using belts of various shapes. The size of the X, H, Lap/Shoulder and three-point belt were chosen to be 1 in and that of V belt to be 0.2 in. Since the dimension of the V belt does not match that of the other belts, the results of the analysis with the V belts has not been show as part of the comparison plots. In Figure B.4g to B.4h, there is a peak of X belt acceleration curve in sled and frontal simulation. The design of X belt holds the motion of mid torso. It cannot fix the lower torso and upper torso very well on the seat in the motion beginning.

Tables B.3, B.4 and B.5 give a comprehensive summary of the maximum displacement and maximum acceleration values of the lower torso, upper torso and head segment for the various test cases.

Note: The values of displacement and acceleration marked with * as superscript indicate the fact that the analysis terminated before completion due to the extremely high velocities of the nodes of the seat belt contacting the right and left upper legs of the dummy.
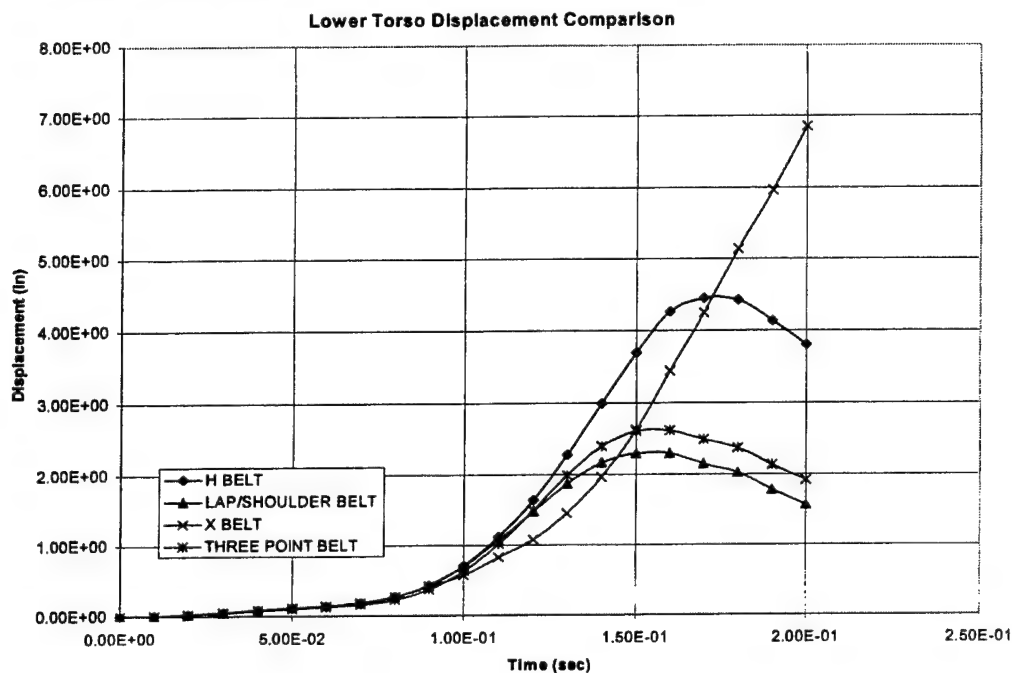
Figure B. 9 Sled simulation lower torso displacement comparison plots
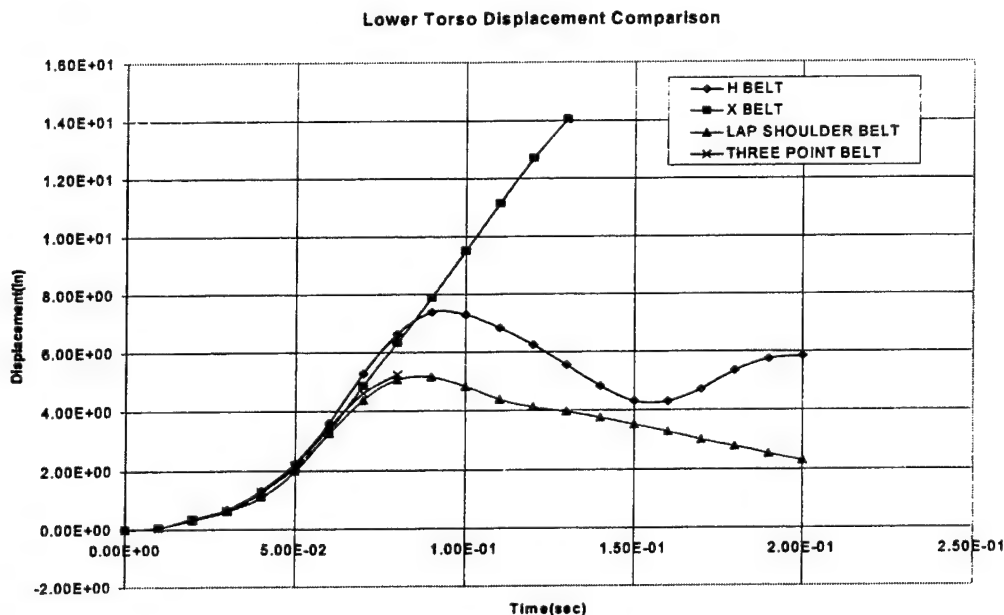
Figure B. 10 Frontal simulation lower torso displacement comparison plots

Lower Torso Acceleration Comparision
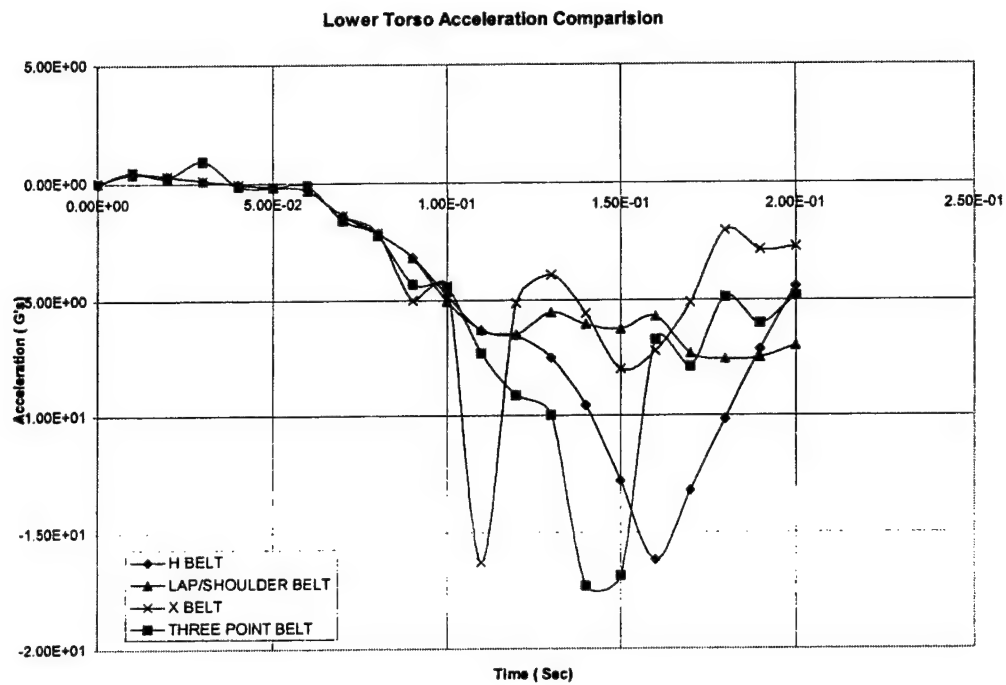
Figure B. 11 Sled simulation lower torso acceleration comparison plots

Lower Torso Acceleration comparison
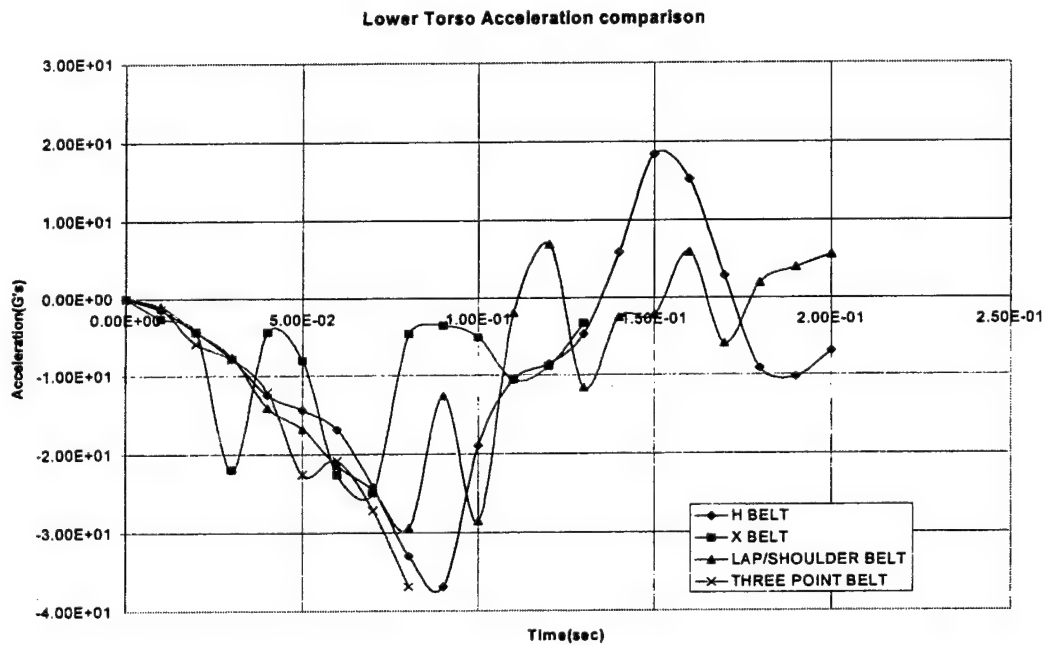
Figure B. 12 Frontal simulation lower torso acceleration comparison plots

53

Upper Torso Displacement Comparison
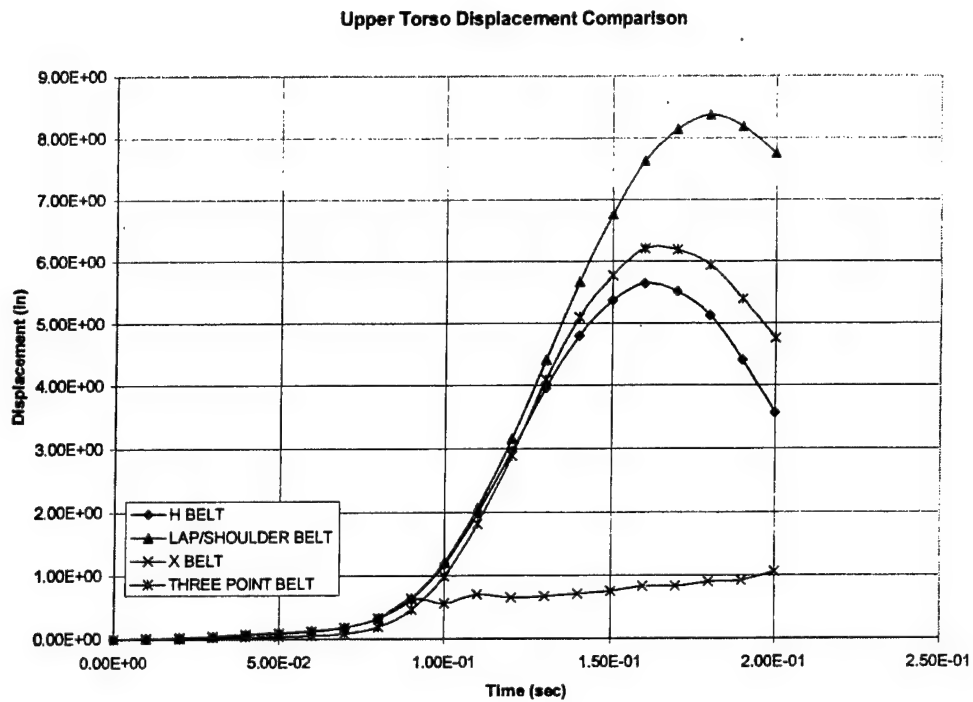
Figure B. 13 Sled simulation upper torso displacement comparison plots

Upper torso displacement comparision
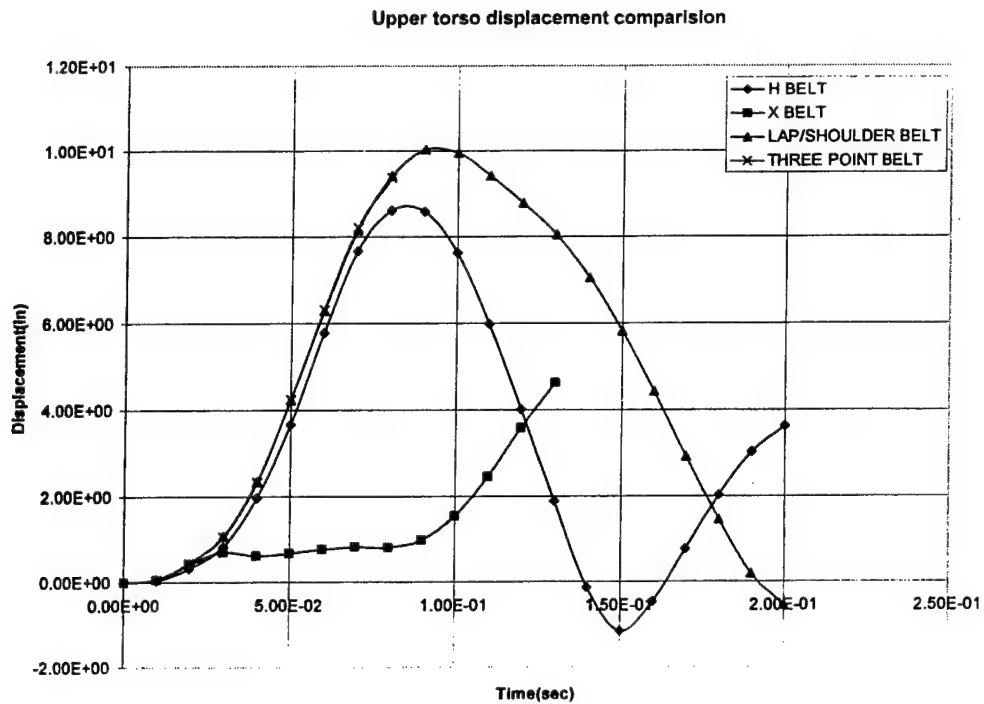
Figure B. 14 Frontal simulation upper torso displacement comparison plots

Upper Torso Acceleration Comparison
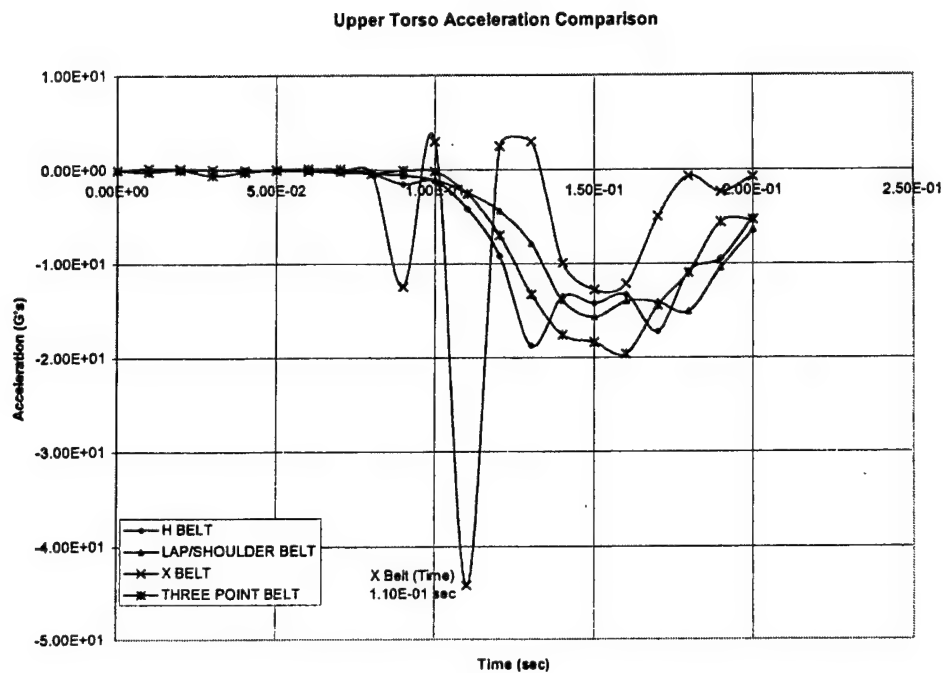
Figure B. 15 Sled simulation upper torso acceleration comparison plots

Upper Torso Accleration Comparison
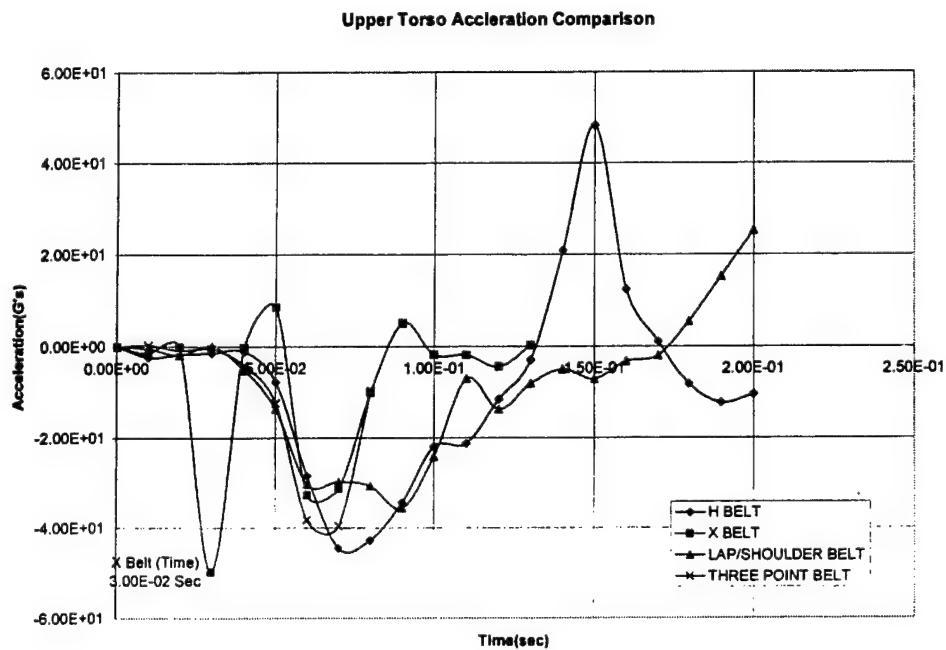
Figure B. 16 Frontal simulation upper torso acceleration comparison plots

55

Head Displacement Comparison
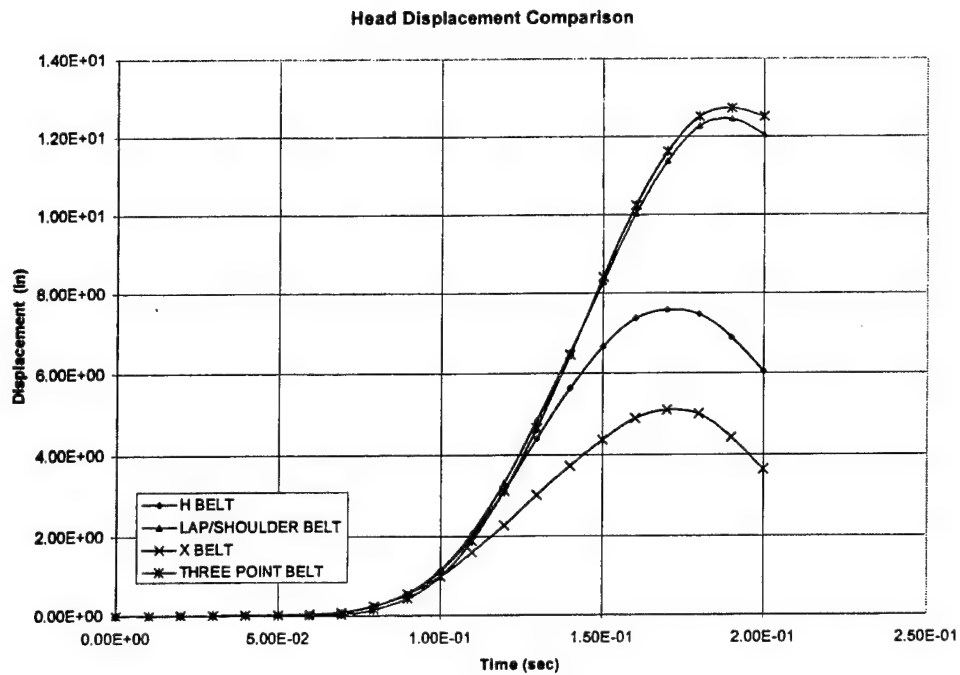
Figure B. 17 Sled simulation head displacement comparison plots

Head Displacement Comparison
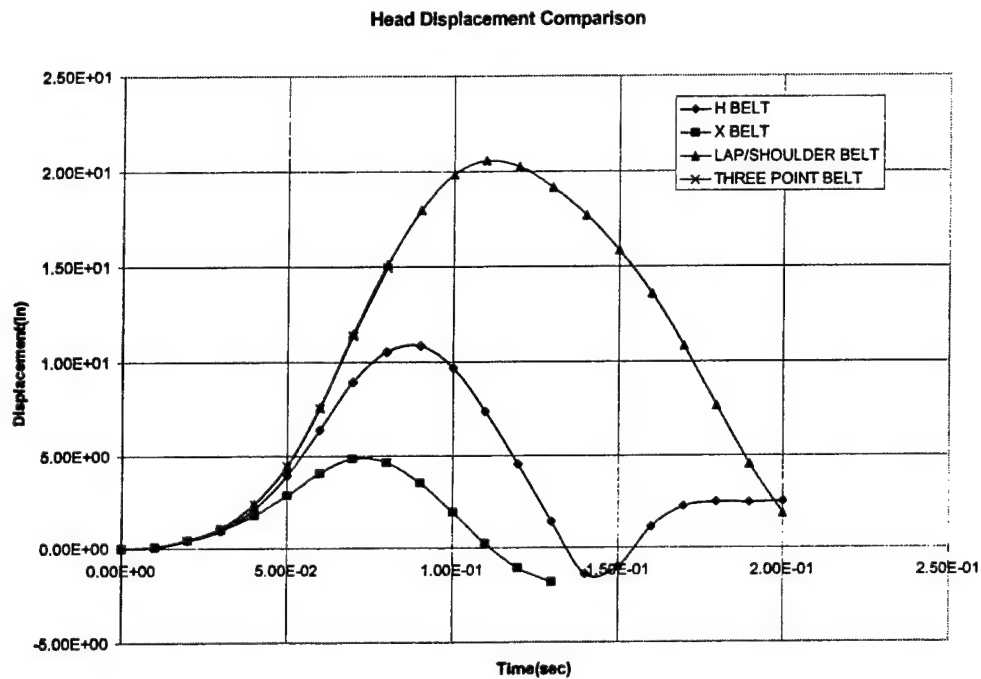
Figure B. 18 Frontal simulation head displacement comparison plots

56

Head Acceleration Comparison
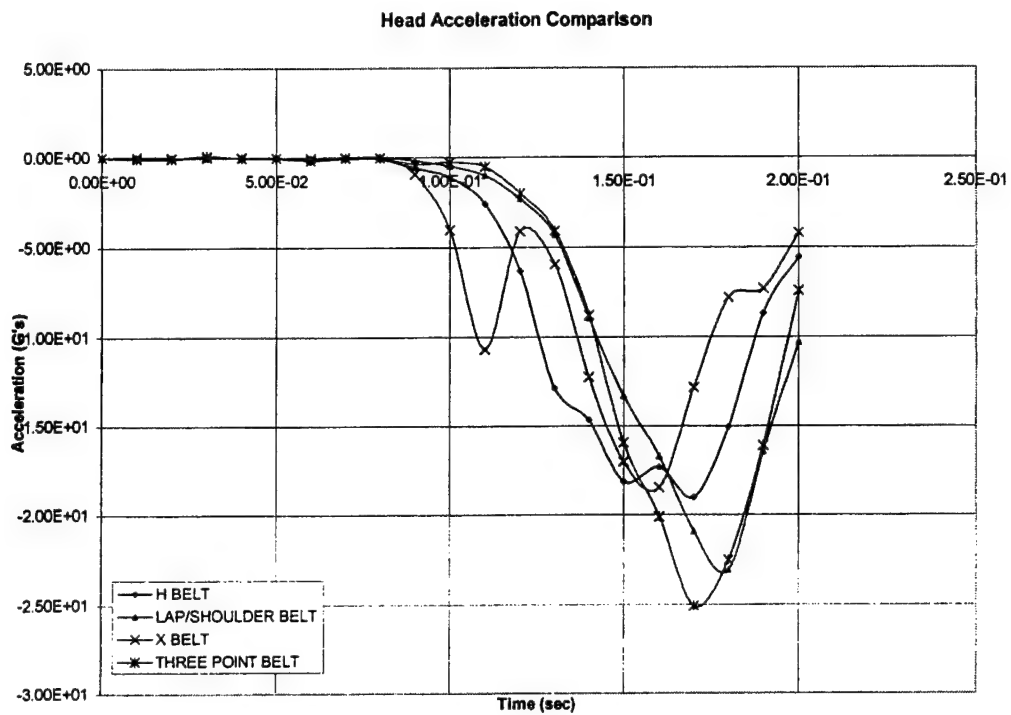
Figure B. 19 Sled simulation head acceleration comparison plots

Head Accleration Comparison
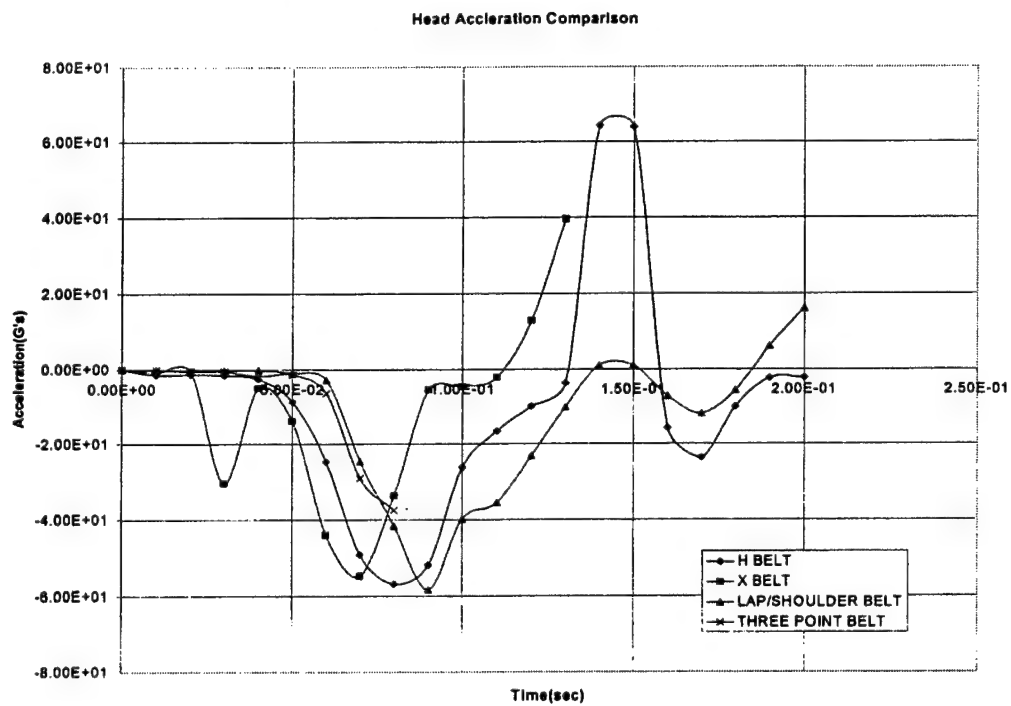
Figure B. 20 Frontal simulation head acceleration comparison plots

Tabular summary of maximum displacement and acceleration values

Table B. 3 Lower torso maximum displacement and maximum acceleration

Simulation	Belt	Dimension (In)	Max.Displacement (in)	Max.Acceleration (G's)
Frontal	X belt	1	14.1*	24.9*
Frontal	H belt	1	7.38	36.9
Frontal	Three Point belt	1	5.25*	36.9*
Frontal	Lap/Shoulder belt	1	5.16	29.4
Sled	X belt	1	6.85	16.3
Sled	H belt	1	4.45	16.2
Sled	Three Point belt	1	2.6	17.27
Sled	Lap/Shoulder belt	1	2.29	7.48

Table B. 4 Upper torso maximum displacement and maximum acceleration

Simulation	Belt	Dimension (In)	Max.Displacement (In)	Max.Acceleration (G's)
Frontal	X belt	1	4.62*	49.8*
Frontal	H belt	1	8.65	48.2
Frontal	Three Point belt	1	9.36*	39.7*
Frontal	Lap/Shoulder belt	1	10	35.7
Sled	X belt	1	1.06	44.1
Sled	H belt	1	5.64	18.8
Sled	Three Point belt	1	6.2	19.62
Sled	Lap/Shoulder belt	1	6.02	15.7

Table B. 5 Head maximum displacement and maximum acceleration

Simulation	Belt	Dimension (In)	Max.Displacement (In)	Max.Acceleration (G's)
Frontal	X belt	1	4.87*	54.8*
Frontal	H belt	1	10.8	64.3
Frontal	Three Point	1	1.49*	37.5*
Frontal	Lap/Shoulder belt	1	20.6	58.3
Sled	X belt	1	5.09	18.5
Sled	H belt	1	7.59	19
Sled	Three Point	1	12.7	25.06
Sled	Lap/Shoulder belt	1	12.5	23.1

58

Screen captures of simulation using the various belts

Figures B.5a, B,5b, B.5c and B.5d show the dummy configuration at time step 17, which corresponds to simulation time of 0.16 sec. The screen captures correspond to the sled simulation performed on the 50th percentile male. The displacement of the upper torso is 6.36 in, 5.64 in, 10.4 in and 11.2 in for H belt, three-point belt, V belt and X belt respectively.
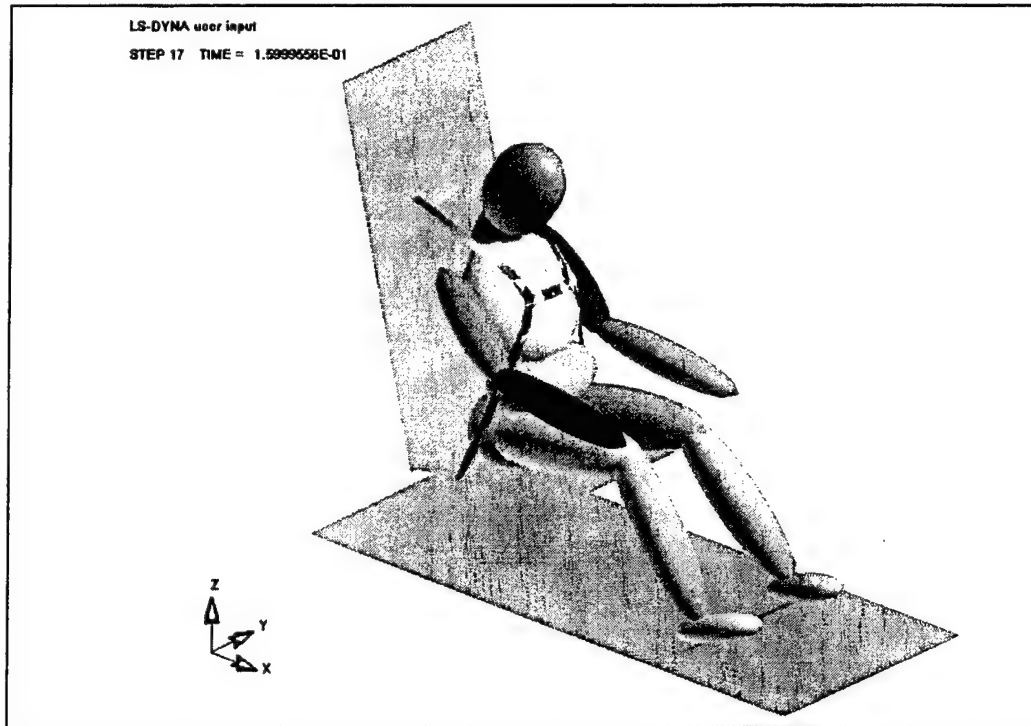
Figure B. 21 Dummy position at time 0.16 sec wearing H belt
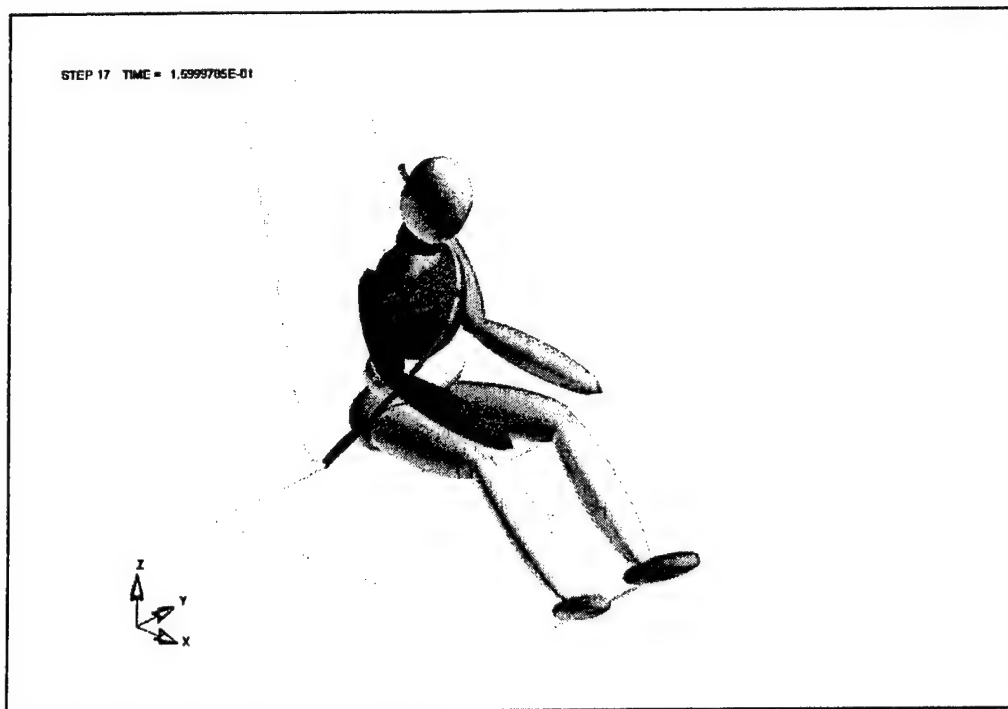
Figure B. 22 Dummy position at time 0.16 sec wearing three-point belt
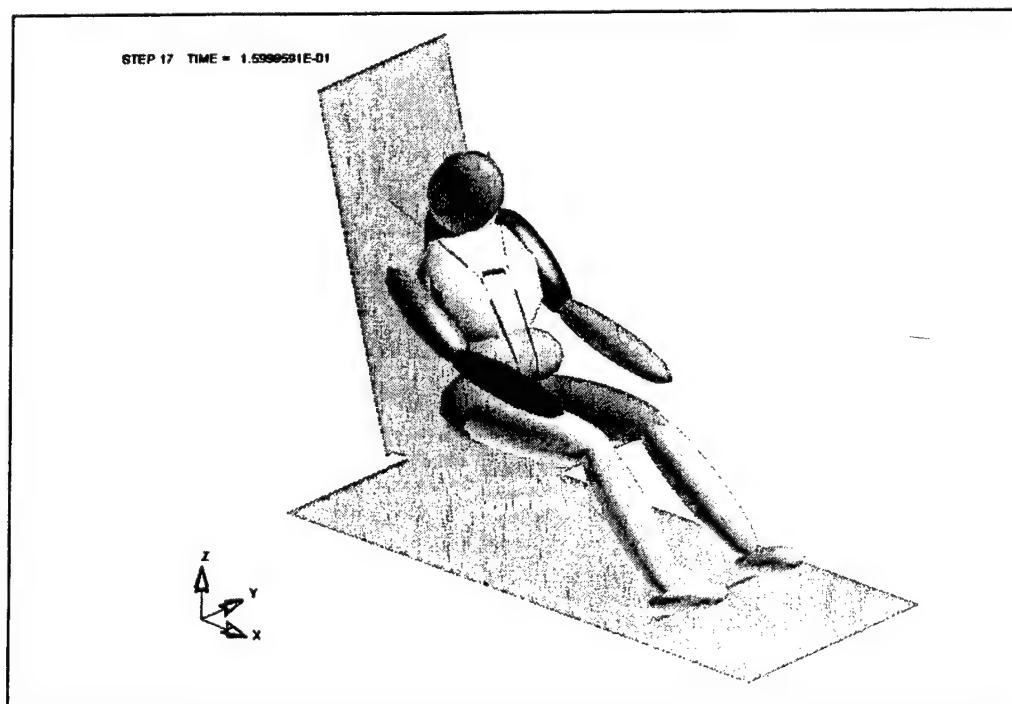
Figure B. 23 Dummy position at time 0.16 sec wearing V belt

STEP 17   TIME = 1.5999649E-01
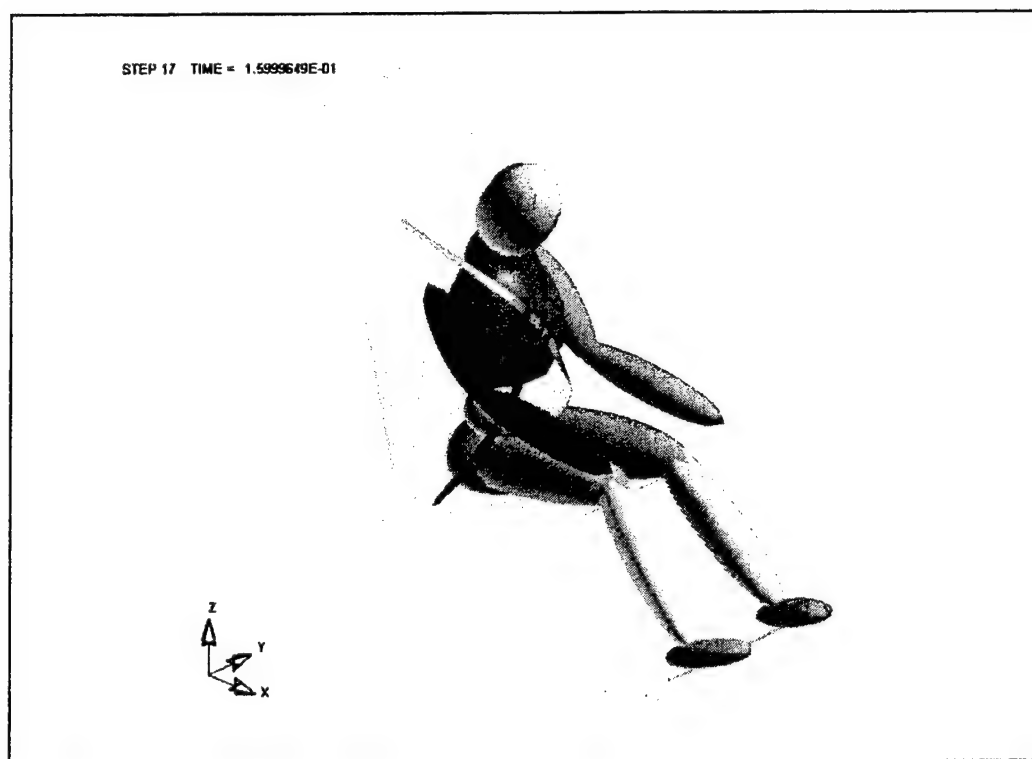
Figure B. 24 **Dummy position at time 0.16 sec wearing X belt**

Comparison of effectiveness based on width of the belt

In order to determine the optimum width of the seat belt that would be most effective for majority of accident situations, sled and frontal simulations were performed using each of these belts. The dummy used was the 50th percentile male.

Figure B.6a to B.6h show the plots of the displacement and acceleration of the upper torso, for the simulation using belts of various shapes. The size of the X, H and Lap/Shoulder belt were chosen to be 0.8 in, 1 in and 1.5 in and, that of V belt to be 0.2 in and 0.4 in.

- **H belt**
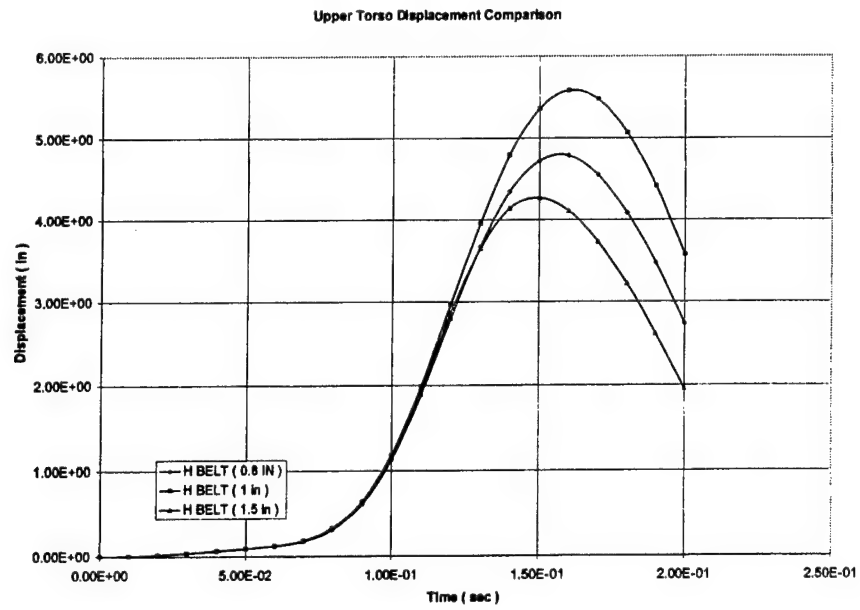
Figure B. 25 H belt displacement comparison plots
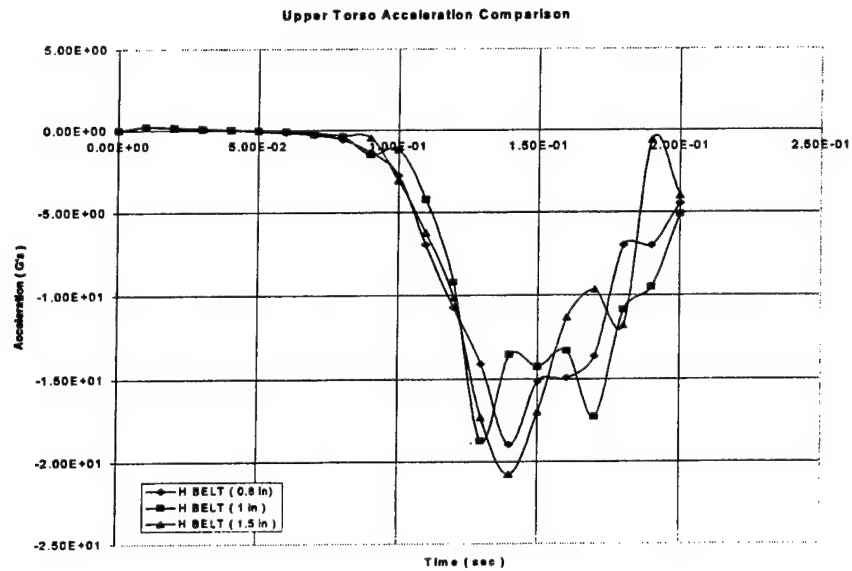
Figure B. 26 H belt acceleration comparison plots

• Lap/Shoulder belt
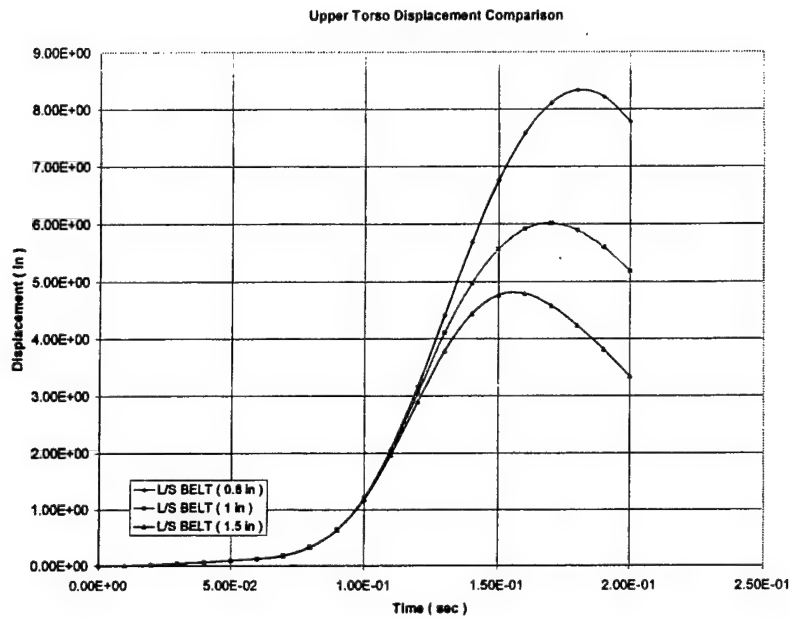
Figure B. 27 Lap/Shoulder belt displacement comparison plots
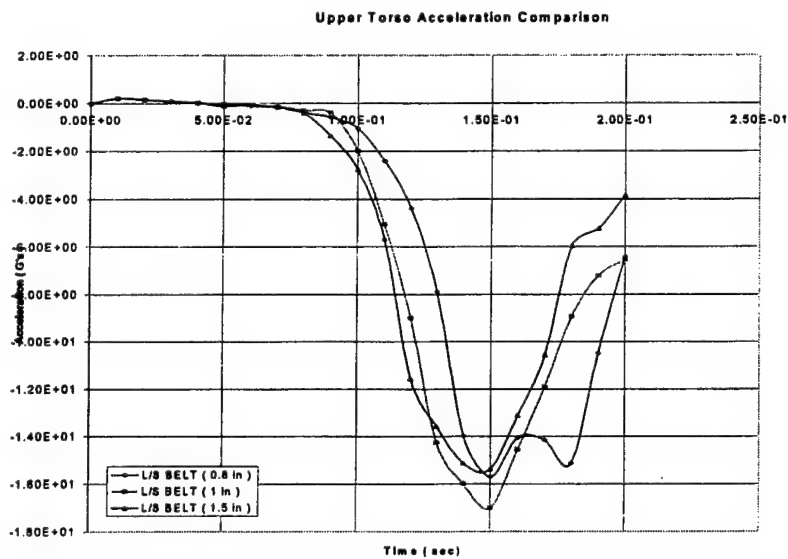
Figure B. 28 Lap/Shoulder belt acceleration comparison plots

- **V belt**

Upper Torso Displacement Comparison
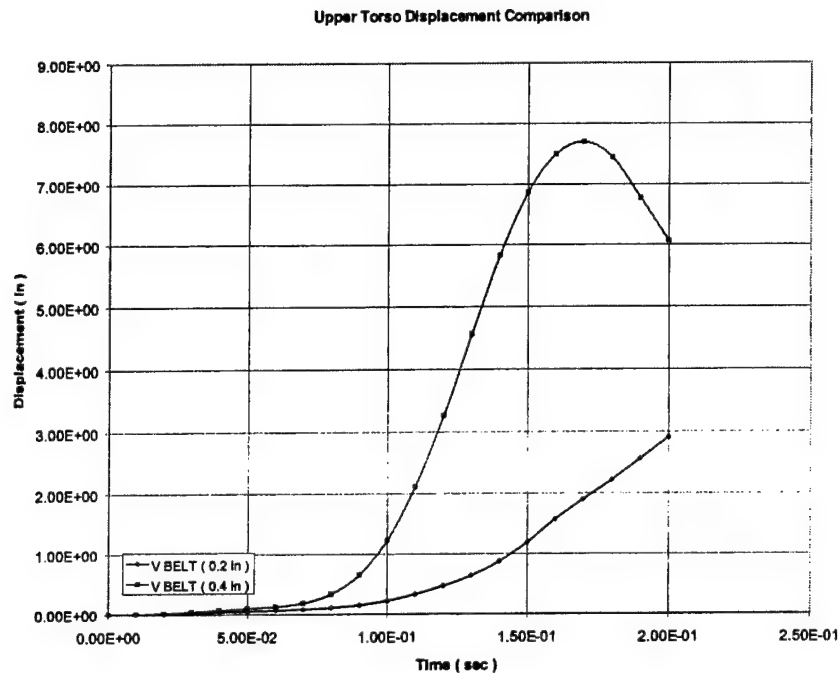
Figure B. 29 V belt displacement comparison plots

Upper Torso Acceleration Comparison
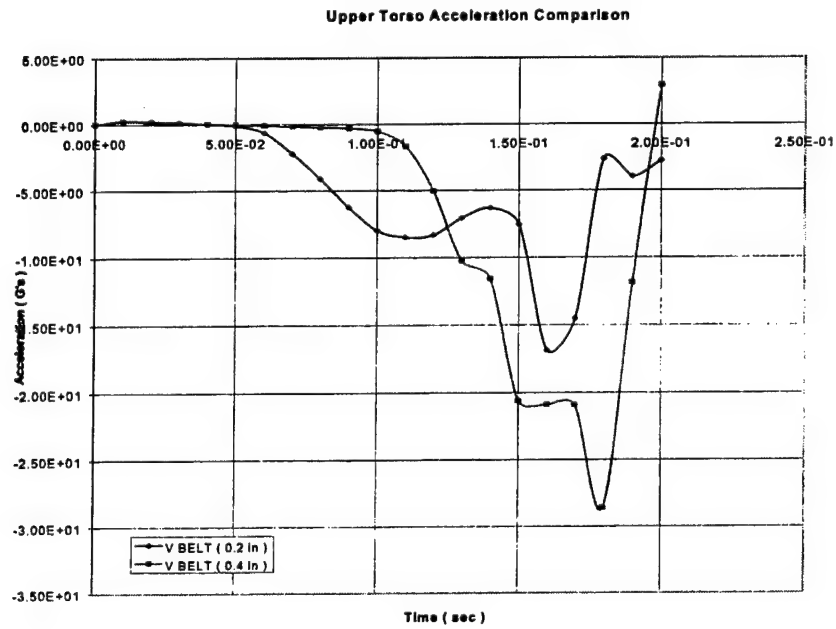
Figure B. 30 V belt acceleration comparison plots

- **X belt**

Upper Torso Displacement Comparison
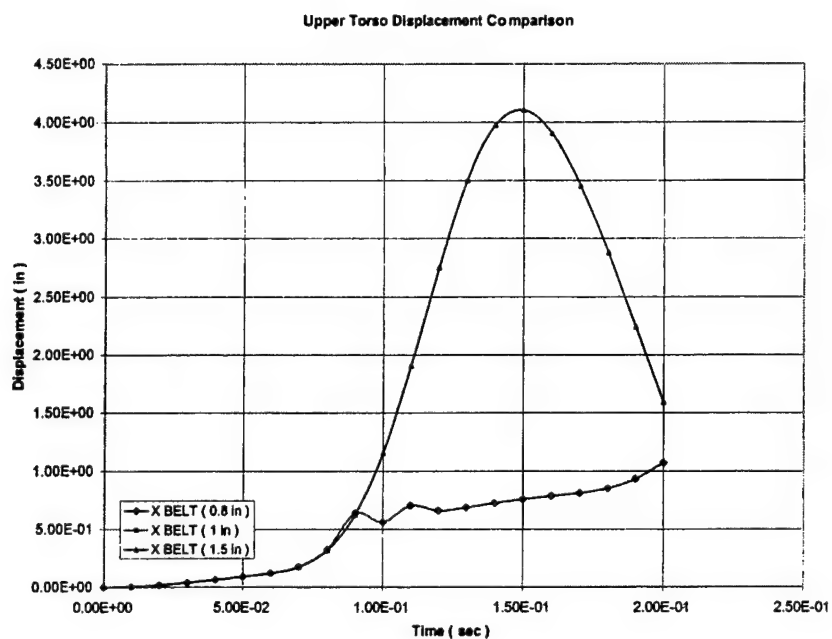
Figure B. 31 X belt displacement comparison plots

(Note. The 0.8 in and the 1.0 in data are almost identical)

Upper Torso Acceleration Comparison
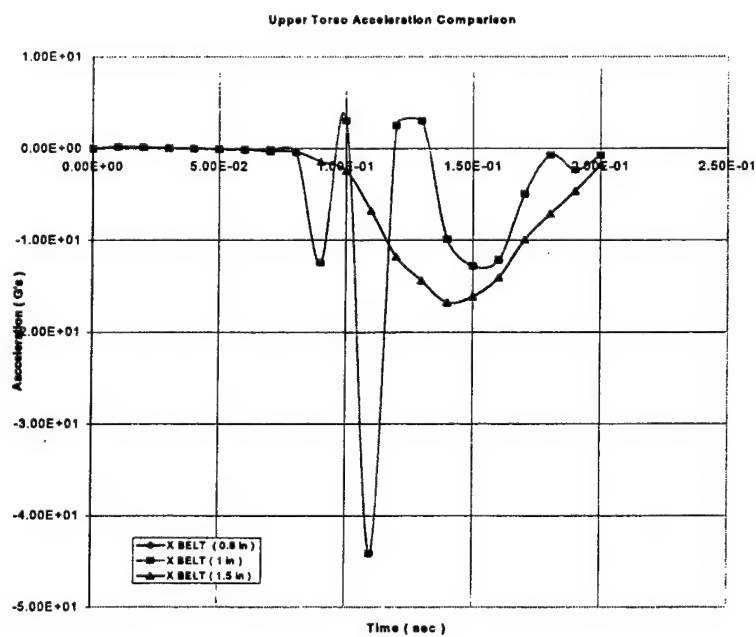
Figure B. 32 X belt acceleration comparison plots

(Note. The 0.8 in and the 1.0 in data are almost identical)

65

Tables B.6 and B.7 give a comprehensive summary of the maximum displacement and maximum acceleration values of the upper torso, for the sled simulation.

Table B. 6 Maximum displacement/acceleration values for H, X and L/S belts

Simulation	Belt Type	Max.Displacement (in)			Max.Acceleration (G's)		
		0.8	1	1.5	0.8	1	1.5
Sled	H belt	4.79	5.58	4.27	19	18.8	20.8
Sled	X belt	1.07	1.07	4.1	44.1	44.1	16.8
Sled	Three Point belt	N/A	6.2	N/A	N/A	19.62	N/A
Sled	Lap/Shoulder belt	8.37	6.02	4.8	15.7	17	15.4

Table B. 7 Maximum displacement/acceleration values for V belt

Simulation	Belt Type	Max.Displacement (in)		Max.Acceleration (G's)	
		0.2	0.4	0.2	0.4
Sled	V belt	2.91	7.70	16.9	28.6

66

Comparison of simulation with different dummies

For the purpose of comparative analysis of two different dummies, the 50th percentile male and female dummy (height 57 in and weight 140 lbs) were chosen. Both the dummies were subjected to sled and frontal simulations with a three-point belt of width 1 in.

This comparative analysis was done in order to ensure the consistency of the results generated by the coupled software.

Table B. 8 Mass of the various dummy segments

MASS OF DUMMY SEGMENTS (lbs)		
	Male	Female
Lower Torso	23.35	21.03
Upper Torso	49.95	34.02
Head	9.21	7.79

The plots B.33nd B.34how the displacement and accelerations of the Lower Torso segments of the two dummies, for the sled simulation.
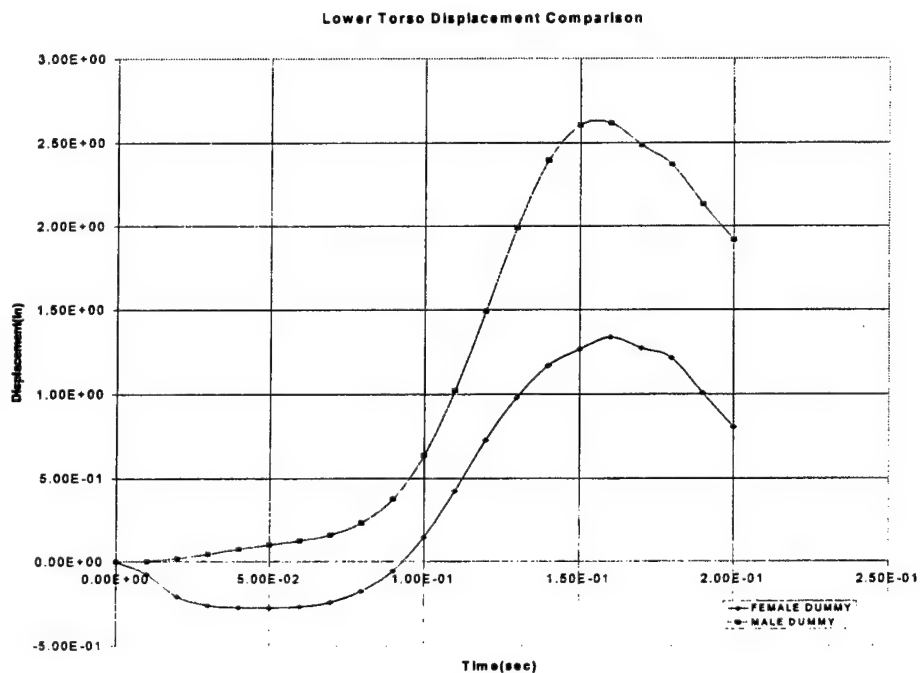
Figure B. 33 Sled simulation lower torso displacement comparison

Lower Torso Acceleration Comparison
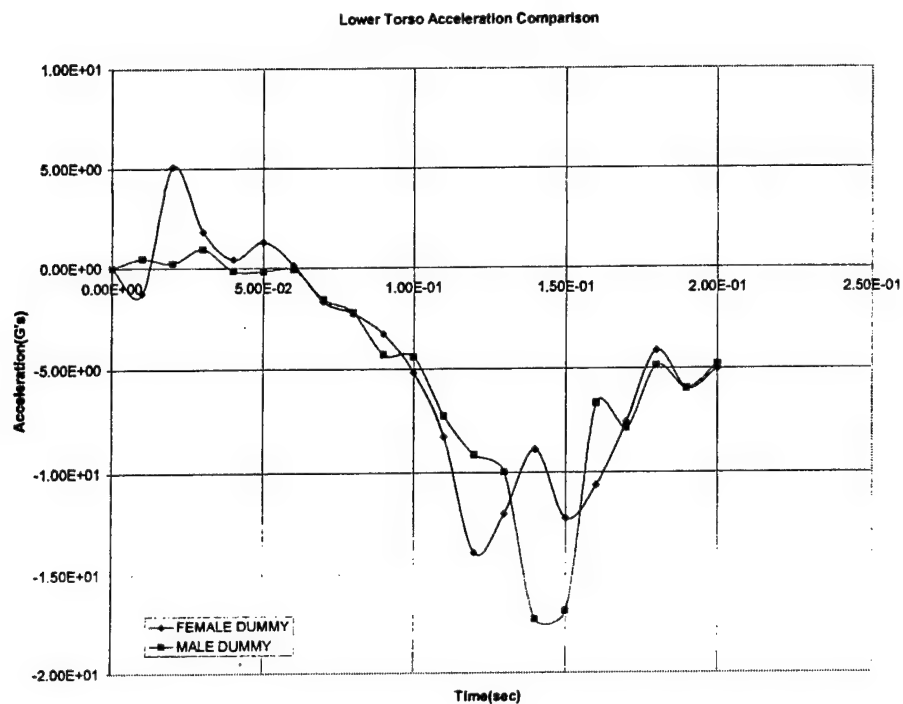
Figure B. 34 Sled simulation lower torso acceleration comparison

The plots B.35 B.36 show the displacements and accelerations of the lower torso segments of the two dummies, for the frontal simulation.

Lower Torso Displacement Comparison
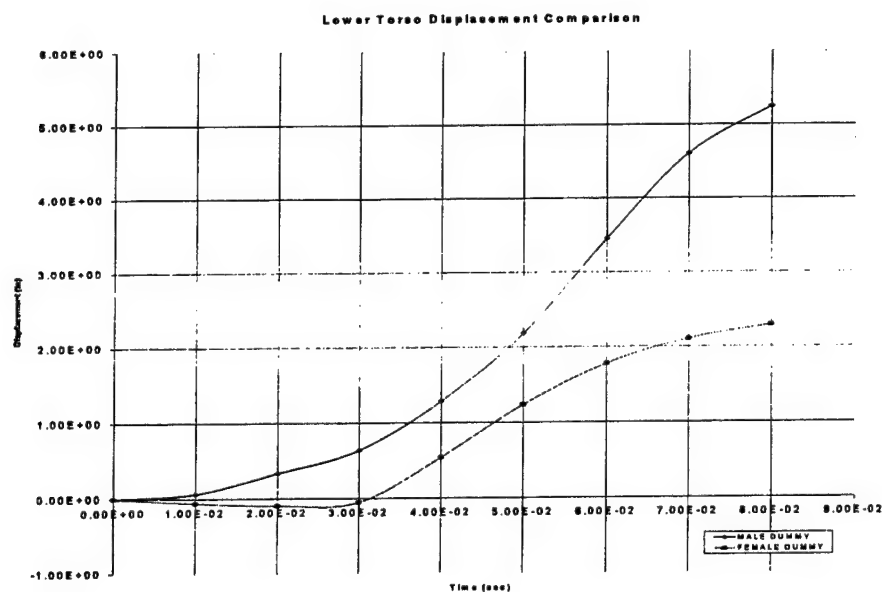
Figure B.7c:

Figure B. 35 Frontal simulation lower torso displacement comparison

68
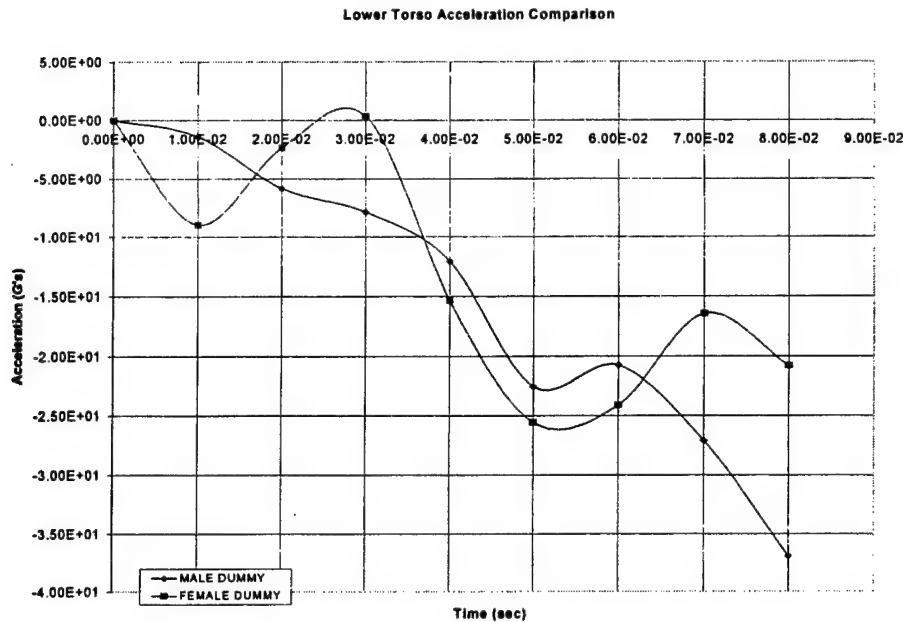
Figure B. 36 Frontal simulation lower torso acceleration comparison

From the analysis of the plots of the lower torso displacement and acceleration of the two dummies, it can be seen that the increase or decrease in the displacement and acceleration values follows a similar pattern.

Also, the differences in the displacement or acceleration values, at any given time step can be attributed to the mass and moment of inertia of the segments. For example, at time 0.15 sec of the sled simulation, the lower torso displacement of the male dummy was 2.6 in and that of the female dummy is 1.27 in. Since the mass of male dummy's lower torso is larger than the female dummy's, it can be expected that for the same simulation conditions the male will have a higher displacement than the female, which verifies the consistency of the results generated by the coupled software.

Effectiveness of retractors and pretensioners

In order to evaluate the effectiveness of the retractors and pretensioners, a 1D lap/shoulder belt was modeled in FEMB and the retractor and pretensioner elements were added using the *ELEMENT_RETRACTOR and *ELEMENT_PRETENSIONER cards, in LS-DYNA. The sensor to trigger the retractor and pretensioner was implemented using the *ELEMENT_SENSOR card. The situation modeled was the sled simulation and the dummy used was the 50th percentile male.

The sensor was modeled to trigger when the acceleration of the seat exceeded 2G, which activates the retractor after 0.05sec. The pretensioner was modeled to activate immediately after the sensor triggers.

From the analysis of the plots (Figures B.37 and B.38), it was observed that merely using the retractors does not have any effect on reducing the displacement or acceleration of the upper torso. On the other

69

hand, using retractors in combination with a pretensioner results in the lowest values of displacement (4.26in), although the acceleration values are the highest (37.8G's).

Upper Torso Displacement Compaison
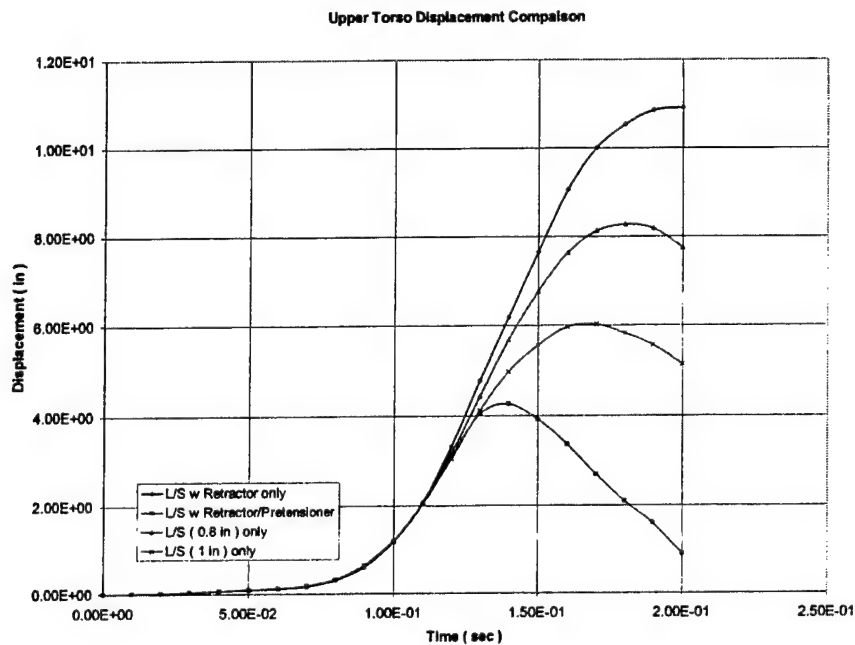
Figure B. 37 Retractor/Pretensioner effectiveness- displacement plots

Upper Torso Acceleration Comparison
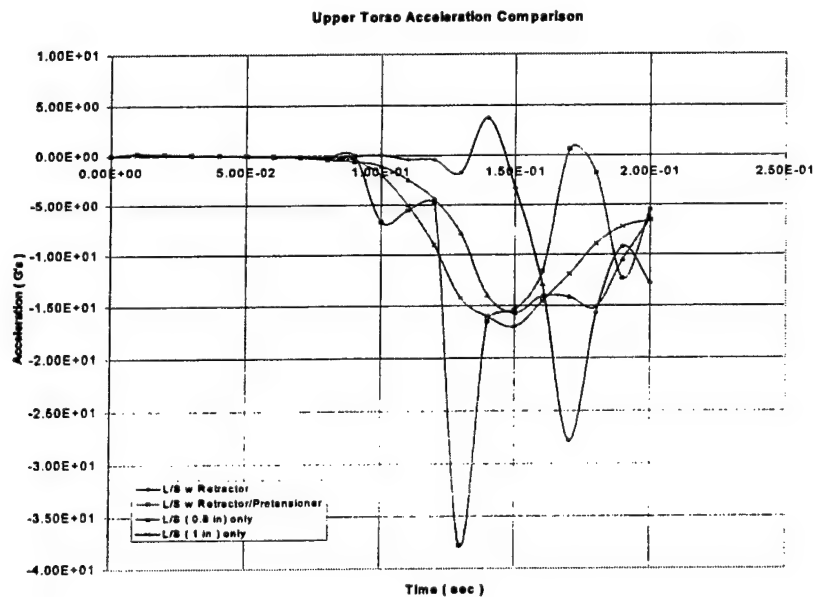
Figure B. 38 Retractor/Pretensioner effectiveness- acceleration plots

70

Table B. 9 Maximum displacement/acceleration values

Simulation	Belt	Max Displacement (in)	Max Acceleration (G's)
Sled	1D L/S belt w Retractor	10.9	27.8
Sled	1D L/S belt w Pretensioner/Retractor	4.26	37.8
Sled	2D L/S belt (0.8in)	4.79	19
Sled	2D L/S belt (1in)	5.58	18.8

APPENDIX C. AIRBAG AND DEFORMABLE DUMMY MODELING

In this research, the profile of the airbag is circular, and it was folded four different ways (shown in the figures below).
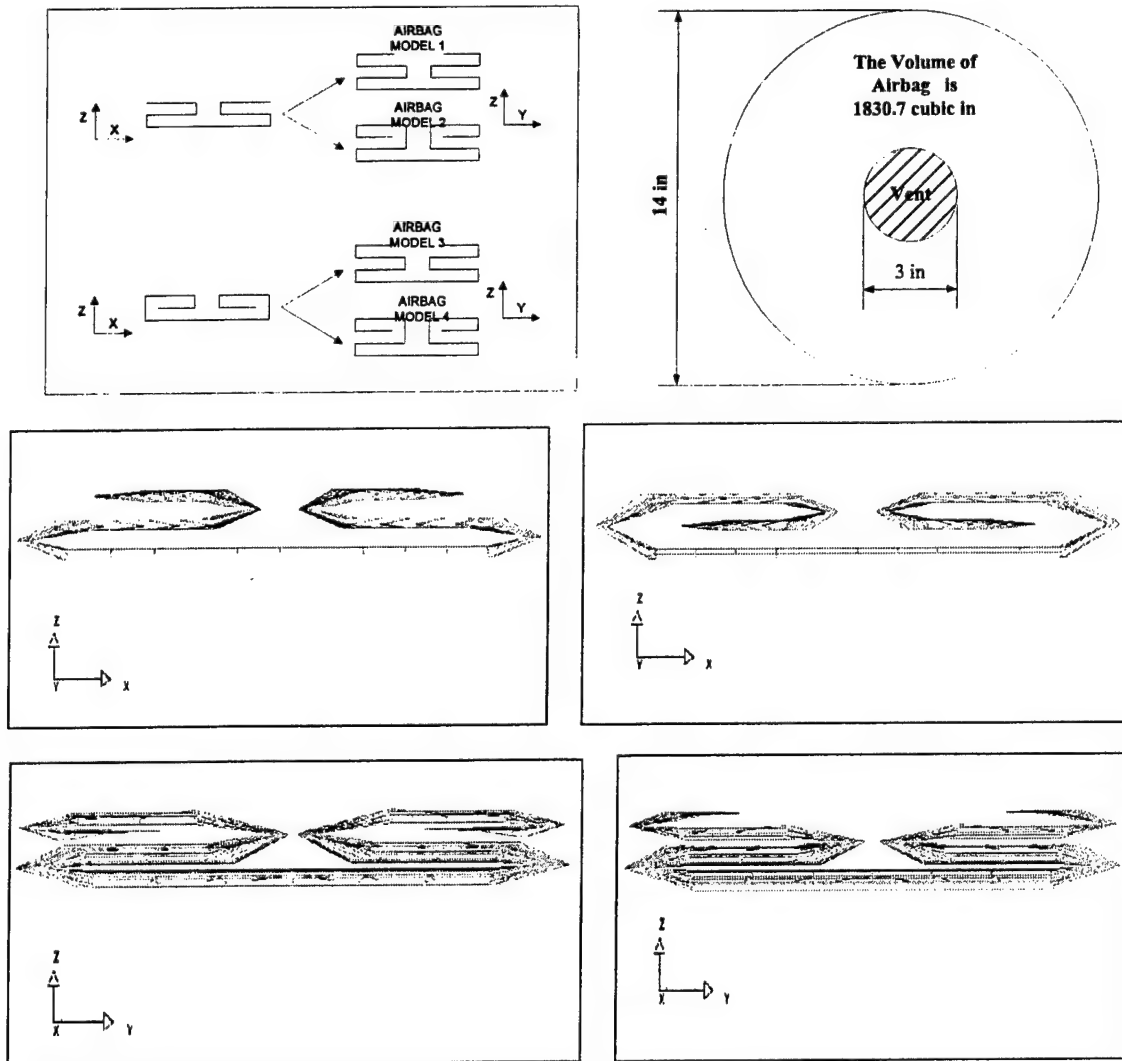
Figure C. 1 The airbag dimension and folding type

The material of airbag is Fabric that was created under MSC.PATRAN, and then INGRID software was used to do the airbag folding.

The material of airbag set to MAT_FABRIC in LS-DYNA. (The material data is from The FHWA/NHTSA National Crash Analysis Center). Its contact option is *CONTACT_AIRBAG_SINGLE_SURFACE (between the airbag fabric layers) and *CONTACT_ENTITY (between Dummy and airbag).

```
*MAT_FABRIC
$      mid        ro        ea        eb        ec      prba      prca      prcb
        2  0.298E-01 2.845E+05 2.845E+05 2.845E+05 0.300E+00 0.300E+00 0.300E+00
$      gab       gbc       gca       gse        el       prl    lratio      damp
2.845E+05 2.845E+05 0.380E+02 0.000E+00 0.000E+00 0.000E+00 0.000E+00 0.500E-01
```

The initial pressure of airbag is showing in the following figure.
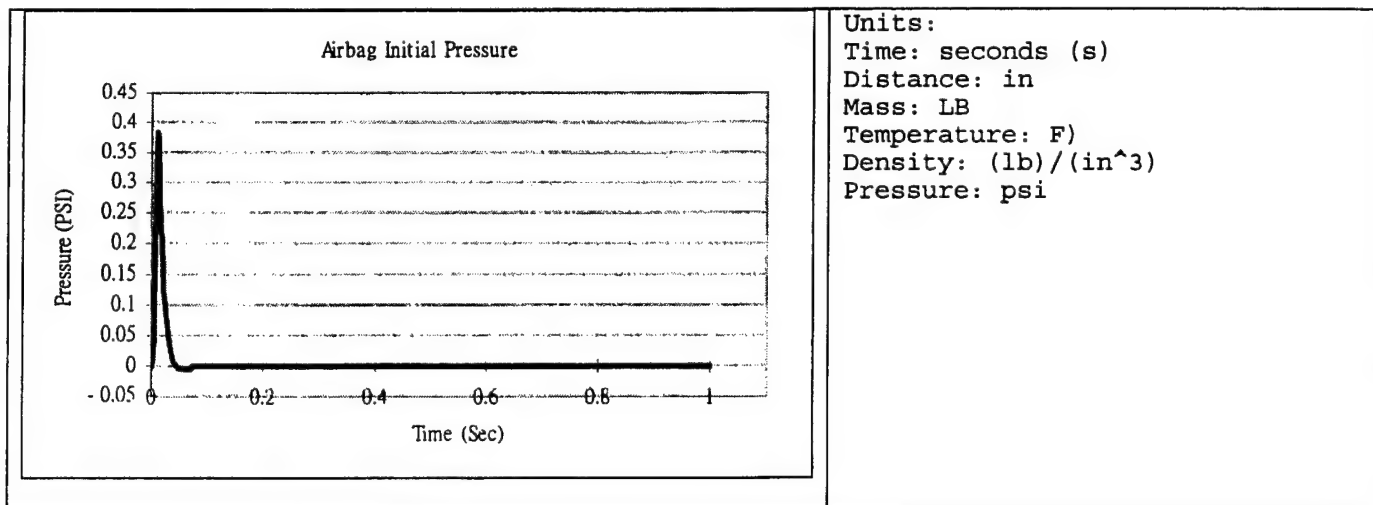
Figure C. 2 Airbag initial pressure

The following figure will show the airbag folding in INGRID.
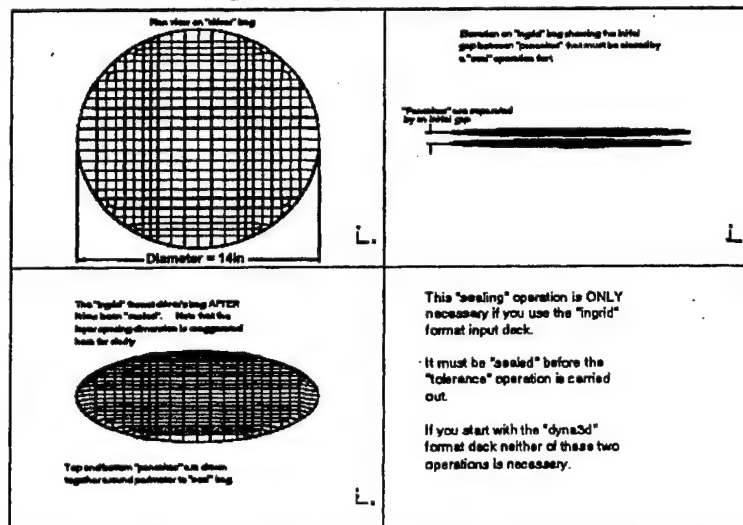
Figure C. 3 The airbag folding in INGRID

Two views of airbag sealed in INGRID

| Airbag folding line | Effect of adjusting mesh for airbag folding |
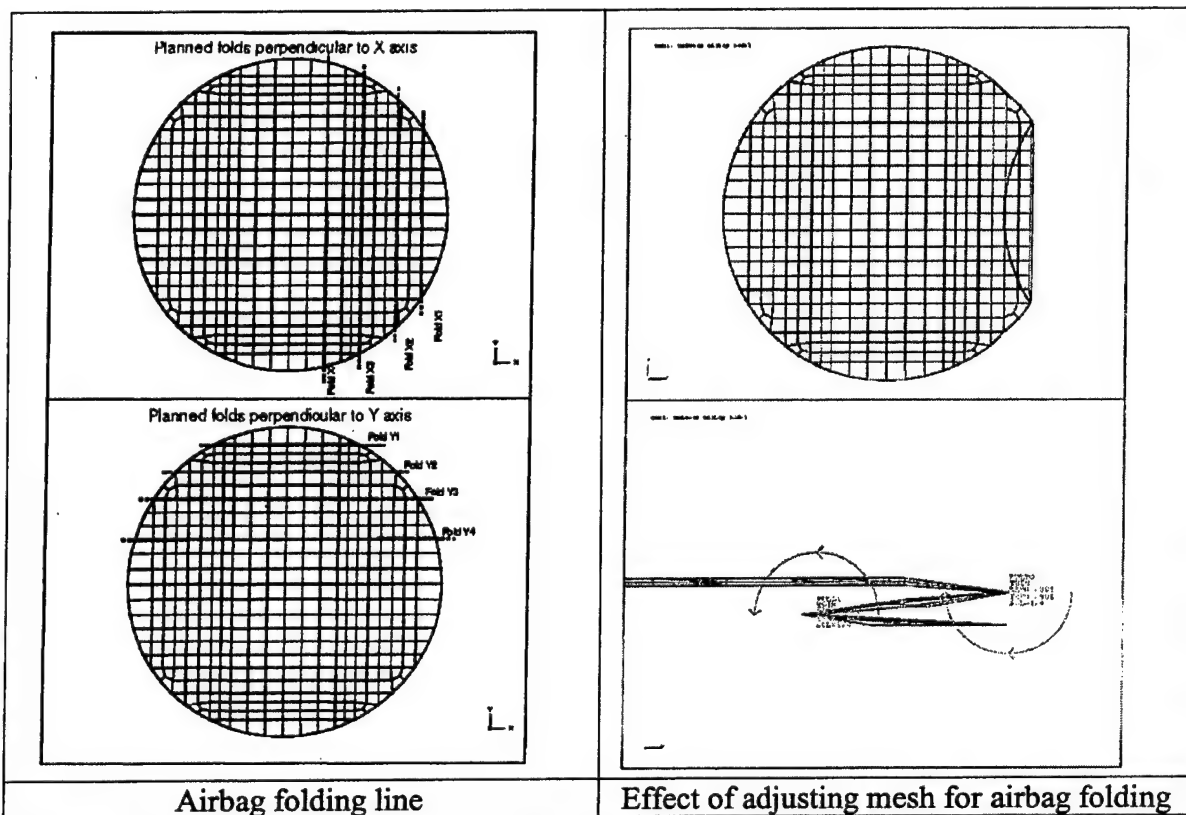
Figure C. 4 The airbag folding in INGRID

For the following simulation, ATB motion and Dummy were used. The airbag (The airbag did not have any sensor, and is deployed in the beginning of motion), seat and seat belt were created using LSDYNA as seen in the figures below.
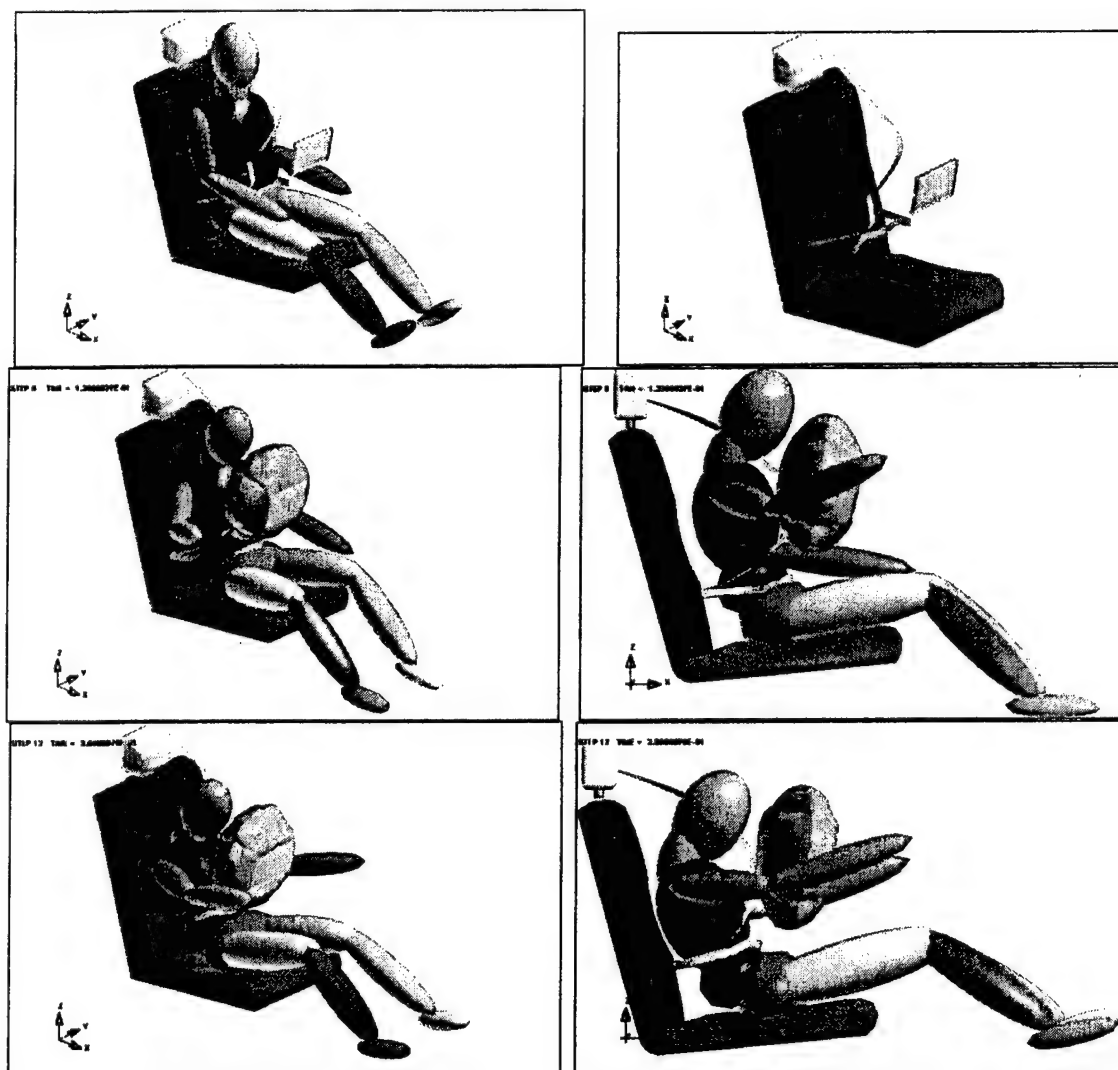
Figure C. 5 The simulation of ATB dummy with FEM (LS-DYNA) airbag, seat belt and seat

Comparing the displacement, velocity and acceleration on segment 3 (dummy chest) one can observe that the airbag folding has some effect, especially in acceleration, on the above quantities as shown in the figures below.
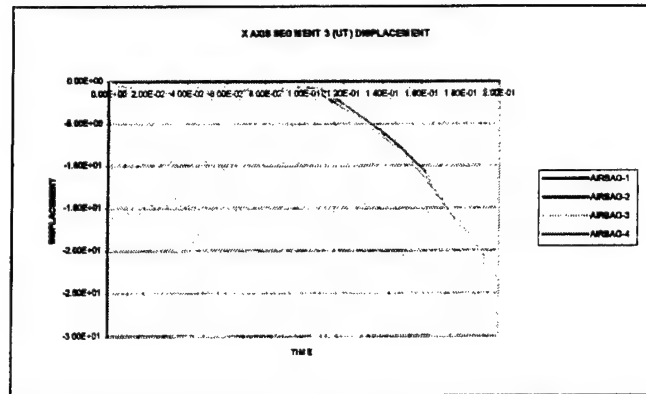
Figure C. 6 The comparison of displacement between 4 different folding airbag
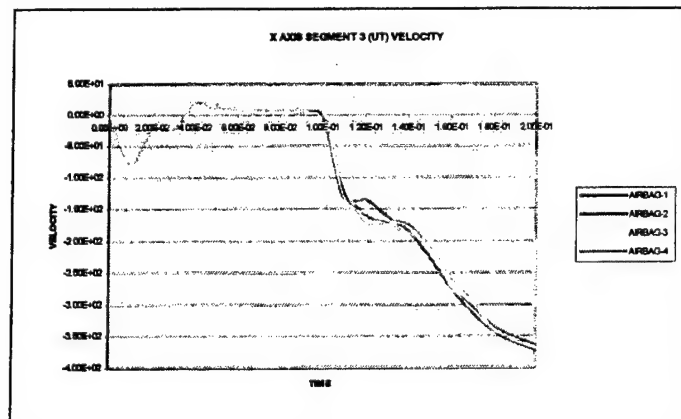
Figure C. 7 The comparison of Velocity between 4 different folding airbag
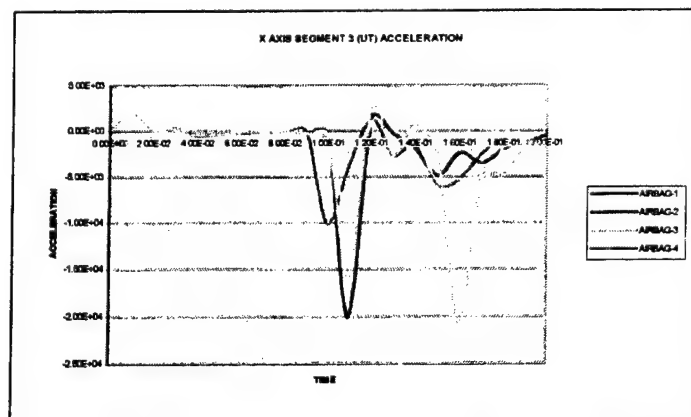
Figure C. 8 The comparison of acceleration between 4 different folding airbag

76

The following figures show the simulation of ATB dummy, seat and airbag with four different types of seat belts.

ATB Dummy with one lap seat belt
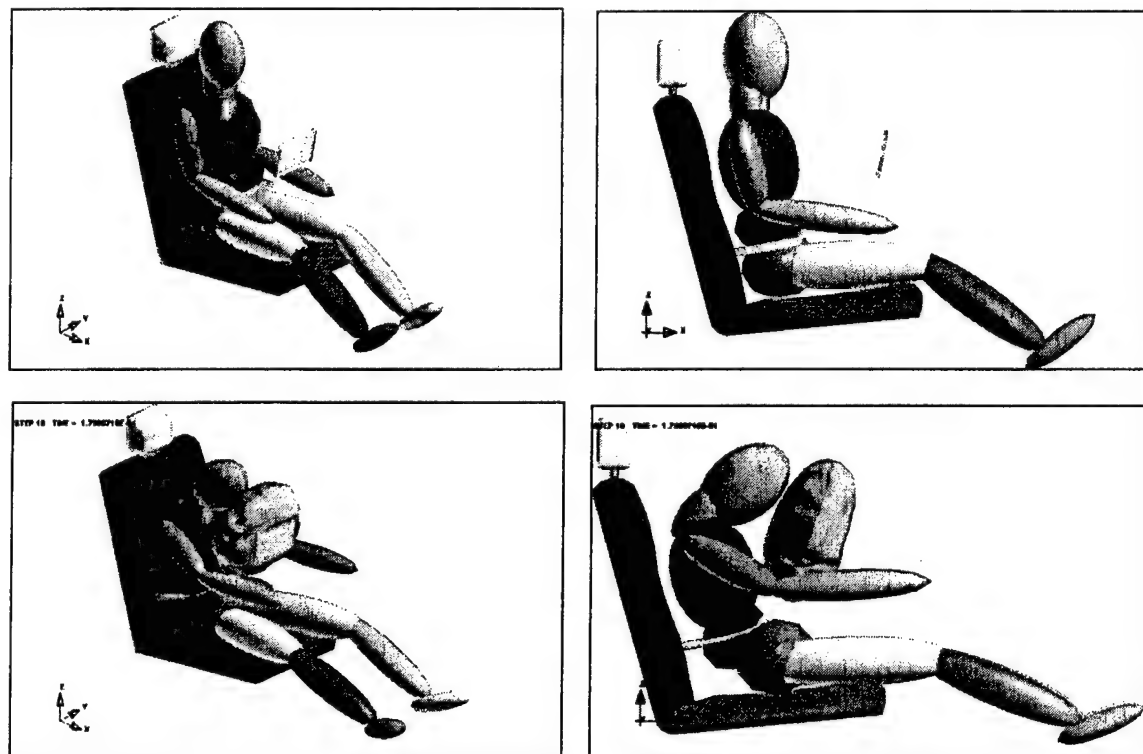
Figure C. 9 The simulation of ATB dummy with one lap seat belt

ATB Dummy with one shoulder seat belt
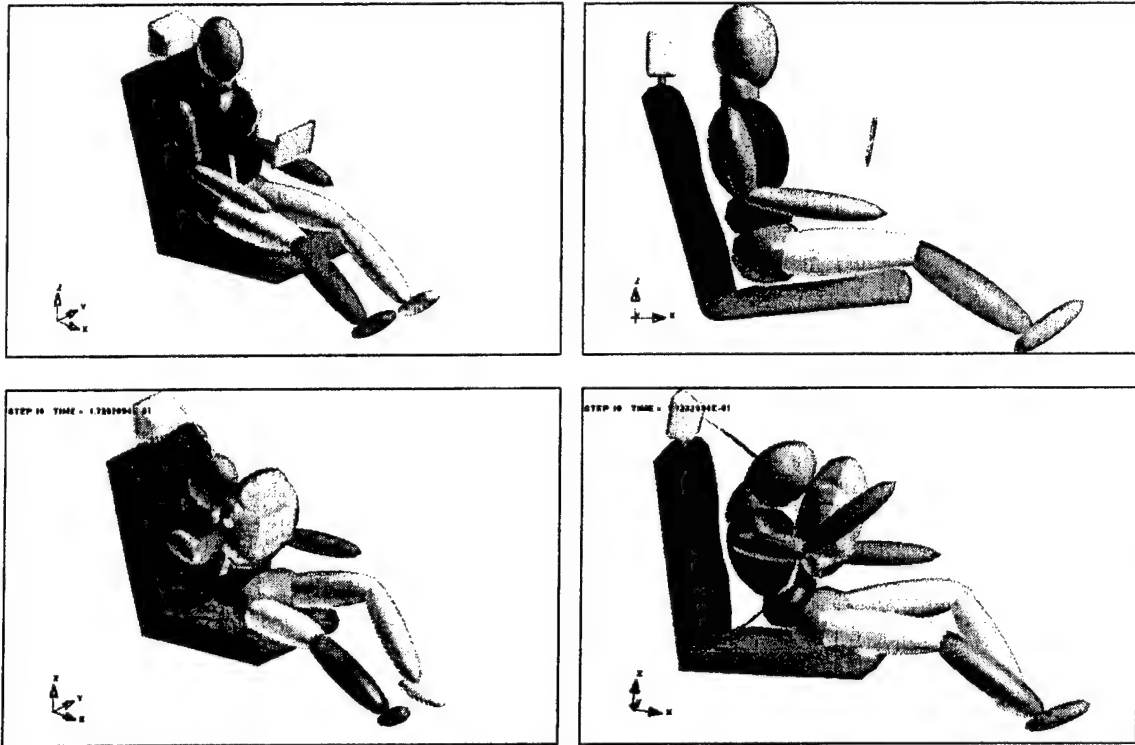
Figure C. 10 The simulation of ATB dummy with one shoulder seat belt

ATB Dummy with three-point seat belts
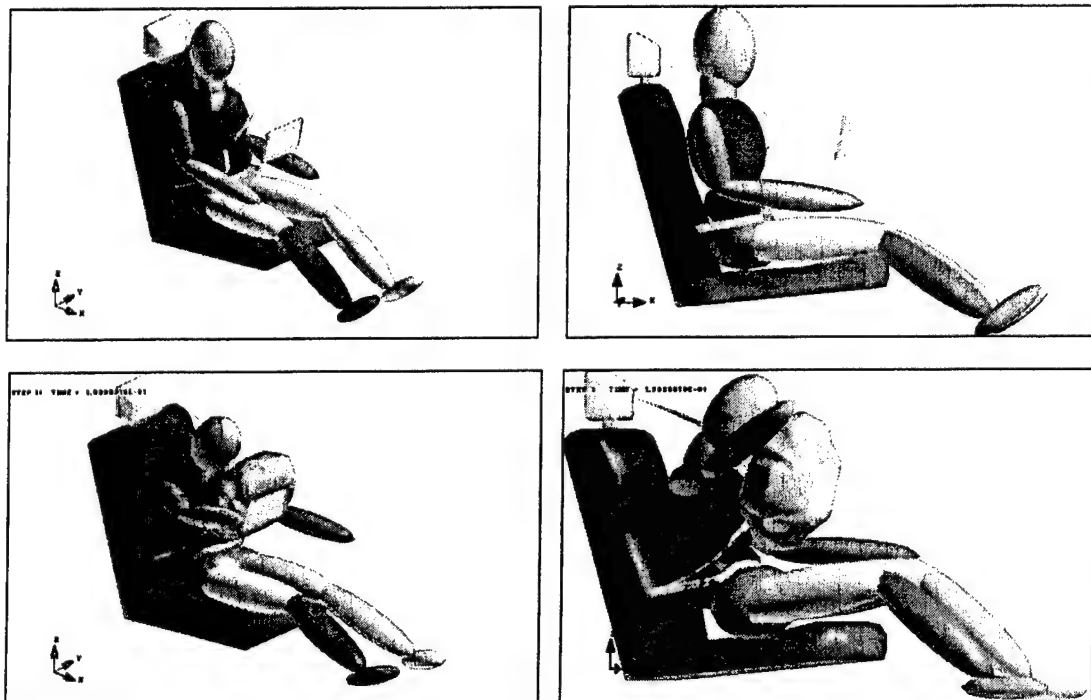
Figure C. 11 The simulation of ATB dummy with three-point seat belt

ATB Dummy with five-point seat belt
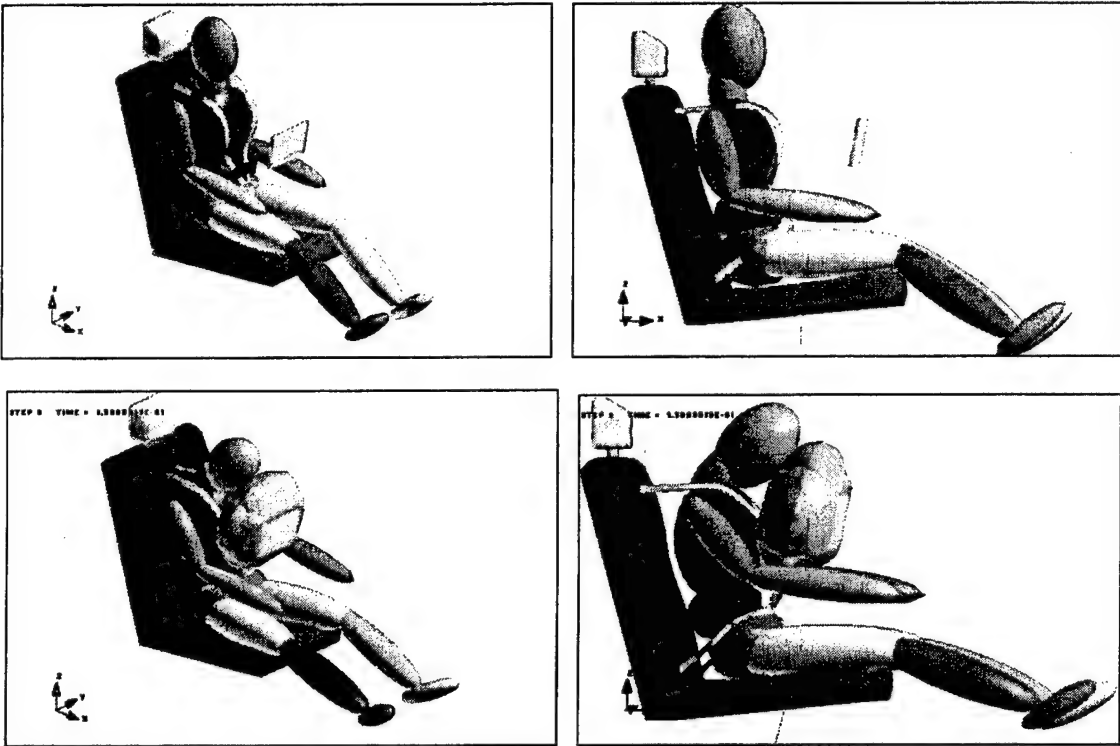
Figure C. 12 The simulation of ATB dummy with five-point seat belt

DEFORMABLE HEAD

A larger size FEM segment covered the ATB head segment. The FEM head segment can use ATB joint information. The FEM segment has deformation when it hits the green rigid cylinder as seen in the figure below.
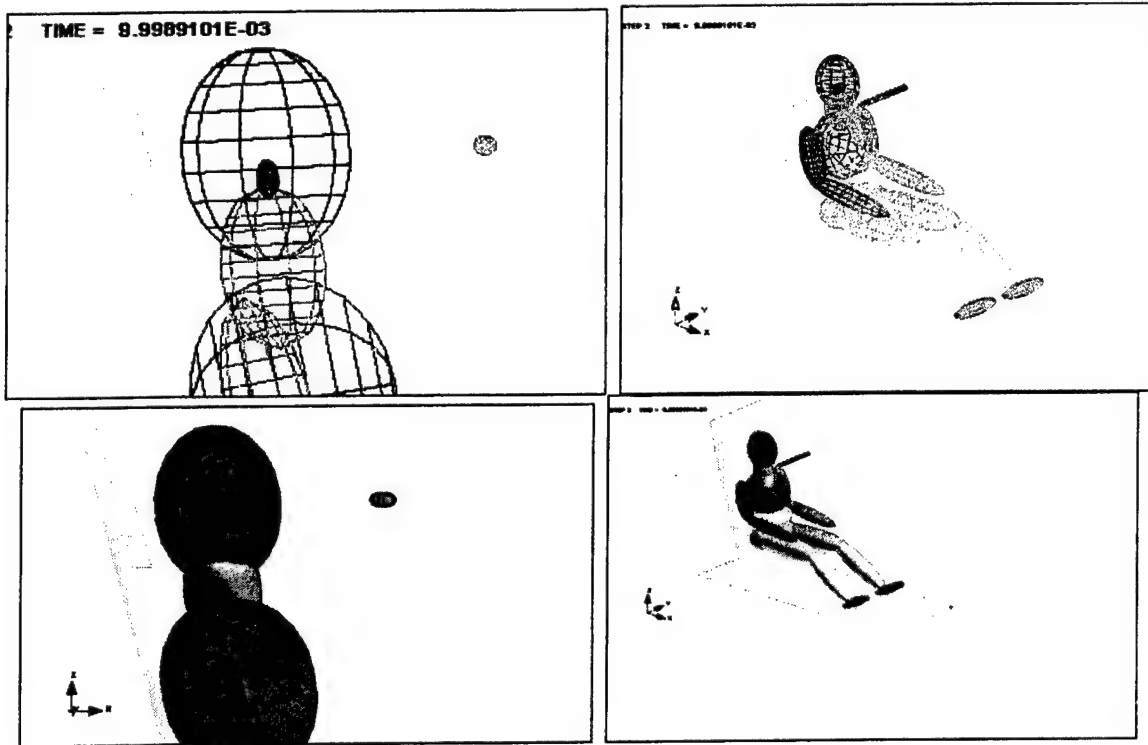
Figure C. 13 The designing idea of deformable head segment

The head segment is deformable; therefore one can visualize the stress distribution, when the head segment impacts the green rigid cylinder. The following figures show the deformation of head and the VON-MISES stress contours.
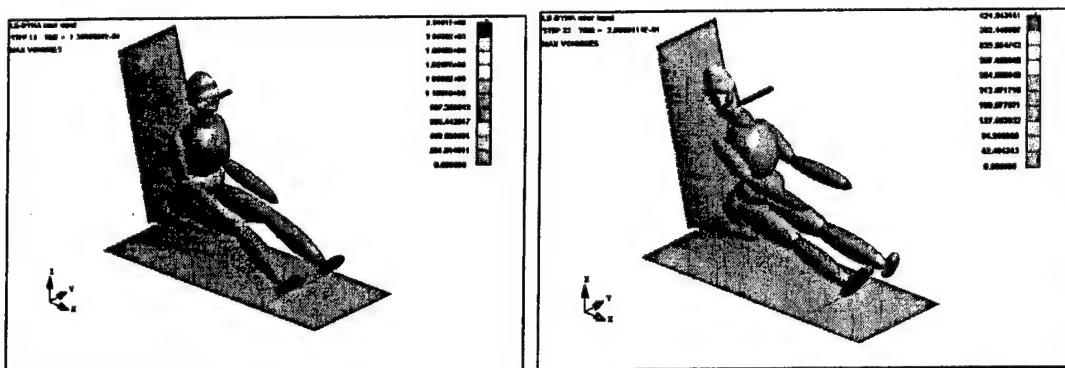
Figure C. 14 The simulation of deformable head segment

80

DEFORMABLE LEG

In this case the FEM Leg segment was used to replace the ATB leg segment. There was no ATB rigid body segment inside the FEM segment.
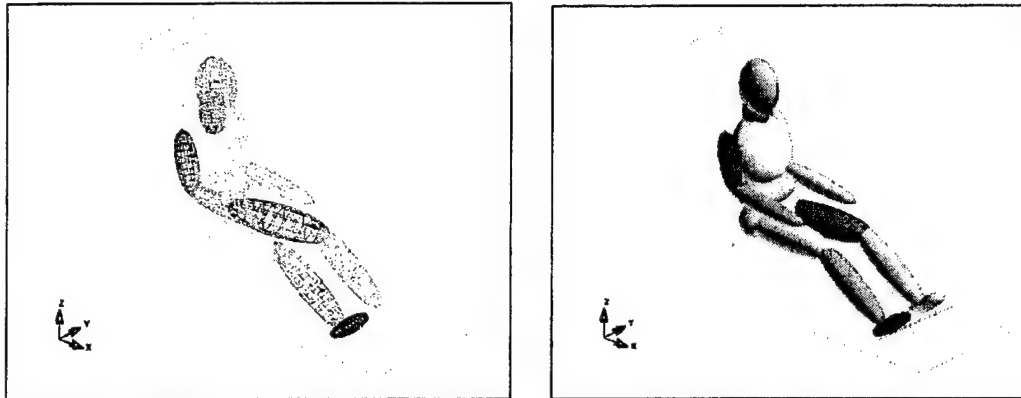
Figure C. 15 The designing idea of deformable left lower leg segment

The FEM leg segment uses the joint information from ATB so one can obtain the deformation and stress information during simulation. The following figures show the FEM segment deformation and stress information.
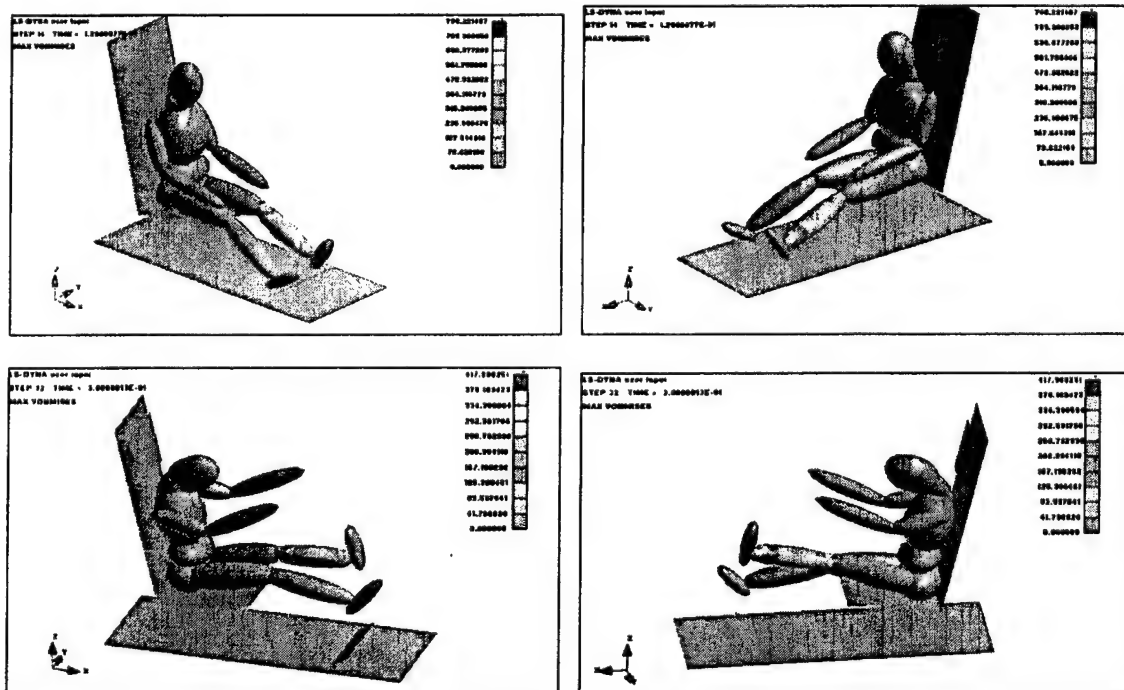
Figure C. 16 The simulation of deformable left lower leg segment

The deformable part is not a complete model, the above figure is just showing an example of creating deformable dummy by another method.

Coupled ATB/LS-DYNA Software User Manual

By:

Robert L. Williams II, Bhavin V. Mehta, Shr-Hung Chen, Srikanth Patlu
Department of Mechanical Engineering
Ohio University, Athens, Ohio 45701

James M. Kennedy
KBS2, Inc.

Coupled ATB/LS-DYNA Software User Manual

This document serves as the user manual for operating the coupled ATB and LS-DYNA software. The Articulated Total Body (ATB) simulation software, developed by the Air Force, is a 3D rigid body dynamics code for modeling human occupants and manikins in crashes and other hazardous events. LS-DYNA, developed by Livermore Software Technology Corporation (LSTC) and marketed by KBS2 Inc., is a general 3D nonlinear dynamic finite element code.

This User's Guide cannot replicate the extensive manuals for ATB and LS-DYNA; the user is referred to those documents that are also applicable for the coupled software. Instead, this guide explains how to run a model in the coupled software, how to view the results in a post-processor (in the LS-DYNA environment), and presents the important software flags and parameters for preparing models in the coupled software environment. Examples are then presented for running models in the coupled ATB/LS-DYNA software.

To Run an Existing Model

Ensure the required files are in the same directory folder: *ls960ATB.exe*
         fn.k
         fn.ain

ls960ATB.exe is the executable for the coupled ATB/LS-DYNA software. The extension of *.k* and *.dyn* represent LS-DYNA input files. The *.ain* extension is used for ATB input files. LS-DYNA input files are given the *.dyn* extension when generated by the pre-processor in FEMB. Files with the *.k* extension are examples provided by KBS2 Inc., identical in function to *.dyn* files. All three input file types (*.k*, *.dyn*, *.ain*) are ASCII files.

To run the coupled software model, from a MS-DOS prompt pointing to the directory folder containing the required files, type:

$$Ls960ATB \quad i{=}fn.k \quad y{=}fn$$

note the *.k* extension is required (*i=fn.k*) while the *.ain* extension may be left off as shown (*y=fn*). This is sufficient to run an example in the coupled software. A more complete list of available options for command-line execution is given below.

i	=	LS-DYNA input file (*fn.k* or *fn.dyn*)
y	=	ATB input file (*fn.ain*); or CAL3D input file
m	=	Stress initialization
r	=	Restart file
l	=	Interface segment
v	=	VDA geometry
t	=	TOPAZ3D file
o	=	*fn.otf* output printer file (default file is *d3hsp.otf*)
ncpu	=	*N* (integer number of multiple processors)

Upon typing *ls960ATB i=fn.k y=fn* at the MS-DOS prompt , the program will execute the requested model. Information will flash by during execution; press ctrl-c and then type *sw2* to see detailed run information. Press ctrl-c and type *sw1* to terminate execution of the model. After successful completion of the program, many files are created. Three output files of note are:

fn.aou	ATB numeric output file
fn.sal	ATB output plot file
d3plot	LS-DYNA output file for post-processing

note the ATB output files contain the model name but the LS-DYNA output file always uses the generic *d3plot* filename, with no extension. Now modeling results may be viewed in a post-processor.

Software Flags for Coupled ATB/LS-DYNA Models

This section discusses software flags required for operating the coupled ATB and LS-DYNA software. All flags in this section will appear in the *fn.k* LS-DYNA input file; no changes are necessary in the *fn.ain* ATB input file.

In the lines from a sample *fn.k* LS-DYNA input file below, '$' indicates a comment line. The comment lines starting with '$...>....1....>....2' are given to show the fixed format of the input lines to follow. A line starting with an asterisk and having capitalized text (with underbars) gives the various keywords, from LS-DYNA. Data in **boldface** indicates a required coupled flag which must be set as given. Data in *italics* indicates that its lines should be repeated and the *italics* items changed (for example, for all Human Model segment part IDs from 1 through 15). All other data in plain text can be set as desired for using LS-DYNA. Please refer to the LS-DYNA manuals to identify standard LS-DYNA options.

Categories for the required software flags given below are Coordinate Frames, Material, Element Type, Part, and Contact. With the exception of the Control Coupling, these categories are further divided into lines for the Human Model, Plane(s) and Seat Belt coming from the ATB input file.

Coordinate Frames

The Control Coupling lines must be used to ensure the *XYZ* Cartesian coordinate frame directions agree between ATB and LS-DYNA. In particular, both the *Y* and *Z* axes must be flipped. As shown below, both FLIPY and FLIPZ must be set to '1'.

```
*CONTROL_COUPLING
$...>....1....>....2....>....3....>....4....>....5....>....6....>....7....>....8
$   UNLENG   UNTIME   UNFORV   TIMIDL   FLIPX    FLIPY    FLIPZ    SUBCYL
                                                    1        1
```

Material

When obtaining model components from ATB, LS-DYNA must be told that these materials are all rigid bodies, as shown in the lines below.

For Human Model

```
* MAT_RIGID
$...>....1....>....2....>....3....>....4....>....5....>....6....>....7....>....8
$      MID        RO         E        PR         N    COUPLE         M     ALIAS
         1 1.00000-4 1.00000+5 0.3000000 0.0000000 2.0000000 1.0000000
$      CMO       CON1       CON2
 0.0000000 0.0000000 0.0000000
$       A1         A2         A3        V1        V2        V3
 0.0000000 0.0000000 0.0000000 0.0000000 0.0000000 0.0000000 0.0000000 0.0000000
```

Notes:
- MID is the human model segment number (shown as italic boldface *1*). These * MAT_RIGID lines must be repeated for all segments, incrementing MID for each (e.g. MID = 1,2, 3, ..., 15 for a 15 segment Human Model).
- COUPLE must be set to '2', indicating the data is to come from ATB.
- M is equal to MID.
- CMO, CON1, and CON2 " must be set to '0'.

For ATB Plane (seat, seat-back, floor, pedals, etc.)

```
        16 1.00000-4 1.00000+5 0.3000000 0.0000000 2.0000000 -1.000000
 0.0000000 0.0000000 0.0000000
 0.0000000 0.0000000 0.0000000 0.0000000 0.0000000 0.0000000 0.0000000 0.0000000
```

Notes:
- The material number for all planes is *16* (assuming a 15-segment Human Model).
- COUPLE must be set to '2', indicating the data is to come from ATB.
- M must be set to '-1'.

For ATB Seat belt

```
        17 1.00000-4 1.00000+5 0.3000000 0.0000000 3.0000000  0.000000
 0.0000000 0.0000000 0.0000000
 0.0000000 0.0000000 0.0000000 0.0000000 0.0000000 0.0000000 0.0000000 0.0000000
```

Notes:
- The seat belt material number is *17* (assuming a 15-segment Human Model).
- COUPLE must be set to '3', which is a new option added for the coupled software.
- M must be set to '0'.

Element Type

When importing rigid-body components from ATB, LS-DYNA must be told which element types to use. The Human Model and ATB Plane use shell elements, while the ATB Seat belt uses beam elements, as shown below.

For Human Model

```
*SECTION_SHELL
$...>....1....>....2....>....3....>....4....>....5....>....6....>....7....>....8
```

$	SECID	ELFORM	SHRF	NIP	PROPT	QR/IRID	ICOMP
	1	0	0.0000000	0.0000000	0.0000000	0.0000000	0

$	T1	T2	T3	T4	NLOC
	1.0000000	1.0000000	1.0000000	1.0000000	0.0000000

Notes:
- SECID is the section number (The Human Model segment number, again repeated for segments 1 through 15).
- ELFORM, SHRFM, and NIP must be set to '0.00'.
- T1, T2, T3, and T4 are element thicknesses at the four corners.

For ATB Plane

The element-type setup for ATB Plane(s) is the same as for the Human Model, using SECID=16.

For ATB Seat belt

```
*SECTION_BEAM
$...>....1....>....2....>....3....>....4....>....5....>....6....>....7....>....8
```

$	SECID	ELFORM	SHRF	QR/IRID	CST
	17	3			

$	T1	T2	T3	T4	NLOC
	1.000000	1.0000000	1.0000000	1.0000000	0.0000000

Notes:
- SECID is 17 (again, assuming a 15-segment Human Model).
- ELFORM must be set to '3'.
- T1, T2, T3, and T4 are element thicknesses at the four corners.

Part

The following lines are used to define the part numbers and correlate them to the section and material numbers. It is logical to choose the same integer for each for a given part, if possible.

For Human Model

```
*PART
$...>....1....>....2....>....3....>....4....>....5....>....6....>....7....>....8
$      PID     SECID      MID    EOSID      HGID      GRAV    ADPORT      TMID
         1         1        1        0         0         0         0         0
```

Notes:
- PID is the Human Model segment number.
- SECID is the section number.
- MID is the material number.
- Each of these must be repeated for segments 1 through 15.

For ATB Plane

The part setup for ATB Plane(s) is the same as for the Human Model, using 16 for PID, SECID, and MID.

For ATB Seat belt

The part setup for the ATB Seat belt is the same as for the Human Model, using 17 for PID, SECID, and MID.

Contact

Determination of contact between components is performed when LS-DYNA is told which components may come into contact. This is accomplished through the *CONTACT_ENTITY keyword. This must be defined for the Human Model only. It is not necessary for the ATB Plane(s) and ATB Seat belt.

For Human Model

```
*CONTACT_ENTITY
$...>....1....>....2....>....3....>....4....>....5....>....6....>....7....>....8
$   PID  GEOTYP   SSID   SSTYP    SF     DF     CF   INTORD
        1           7      4        0 0.0000000 0.0000000 0.4000000          0
$   BT    DT    SO    GO
 0.0000000 0.0000000
$   XC    YC    ZC    AX    AY    AZ
 0.0000000 0.0000000 0.0000000 1.0000000 0.0000000 0.0000000
$   BX    BY    BZ
 0.0000000 1.0000000 0.0000000
$  INOUT    G1    G2    G3    G4    G5    G6    G7
        0 1.0000000 0.0000000 0.0000000 0.0000000 0.0000000 0.0000000 0.0000000
```

Notes:
- GEOTYP must be set to '7', which indicates ellipse.
- SSID is the ID of the slave component.
- This must be repeated for segments 1 through 15.

To View Simulated Results via Post-Processing

Two post-processing capabilities are provided by KBS2 Inc., FEMB within LS-DYNA and stand-alone program PostGL. Either may be used to similar effect for viewing simulation results. PostGL has a better shading capability.

FEMB Post-Processing

The following steps are used to view the modeling results in output file *d3plot* using FEMB, the pre- and post-processor of LS-DYNA.

- Run LS-DYNA under Windows NT (the existing non-coupled version).
- Click the FEMB icon (magnifying glass). Open a database file:
- Choose the output file *d3plot* that was created in running the coupled software.
- ENTER LS-DYNA VERSION; Choose LS936/LS940.
- When model displays, viewing functions can be used: zoom, pan, fill, rotations, standard views.
- Using the pull-down menu choose Post → Animate → Deformation
- STEPS TO ANIMATE; make desired selection (ALL AVAILABLE STEPS).
- SELECT ANIMATION OPTION; make desired selection (Hidden Line Color Fill).
- While animation is running (repeats continuously), right click to quit (End Select) or to see other options (such as creating an .AVI file and setting the frame rate).

PostGL Post-Processing

The following steps are used to view the modeling results using PostGL, a stand-alone post-processor that accepts LS-DYNA output file *d3plot*.

- Run PostGL under Windows NT. From the pull-down menu File:
- Open the output file *d3plot* that was created in running the coupled software.
- SELECT LS-DYNA VERSION; Choose LS940/LS950.
- Do you want to process output acceleration and velocity? YES.
- SELECT TIME STEPS; make desired selection (ALL AVAILABLE STEPS).
- Select Result Components; make desired selection for stress/strain components (Cancel).
- When model displays, viewing functions can be used: zoom, pan, fill, rotations, standard views.
- Under the Current Visual area (lower toolbar), click the Shade Model button ON/OFF as desired.
- On right toolbar click Frame Range; make desired selection (all frames).
- Click Play to run animation continuously.
- Click Cancel/End button on lower toolbar to quit.

The first time a new d3plot file is viewed using FEMB (or PostGL), the file *d3plot.pp* (or *PostGL.pp*) is created. This file may be Opened to view the animation more quickly in the future.

To Plot Analysis Results

In order to enable plotting results from running the coupled ATB/LS-DYNA software, add the following lines to the *fn.k* LS-DYNA input file, immediately following the *DATABASE_BINARY_D3PLOT lines:

```
*DATABASE_RBDOUT
$ dt/cycl        lcdt
 0.001
```

This instructs LS-DYNA to record data for plotting every 0.001 seconds. No entry is required for lcdt. Upon execution of the coupled software with this change, a new output file is written, with no file extension: *rbdout*. This file must be opened in LS-DYNA to view plot results of the desired variables. In addition, the output file *abstat* contains airbag plot information. There are two ways to generate these plots.

FEMB Pre-Processing

The following steps are used to graph the desired results from output file *rbdout* using FEMB, the pre- and post-processor of LS-DYNA, Version 950.
- Run LS-DYNA under Windows NT (the existing non-coupled version).
- Click the FEMB pre-processor icon (magnifying glass with *F*). Open a Database File (choose filetype LS-DYNA3D Graph):
- Choose the output file *rbdout* that was created in running the coupled software.
- SELECT RIGID BODY; make desired selection (rigid body 1) and click Add-->. Click Close.
- Select Rigid Body Time History Components for Graph; make desired selection (z-displacement) and click Add-->. Click Close.
- The graph will now display in a window. To save this graph as a bitmap file (.BMP), under the File pull-down menu choose Save As. Alternatively, the graph may be copied to the clipboard and pasted where desired.

Graph Processing

The following steps are used to graph the desired results from output file *rbdout* using the graph-processing feature of LS-DYNA, Version 950: eta PostGL/Graph 1.0.
- Run LS-DYNA under Windows NT (the existing non-coupled version).
- Click the FEMB icon (magnifying glass with *G*). Open a Database File (choose filetype LS-DYNA3D Graph):
- Choose the output file *rbdout* that was created in running the coupled software.
- Time Interval Selection; make desired selections and click OK.
- In the GRAPH INPUT table make desired selections for Rigid Body(s) Available (Rigid Body #1) and Variable Types (global z-displacement). Click OK.

- The graph will now display in a window. The graph may be copied to the clipboard and pasted where desired.

Examples

Four examples are briefly discussed in this section to demonstrate results from running the coupled ATB/LS-DYNA software. The associated ATB and LS-DYNA input files (available from the contact author) for these examples are listed in the table below.

**Table D. 1 The example of Simulation**

Model	ATB Input File (*fn.ain*)	LSDYNA Input File (*fn.k*)
a. Sphere falling on plane	*Ball.ain*	*Ball.k*
b. ATB Human Model	*Human.ain*	*Human.k*
c. Sphere on inflating airbag	*BallBag.ain*	*BallBag.k*
d. Ohio University Model	*OUModel.ain*	*OUModel.k*

Sample plots of the example simulation output results were given in the Second Payable Milestone report for cases a. and b. in conjunction with the validation and modeling sections. In case a., the coupled software results must be picked out since the plots in Figs. 1 also give ATB-only and LS-DYNA-only results. Case b. gives only the coupled software results in the plots of Figs. 2. Given below are results for model c., the sphere on an inflating airbag. This model cannot be executed in ATB alone and hence was not part of the coupled code verification. Sample results for case d. were also given in the Second Payable Milestone report, Figs. 3.

For example c., a rigid sphere is placed on an airbag. The airbag is inflated and the resulting motion is plotted vs. time. The motion is primarily in the Z direction. The rotational motion demonstrates that, despite the fact that the sphere is uniform and symmetric, the angular motion is significant.

For the rigid sphere, Figs. D.1 through D.3 show the CG translational displacements, CG translational velocities, and CG translational accelerations, for all three XYZ components. Figures D.4 through D.6 show the angular displacements, angular velocities, and angular accelerations, about all three XYZ axes. Both the CG translational accelerations and the angular accelerations are reasonable in this example (i.e. the acceleration values look like the derivative of the velocity curves at all time points).
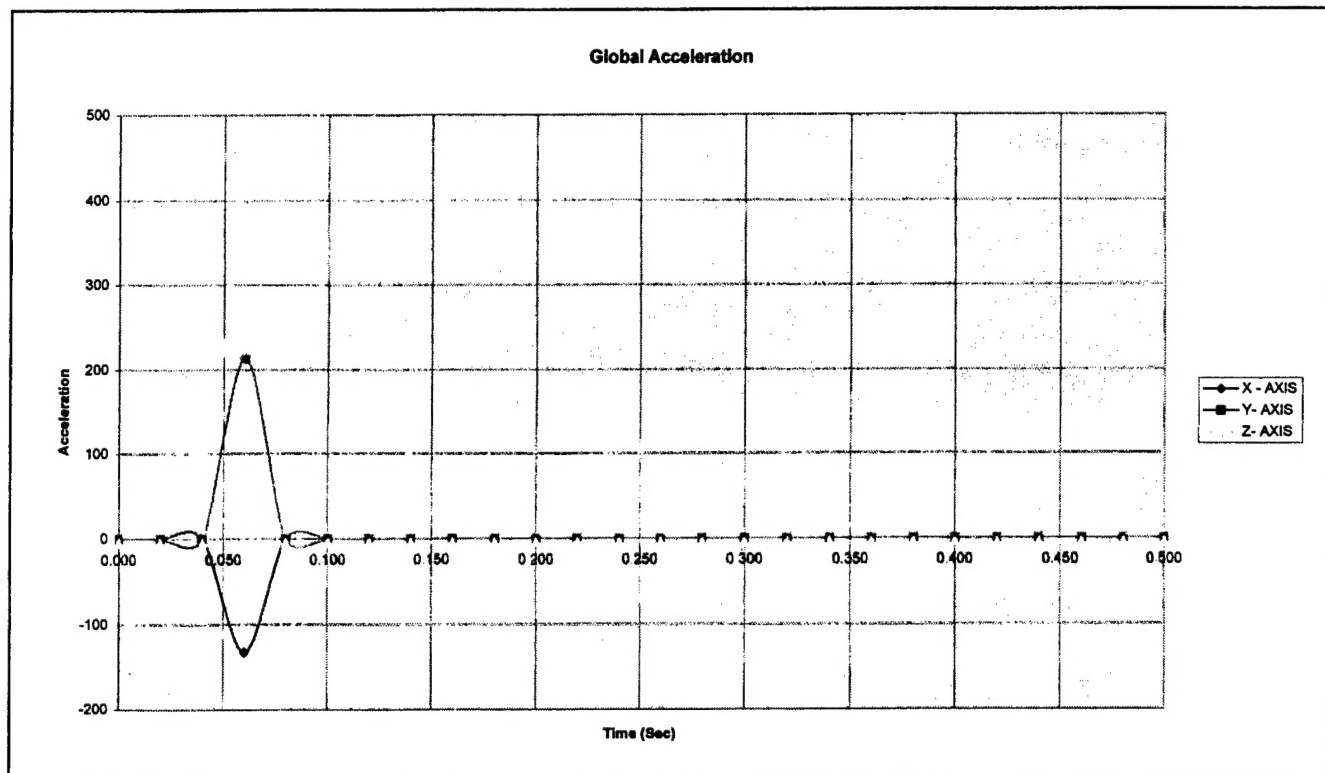
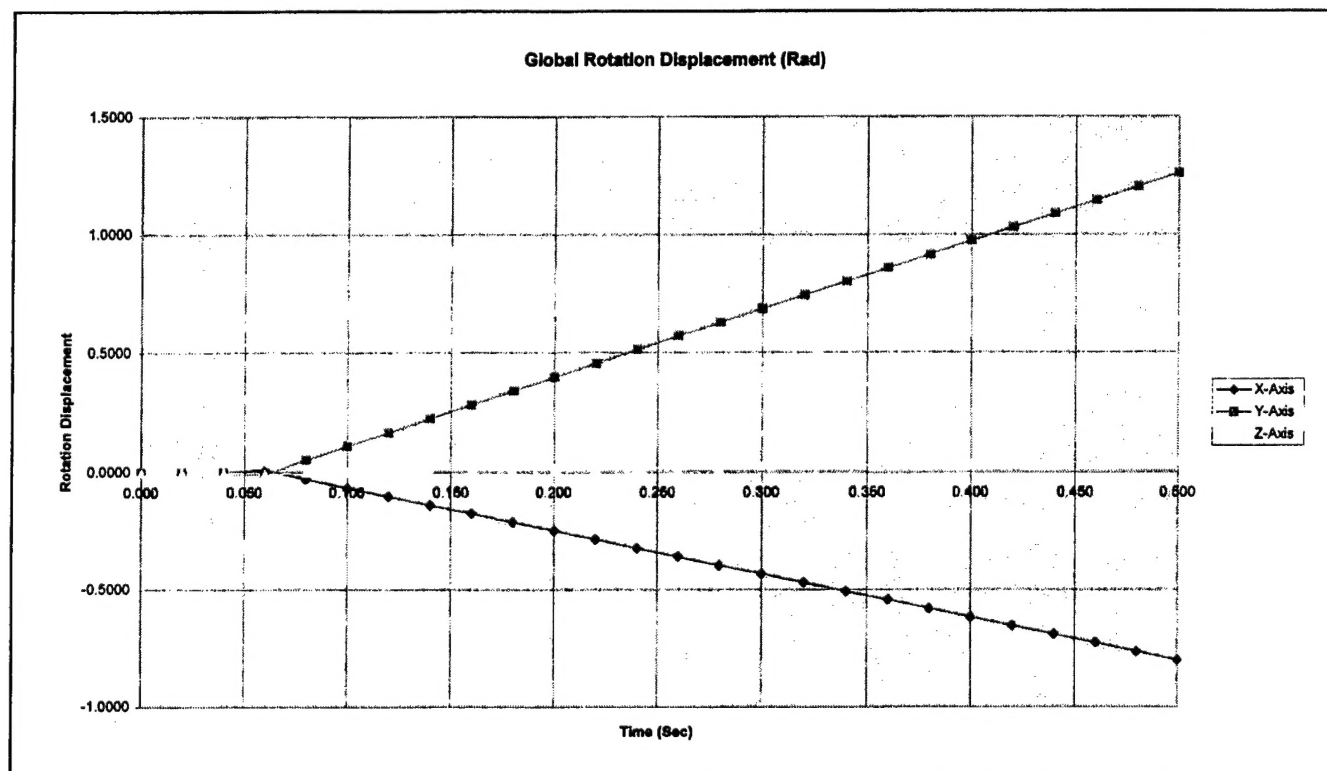Figures D.7 and D.8 present the first and last frame snapshots from the resulting animation for model c.
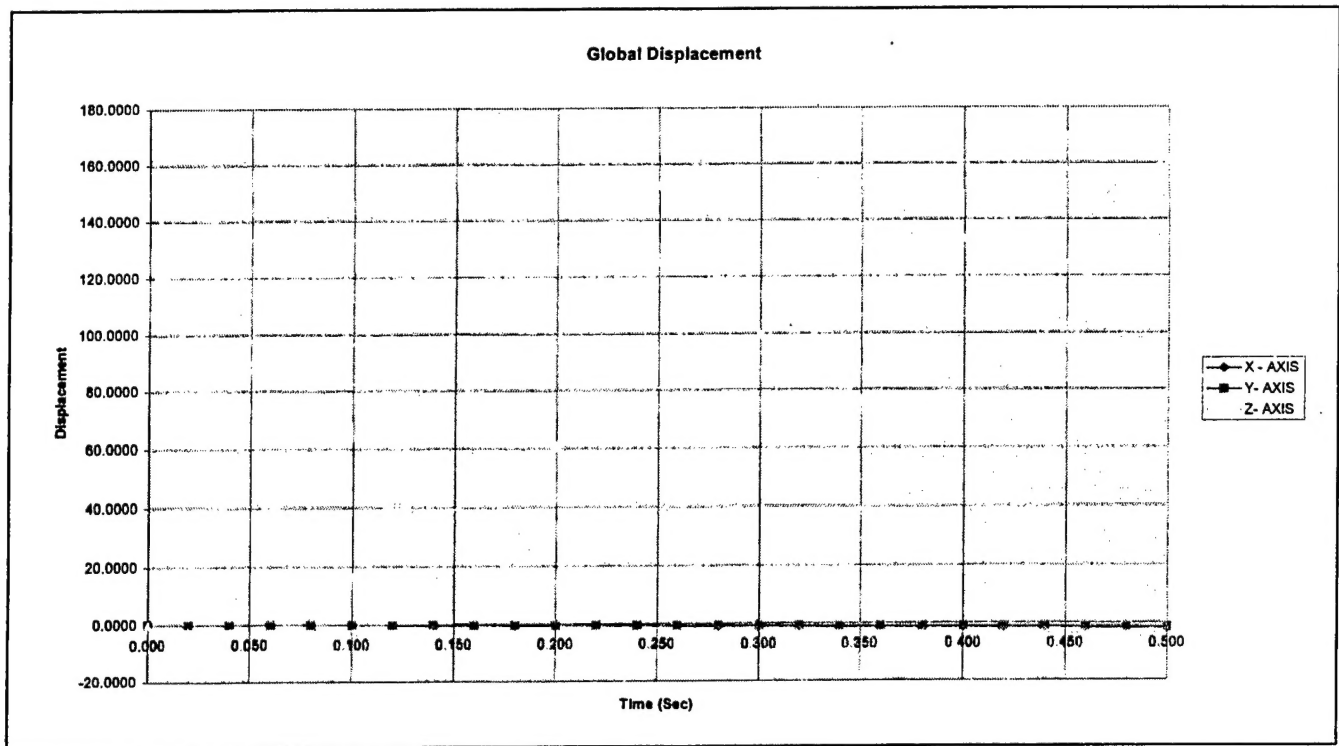
Figure D. 1 Sphere XYZ Translational Displacements
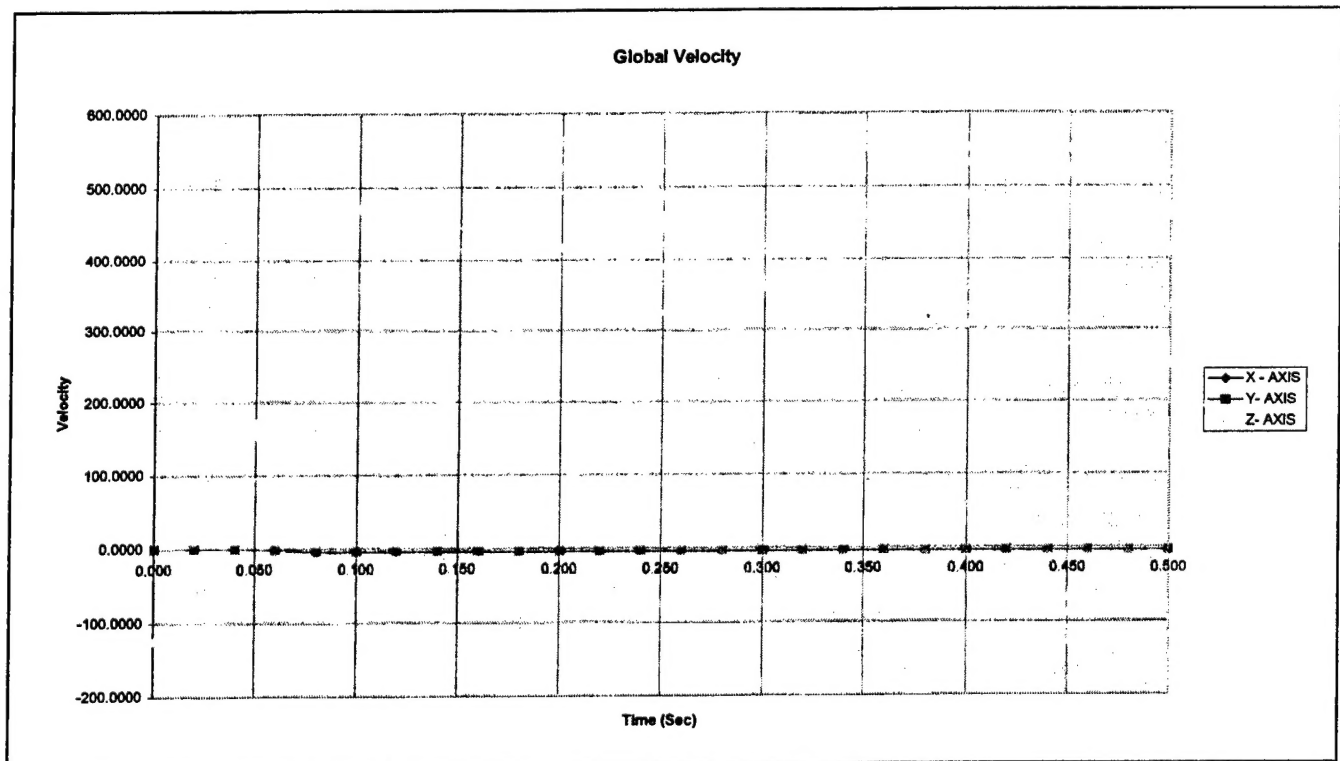
Figure D. 2 Sphere XYZ Translational Velocities

92

Figure D. 3 Sphere XYZ Translational Accelerations

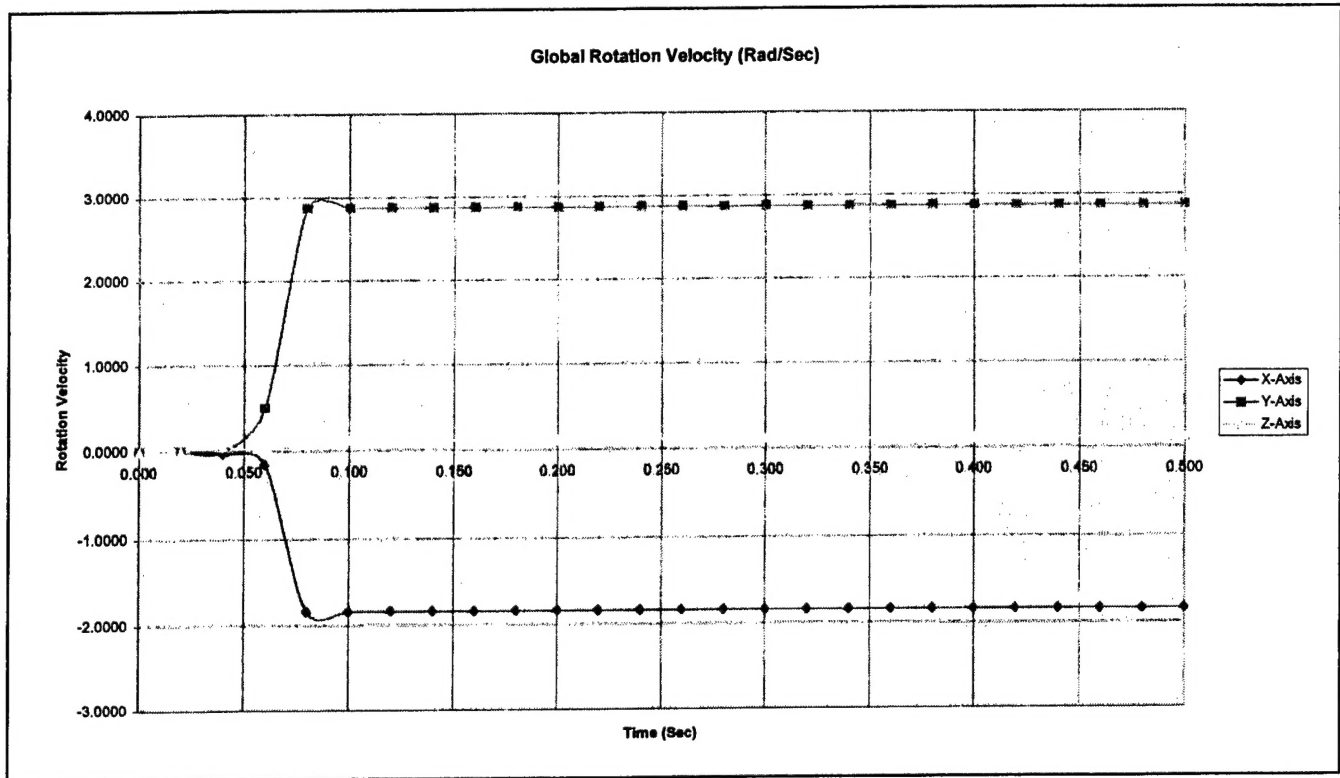**Figure D. 4 Sphere XYZ Angular Displacements**

93

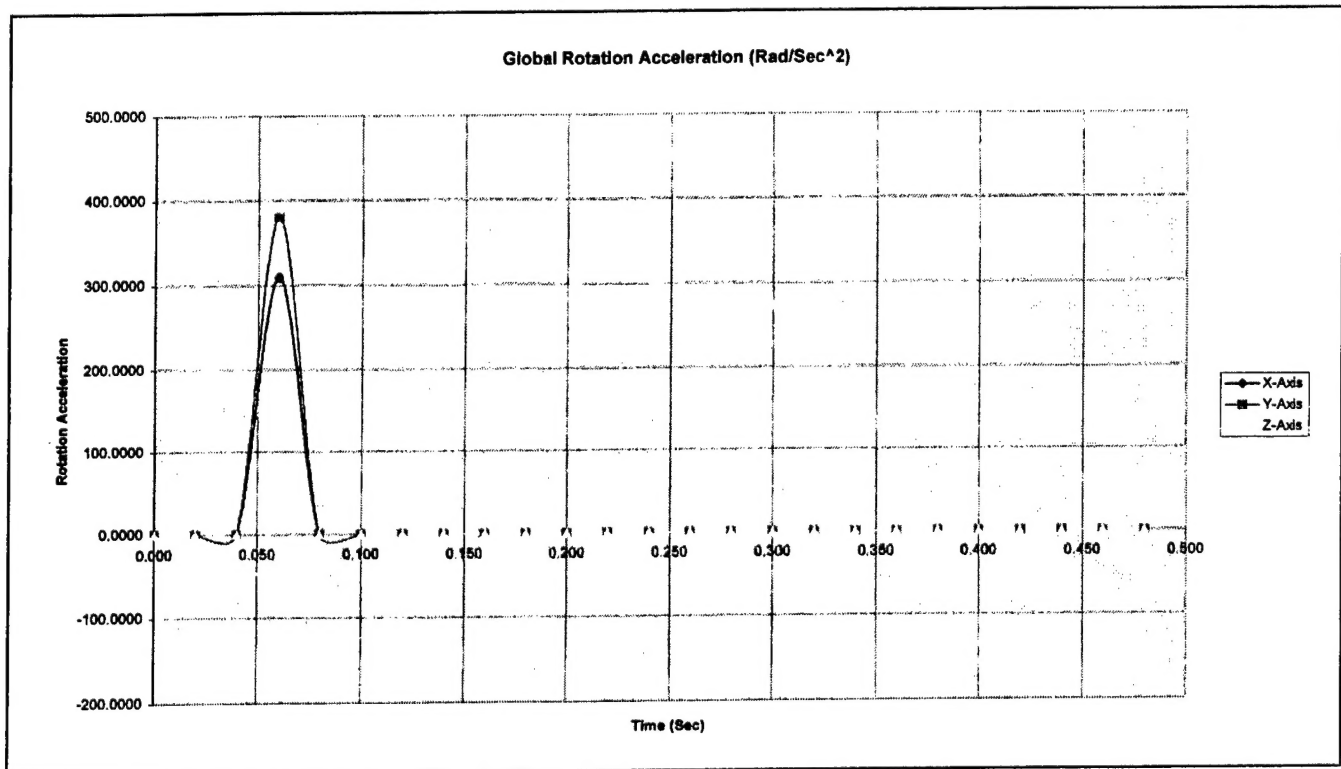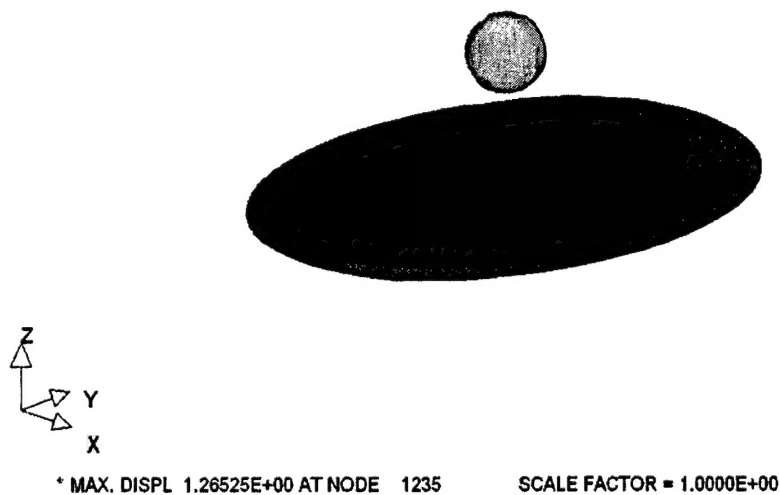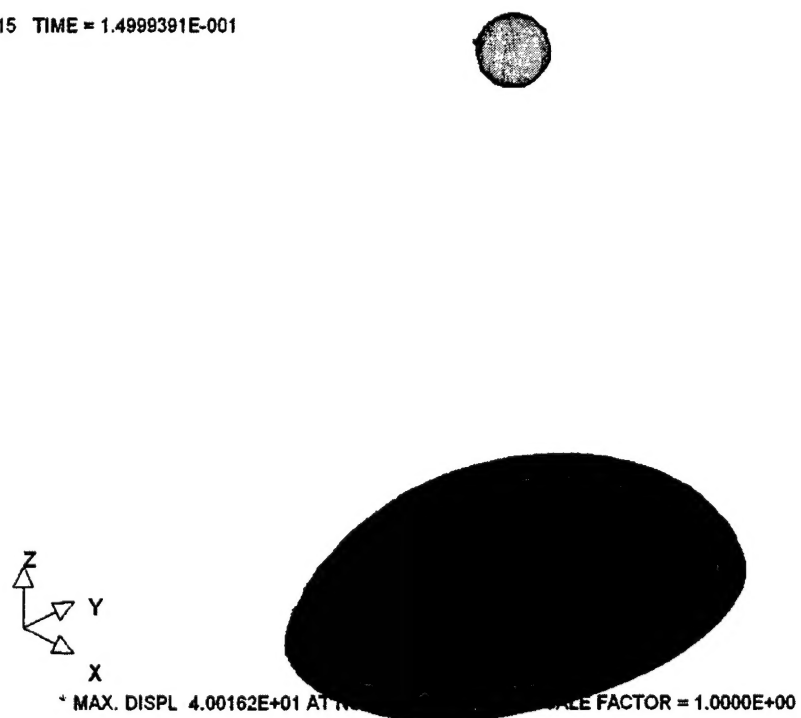**Figure D. 5 Sphere XYZ Angular Velocities**

Figure D. 6 Sphere XYZ Angular Accelerations

94

STEP 1   TIME = 9.9957259E-003

Z
Y
X

* MAX. DISPL 1.26525E+00 AT NODE   1235   SCALE FACTOR = 1.0000E+00

Figure D. 7 First Simulation Frame, Model c.

STEP 15   TIME = 1.4999391E-001

Z
Y
X

* MAX. DISPL 4.00162E+01 A̶T̶ ̶N̶...̶...̶...̶L̶E̶ FACTOR = 1.0000E+00

Figure D. 8 Last Simulation Frame, Model c.